The circadian clock of the carpenter ant *Camponotus floridanus*

Die circadiane Uhr der Rossameise *Camponotus floridanus*

Doctoral thesis for a doctoral degree
at the Graduate School of Life Sciences,
Julius-Maximilians-Universität Würzburg,
Section Integrative Biology

submitted by

Janina Kay

from

Ochsenfurt

Würzburg, 13.12.2017

Submitted on: ……..……..

Office stamp

Members of the *Promotionskomitee*:

Chairperson: Prof. Dr. Jörg Schultz

Primary Supervisor: Prof. Dr. Charlotte Förster

Supervisor (Second): Prof. Dr. Flavio Roces

Supervisor (Third): Prof. Dr. Monika Stengl

Date of Public Defence: ……..……

Date of Receipt of Certificates: ……..

CONTENT:

SUMMARY:

Due to the earth´s rotation around itself and the sun, rhythmic daily and seasonal changes in illumination, temperature and many other environmental factors occur. Adaptation to these environmental rhythms presents a considerable advantage to survival. Thus, almost all living beings have developed a mechanism to time their behavior in accordance. This mechanism is the endogenous clock. If it fulfills the criteria of (1) entraining to zeitgebers (2) free-running behavior with a period of ~ 24 hours (3) temperature compensation, it is also referred to as “circadian clock”. Well-timed behavior is crucial for eusocial insects, which divide their tasks among different behavioral castes and need to respond to changes in the environment quickly and in an orchestrated fashion. Circadian rhythms have thus been studied and observed in many eusocial species, from ants to bees. The underlying mechanism of this clock is a molecular feedback loop that generates rhythmic changes in gene expression and protein levels with a phase length of approximately 24 hours. The properties of this feedback loop are well characterized in many insects, from the fruit fly *Drosophila melanogaster*, to the honeybee *Apis mellifera*. Though the basic principles and components of this loop are seem similar at first glance, there are important differences between the *Drosophila* feedback loop and that of hymenopteran insects, whose loop resembles the mammalian clock loop. The protein PERIOD (PER) is thought to be a part of the negative limb of the hymenopteran clock, partnering with CRYPTOCHROME (CRY). The anatomical location of the clock-related neurons and the PDF-network (a putative in- and output mediator of the clock) is also well characterized in *Drosophila*, the eusocial honeybee as well as the nocturnal cockroach *Leucophea maderae*. The circadian behavior, anatomy of the clock and its molecular underpinnings were studied in the carpenter ant *Camponotus floridanus*, a eusocial insect Locomotor activity recordings in social isolation proved that the majority of ants could entrain to different LD cycles, free-ran in constant darkness and had a temperature-compensated clock with a period slightly shorter than 24 hours. Most individuals proved to be nocturnal, but different types of activity like diurnality, crepuscularity, rhythmic activity during both phases of the LD, or arrhythmicity were also observed. The LD cycle had a slight influence on the distribution of these activities among individuals, with more diurnal ants at shorter light phases. The PDF-network of *C. floridanus* was revealed with the anti-PDH antibody, and partly resembled that of other eusocial or nocturnal insects. A comparison of minor and major worker brains, only revealed slight differences in the number of somata and fibers crossing the posterior midline. All in all, most PDF-structures that are conserved in other insects where found, with numerous fibers in the

optic lobes, a putative accessory medulla, somata located near the proximal medulla and many fibers in the protocerebrum. A putative connection between the mushroom bodies, the optic lobes and the antennal lobes was found, indicating an influence of the clock on olfactory learning. Lastly, the location and intensity of PER-positive cell bodies at different times of a 24 hour day was established with an antibody raised against *Apis mellifera* PER. Four distinct clusters, which resemble those found in *A. mellifera,* were detected. The clusters could be grouped in dorsal and lateral neurons, and the PER-levels cycled in all examined clusters with peaks around lights on and lowest levels after lights off.

In summary, first data on circadian behavior and the anatomy and workings of the clock of *C. floridanus* was obtained. Firstly, it´s behavior fulfills all criteria for the presence of a circadian clock. Secondly, the PDF-network is very similar to those of other insects. Lastly, the location of the PER cell bodies seems conserved among hymenoptera. Cycling of PER levels within 24 hours confirms the suspicion of its role in the circadian feedback loop.

ZUSAMMENFASSUNG:

Durch die Rotation der Erde um die Sonne, entstehen rhythmische, tägliche und saisonale Änderungen in der Beleuchtung, Temperatur und vielen anderen Umweltfaktoren. Die Anpassung an diese Umweltrhythmen stellt einen großen Überlebensvorteil dar. Deshalb haben fast alle bekannten Lebewesen einen Mechanismus zur Steuerung ihres Verhaltens in Relation zu diesen Änderungen entwickelt. Dieser Mechanismus ist die innere Uhr, die auch als zirkadiane Uhr bezeichnet wird wenn sie die folgenden Kriterien erfüllt: (1) Entrainment auf Zeigeber (2) Freilaufendes Verhalten mit einer Periodenlänge von ungefähr 24 Stunden (3) Temperatur-Kompensation. Den korrekten Zeitpunkt für ein bestimmtes Verhalten einzuhalten ist äußerst wichtig für soziale Insekten. Sie verteilen ihre Aufgaben unter verschiedenen Verhaltens-Kasten und müssen in der Lage sein schnell und organisiert auf Umweltänderungen zu reagieren. Deshalb stellen sie interessante Objekte für das Studium circadianen Verhaltens dar, welches schon in vielen eusozialen Spezies wie Ameisen und Bienen beobachtet wurde. Der der inneren Uhr zugrunde liegende Mechanismus ist eine molekulare Rückkopplungsschleife, die rhythmische Veränderungen in der Expression von Genen und dem Akkumulationsniveau von Proteinen in einem 24 Stunden Zyklus hervorruft. Die Eigenschaften dieser Rückkopplungsschleife sind in vielen Organismen, von der Taufliege *Drosophila melanogaster*, bis zur Hongbiene *Apis mellifera*, bereits gut charakterisiert. Obwohl die Gemeinsamkeiten der zugrunde liegenden Prinzipien und Bestandteile stark auffallen, gibt es wichtige Unterschiede zwischen der Rückkopplungsschleife von *Drosophila* und der eher

mammal organisierten Rückkopplungsschleifen hymenopterer Insekten. Das PERIOD (PER) Protein ist vermutlich ein Bestandteil des hemmenden Teils der Schleife und verbindet sich mit CRYPTOCHROME (CRY). Die anatomischen Eigenschaften der Uhrneurone und des PDF-Netzwerks (vermutlich der Ein- und Ausgang für Informationen im Uhrnetzwerk) sind ebenfalls in der Taufliege, eusozialen Honigbiene, sowie in der nachtaktiven Schabe *Leucophea maderae* sehr gut beschrieben. Die Rossameise *Camponotus floridanus* wurde hier als Studienobjekt verwendet, um zirkadianes Verhalten, die Anatomie der Uhr sowie die ihr zu Grunde liegenden molekularen Strukturen in einem weiteren eusozialen Organismus zu analysieren. Die Aufzeichnung von Lauf-Verhalten in sozialer Isolation bewies, dass der Großteil der Ameisen in der Lage ist auf verschiedene LD-Zyklen zu entrainen, freilaufendes Verhalten im Dunkeln aufweist und eine temperaturkompensierte Uhr mit einer Periodenlänge von etwa 24 Stunden besitzt. Die meisten Individuen waren nachtaktiv, aber es wurden auch andere Verhaltensmuster wie Tagaktivität, Dämmerungsaktivität, Rhythmische Aktivität während beiden LD Phasen sowie Arrhythmizität beobachtet. Der LD-Zyklus hatte einen leichten Einfluss auf die Verteilungsmuster dieser Aktivitätstypen. Mehr tagaktive Tiere wurden bei kurzen Lichtphasen beobachtet. Das PDF-Netzwerk in *C. floridanus* konnte mit Hilfe des anti-PDH Antikörpers sichtbar gemacht werden und ähnelte in Teilen dem anderer eusozialer oder nachtaktiver Insekten. Ein Vergleich zwischen den Gehirnen kleiner und großer Arbeiter zeigte nur geringe Unterschiede in der Anzahl von Zellkörpern und Fasern die die posteriore Mitte des Gehirns überschreiten. Im Gesamten konnte die Mehrzahl der zwischen den anderen Insektengehirnen konservierten PDF-Strukturen, wie viele Fasern in den optischen Loben, eine akzessorische Medulla, Zellkörper neben der proximalen Medulla und viele Verzweigungen im Protozerebrum, gefunden werden. Eine mögliche Verbindung zwischen den Pilzkörpern, optischen Loben und den Antennalloben wurde identifiziert und weist auf einen Einfluss der Uhr auf olfaktorisches Lernen hin. Zu guter letzte wurde mit Hilfe eines gegen Bienen-PER gerichteten Antikörpers die Lage und Intensität der PER-Zellkörper während mehrerer Zeitpunkte im Verlauf von 24 Stunden bestimmt. Vier abgegrenzte Gruppen von Zellkörpern, die den Gruppen in *A. mellifera* ähneln, konnten identifiziert werden. Diese Gruppen teilen sich in dorsale und laterale Neuronen und der Proteingehalt an PER oszilliert in allen untersuchten Gruppen, mit dem Höhepunkt bei Licht-an und dem Tiefpunkt kurz nach Licht-aus.

Zusammenfassend ist zu sagen, dass erste Erkenntnisse über zirkadianes Verhalten, die Anatomie und die Grundlagen der inneren Uhr von *C. floridanus* gewonnen werden konnten. Erstens, erfüllt das Verhalten alle Kriterien für die Präsenz einer inneren Uhr. Zweitens, ist das PDF-Netzwerk ähnlich dem anderer Insekten. Letztens, scheint die Lage der PER-positiven

Neurone innerhalb der Hymenopteren konserviert. Die Oszillation von PER bestätigt den Verdacht seiner Beteiligung an der Rückkopplungsschleife der inneren Uhr.

1. INTRODUCTION

1.1 The endogenous clock

The daily changes in light and dark phases, caused by the earth`s rotation around the sun and itself, are one of many environmental factors living beings are exposed to. Not only does the earth's rotation lead to a daily alternation between phases of illumination and darkness, the so-called light-dark cycle (LD), the rotation around the sun also leads to differences in the length and proportion of the LD throughout the year (photoperiod). These rhythmical changes in illumination have an influence on numerous aspects of life, ranging from environmental conditions like temperature (influenced for example by the inclination of the suns' rays towards the earth and the length of the light period) or availability of food to social conditions like visibility/conspicuousness to mates and predators. Evolutionary adaptation to these rhythmical changes developed in form of an internal time-keeping device, the circadian clock. It allows for prediction of these illumination related changes through an endogenous oscillator that receives input from returning environmental events.

The first report of an endogenous oscillation can be found as early as 1729, when Jean Jacques d'Ortous de Mairan conceived the very first circadian experiments (Mairan, 1729). He found that *Mimosa pudica* does not only spread and fold its leaves in response to a LD cycle, but that it persisted in doing so with a period of approximately 24 hours in constant darkness. Further experiments, conducted in the middle of the 20th century on humans (Aschoff, 1984), plants (Bünning, 1973) and insects (Pittendrigh, 1993), showed that an endogenous time-keeping device, a clock, was responsible for the generation of rhythms of approximately 24 hour period-length (τ) that could be coupled to external time-cues. Thus, the term circadian (greek; circa=approximately, dia=day) was established in (Halberg, 1959), referencing the period length of the endogenous clock. Three defining criteria need to be met for an endogenous oscillator to be called "circadian":

[1] The clock must "free-run" in constant conditions. This means, the rhythmic output must persist under constant conditions that do not present any periodic stimuli. The period-length τ witnessed under such conditions is called "free-running period" and is close to 24hours.

[2] The clock must be able to entrain to "zeitgebers". A zeitgeber is any external periodic stimuli the clock can synchronize to. A clock that is synchronized to a zeitgeber is referred to as entrained, the period in which a clock adapts to a new zeitgeber entrainment. The zeitgeber-time is defined in hours. A zeitgeber-time (ZT) of 0 usually refers to the onset of the stimulus, e.g. in a LD-cycle of 12 hours light and 12 hours darkness ZT 0 would be the onset of the light phase, ZT12 the onset of the dark phase.

[3] The clock is temperature compensated. Usually, the speed of biochemical reactions is dependent on ambient temperature, with a 10K rise in temperature doubling the reaction rate (RGT-Regulation, also called Van´t Hoffsch Regulation). Circadian clocks however, work in many different temperature zones and there is no significant difference in the period length at warmer or colder temperatures (Bodenstein et al., 2012; Francois et al., 2012). Thus, the biochemical reactions underlying the molecular basis of the clock must be temperature compensated.

Circadian clocks were found in almost all organisms. In animals, a master clock resides in the brain and several slave clocks in other tissues tissues, like skin, the stomach or the kidneys. These different clocks can be entrained to different factors, like food or light. Input from a zeitgeber is recorded by a receptor (e.g. the eyes record light), then mediated into the endogenous oscillator via an entrainment pathway. This synchronizes the clocks endogenous period-length to the zeitgeber, which in turn generates a rhythmic output through an effector pathway (e.g. a behavior). Two of the most prominent zeitgebers in the environment are light and temperature. Both change throughout the day as well as throughout the year in a rhythmical fashion. Even though temperature cannot speed up or slow down the clock, due to the clock's temperature compensation, it can still set its phase and period (Glaser and Stanewsky, 2005; Tomioka and Yoshii, 2006; Currie et al., 2009; López-Olmeda, 2017). For most animals, light is an even more important zeitgeber. The free-running-period of the circadian clock is closely coupled to the solar day, which is also approximately 24 hours in length. Not only can light set the phase of the clock (reviewed in (Hughes et al., 2015; Schlichting and Helfrich-Förster, 2015b)), it can also influence the period length through its intensity (Pittendrigh, 1960; Aschoff, 1984): period length is increased in nocturnal animals when light intensity is raised, while it is decreased in diurnal animals under the same conditions. Furthermore, a light pulse during the dark phase of a LD period can shift the phase of the clock forward (delaying) or backwards (accelerating) and thus "reset" it. This resetting is one of the mechanisms allowing animals to entrain to different light phases.

1.2 Rhythmic Behavior

Rhythmic behavior is any behavior that is continuously repeated within a fixed period of time. In terms of the endogenous clock, there are numerous rhythms that can be followed, ranging from ultradian rhythms (shorter than 24 hours) like tidal rhythms, to the aforementioned circadian rhythms, to rhythms longer than 24 hours like semilunar (~14 days), lunar (28 days), seasonal and circannual (~ 1 year) rhythms. All these rhythms are entrained by environmental cues and an endogenous time-keeper is necessary to adapt to them. Rhythmic behavior as an output of the clock has been studied extensively in many organisms. As mentioned before, truly endogenous rhythmic behavior is entrained by zeitgebers, mediated by the clock and persists under constant conditions. In the following chapter, only rhythmic behavior in different ant species is discussed, though there is evidence for circadian and other rhythms in numerous other taxa as well.

1.2.1 Rhythmic behavior in selected ants

All species of ants are eusocial, which means their colonies are organized strictly into a reproductive caste (queens and males) and a (mostly) sterile worker caste that is engaged in tasks relating to colony growth and development. Queens and males mating flights happen at a species specific time of day, that is influenced by light intensity and humidity (Boomsma and Leusink, 1981). This timing of the mating flight has been reported for many species (Kannowski, 1959; Kannowski, 1962; Weber, 1972) and is important, since many queens and males die within hours of leaving the nest. McCluskey tested the rhythmic behavior of males and queens of various species extensively in the laboratory (McCluskey, 1958; McCluskey, 1967; McCluskey and Carter, 1969; Mccluskey, 1974). He found that the rhythms males displayed under an LD cycle of 12:12 hours persisted after transition to total darkness and were very precise in their timing. While *Veromessor andrei* males are most active during the first hour of light, with a rise of activity shortly before the end of the dark phase, males of *Camponotus clarithorax* do not show a similar rise in activity but were only active in the first hours of the light phase and males of *Iridomyrmex humilis* are most active at the end of the light period (McCluskey, 1965). Females of *Veromessor pergandei* and *Veromessor andrei* showed similar rhythms under LD cycles and constant conditions while they expressed wings (virgins), but wingless (post-flight) queens did not (McCluskey, 1967). McCluskey later showed that queens of *Pogonomyrmex californicus* exhibit a similar behavior and that the loss of rhythmicity only happens in mated post-flight queens (McCluskey and Carter, 1969). Similar findings were

reported in Sharma et al. (2004) for virgin males and queens of *Camponotus compressus*. Not only did unmated males and queens show strong rhythms in the laboratory, the queens also lost their rhythmicity once they had mated and started laying eggs. After the egg-laying phase had passed, queens resumed their rhythmic activity (Sharma et al., 2004), indicating that rhythmicity was merely suppressed in a phase when it would be counterproductive.

The worker caste of the colony is entrusted with a number of diverse tasks that are vital to colony management and growth and can often be categorized into physical castes according to their morphology (size, shape of head, etc.). These tasks are allocated according either to the physical caste or age polyethism and further classify the worker ants into social castes (characterized by their allocated tasks). Whether this allocation happens according to morphology, age or both is species specific. In *Camponotus rufipes*, for instance, media workers (physical caste) perform both tasks inside the nest, as well as outside (Jaffe and Sanchez, 1984). Here, younger ants tend to stay inside the nest, for example as nurses and older ants perform tasks outside the nest, like foraging or patrolling (Soares et al., 2008). Another example for the distribution of tasks among castes of different morph is *Atta sexdens*, a leaf-cutting ant. A total of 29 tasks are distributed among four size castes (Wilson, 1980b). While some size castes seem to be more adapt at performing special tasks, like medium workers that perform most leaf-cutting tasks and minims that take care of gardening and nursing, it is still possible for ants of other size castes to take over their responsibilities and to perform other tasks as well (Wilson, 1980b; Wilson, 1980a). Some species of ants have been shown to be flexible in their behavior and are able to switch their tasks (Calabi, 1988; Gordon, 1989). This flexibility in task allocation allows ant colonies to quickly respond to unpredictable changes in their environment. Nevertheless, to generate a coordinated colony response daily tasks must be organized and synchronized among all individuals of the colony, inside as well as outside. Colonies of different species of ants have been reported to show preferences for different times of day when entering and leaving the nest, some of them using their specific temporal niche to avoid competitive species with different timing living nearby (Van Pelt, 1966; Hunt, 1974; Hansen, 1978; Levieux and Diomande, 1978). One of the first experiments showing colony specific rhythms for other behavior than just leaving and entering the nest was described in Gordon (1983), which showed rhythmic behavior in specific tasks, like patrolling or midden work in *Pogonomyrmex badius*. Some tasks, like foraging of nectar, require very precise timing, since the forager needs to be present at the flower at the right time of day to be able to harvest. It has been shown for many ant species, like *Camponotus rufipes* (Mildner and Roces, 2017) and *Dinoponera quadriceps* (Medeiros et al., 2014) that their foragers exhibit strong behavioral rhythms in social conditions. *Dinoponera quadriceps'* mainly diurnal foraging

rhythms were revealed to be plastic on a daily and annual basis in accordance with environmental conditions and specific for each colony (Medeiros et al., 2014). Mildner and Roces (2017) also shed some light on the locomotor behavior of foragers in isolation. Most, but not all, were rhythmic under an LD cycle, able to adapt their activity to a shift in the LD cycle, showed a preference for nocturnal behavior and free-ran with a period shorter than 24 hours in constant darkness. Additionally, foragers of the species *Camponotus mus* are able to perceive crop filling times and nectar flow rates and can estimate when a visited nectary can be harvested again (Roces et al., 1998). Another behavioral caste that is important for the thriving of the colony are nurses. Nurses take care of the brood by licking, feeding and transporting it. They are generally thought to be active around the clock. Still, nurses of *Camponotus rufipes* were shown to display rhythmic and nocturnal locomotor behavior in isolation, with a free-running period similar to those of foragers (Mildner and Roces, 2017). This locomotor rhythmicity is lost when nurses are observed in the social context, hinting at a suppression of their endogenous rhythms in presence of the brood (Mildner and Roces, 2017). Furthermore, nurses of *Camponotus mus* show a circadian preference for temperature (Roces and Nunez, 1989b; Roces, 1995). They transport larva to specific temperatures, once in the middle of the light phase and once eight hours later in the dark phase, with the first relocation depending on the duration of the light phase and the second on the preceding one. Another study on differences in rhythmic behavior between worker castes did not compare foragers to nurses, but members of different size castes *Camponotus compressus* (Sharma et al., 2004). While major and media workers of this species entrain to LD cycles and show free-running behavior in constant conditions, minor workers neither entrain nor free-run in isolation. Another difference can be found in their temporal preference for activity, while major workers were uniformly nocturnal and showed a single state of activity in constant conditions, about a quarter of the media workers were diurnal and the rest nocturnal. They switched from period lengths longer than 24 hours to period lengths shorter than 24 hours after several days of DD (Sharma et al., 2004). These differences might be connected to the tasks the differently sized castes are involved in.

1.2.2 Rhythmic behavior in *C. floridanus*

The carpenter ant *Camponotus floridanus* is closely related to all Camponote species in the preceding chapter. Nevertheless, its colony structure, task-allocation and rhythmic behavior differ from theirs in some points. Though *Camponotus floridanus* is a mainly nocturnal species when observed in vicinity of the diurnal ant *Camponotus socius* (Hölldobler and Wilson, 1990), it is thought to be able to switch its activity to other times of the day when necessitated by environmental conditions. Simola et al. (2016) found two distinct morphological castes in *C. floridanus*, minors and majors, which differ significantly in their body size and head length to width ratio, and are thus easily identifiable. A third morphological caste, that exhibits mixed features of the two distinct castes, also exists. Members of the minor caste were found to perform the majority of the foraging and scouting activities, with a rise in these activities directly correlated with age (Simola et al., 2016). These foraging activities were predominantly performed during the night-time.

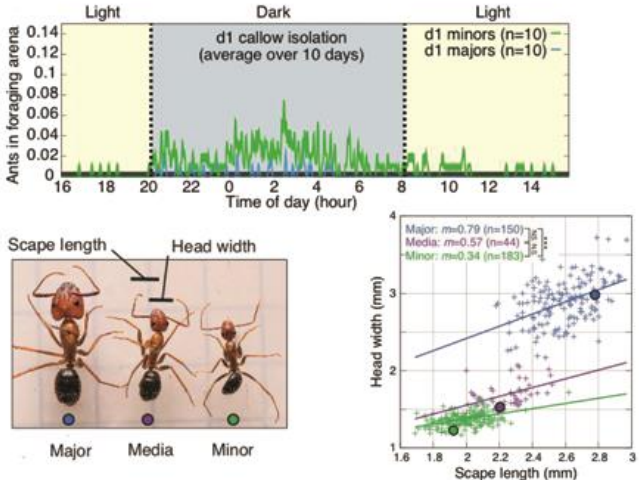

Figure 1: Foraging activity and size caste identification in *C. floridanus*: a) Foraging activity of *C. floridanus* minors and majors during a 12:12 hour light dark cycle. b) Distribution of scape length and head width in the different morphological castes. After (Simola et al., 2016)

1.3 The molecular basis of the circadian clock

The endogenous rhythm-generator mentioned in the preceding chapters is most likely based on cell-autonomous oscillations of proteins that cycle with a period length close to 24 hours. These oscillations are usually sustained by transcriptional-translational feedback loops, post-translational negative-feedback loops or several of the aforementioned in combination (reviewed in (Helfrich-Förster, 2004; Ko and Takahashi, 2006).

1.3.1 The transcriptional-translational feedback-loop

A transcriptional-translational feedback-loop (TTFL) consists of several factors that regulate either their own or that of other factors, which in turn have an influence on them. In the most simplified model, a gene blocks its own transcription through the translated protein, leading to a cyclic accumulation of mRNA and protein. In the circadian clock, this TTFL is much more complicated, listing a number of genes whose products influence each other in several interlocked feedback loops. The following chapters provide an insight into components and workings of the TTFL in different organisms. Since the TTFL has not been characterized in *C. floridanus* yet, closely related species are presented and compared.

1.3.2 Components of the feedback loop in selected insects

1.3.2.1 The molecular feedback loop of *Drosophila melanogaster*

Drosophila melanogaster's feedback loop is among, if not the best characterized feedback loops in all organisms. Indeed, research on the molecular properties of the clock started in this organism when Konopka and Benzer generated the very first clock mutants in 1971 (Konopka and Benzer, 1971). Their mutants were termed per^{s}, per^{l} and per^{01}, representing behavioral phenotypes of short and long period length, and arrhythmic ones (adult locomotor behavior, eclosion). The phenotypes could be traced back to single nucleotide mutations of the *period*-gene (*per*) later on (Yu et al., 1987). The discovery of oscillations of the relative amount of the *per* mRNA (Hardin et al., 1990) and Period (PER) protein (Siwicki et al., 1988; Zerr et al., 1990) under LD and DD conditions, and the fact that these oscillations were altered in accordance with the phenotype in the *per* mutants, lead to a first proposal of a feedback loop in which PER causes cycling of its own mRNA (Hardin et al., 1990). Since the first discovery of a clock-gene in 1971, several other genes that are involved in *Drosophila's* clock have been found. It has since been established that TTFL regulation takes place on transcriptional, post-transcriptional

and post-translational levels (reviewed in (Helfrich-Förster et al., 1998; Allada and Chung, 2010; Hardin, 2011; Özkaya and Rosato, 2012). Sehgal et al found the second gene involved in 1994, the *timeless 1* (*tim1*) gene (Sehgal et al., 1994). *Timeless* also shows circadian oscillations in its mRNA and protein levels, cycles in phase with *per* in LD conditions and seems to have a direct influence on *per* cycling (Sehgal et al., 1994; Sehgal et al., 1995). Additionally, Timeless 1 (TIM1) and PER proteins form a heterodimer (Gekakis et al., 1995) through binding of TIM1 to a PAS-domain expressed by PER, and express a common eBox motif (Hao et al., 1997; Darlington et al., 1998). PAS-domains are known to bind bHLH-PAS transcription factors (Reisz-Porszasz et al., 1994), which led to the discovery of the dClock (CLK, Circadian Locomotor Output Cycles Kaput) protein in *Drosophila* (Darlington et al., 1998). For the mammalian orthologue to this protein, mClock, the presence of its bHLH-PAS domain and its influence on rhythmic behavior had been described earlier in mice (King et al., 1997). This mammalian protein was also known to form a heterodimer with another factor, the BMAL1 (Brain and Muscle ARNT Like 1) protein (Ikeda and Nomura, 1997; Gekakis et al., 1998). This heterodimer was found to bind to eBox motifs and activate expression of *per* and *tim* genes in mice, which in turn where able to bind to bind to the CLK/BMAL1 dimer and repress its function (Gekakis et al., 1998). A homolog to the mammalian BMAL1 was also reported in *Drosophila melanogaster* (Darlington et al., 1998; Rutila et al., 1998) and called Cycle (CYC). Expression levels of *clk* mRNA cycle in antiphase to those of *tim1* and *per* (Bae et al., 1998), but *cyc* does not show changes in expression level (Rutila et al., 1998). Thus, a first basic model of the TTFL was established, the CLK:CYC heterodimer activates expression of *per* and *tim1*, which is in turn blocked by their product PER:TIM1 (Bae et al., 1998; Lee et al., 1998), leading to cyclic repression and expression. The binding of CLK:CYC to the *per* and *tim1* promoter region takes place at approximately ZT 4 to ZT 16 in a LD cycle of 12:12 (Sehgal et al., 1994), leading to accumulation of PER and TIM1 in the cytoplasm. Their mRNA levels peak at ZT 12 (Sehgal et al., 1994), while the peak of their protein levels is delayed by approximately 7 hours until ZT19, when PER and TIM enter the nucleus (Curtin et al., 1995). This delay might be necessary to set the phase length of the clock to 24 hours, since transcription, translation and repression of transcription would usually take much less time. Several factors play a role in mediating this delay, one of them is the protein Doubletime (DBT) (Kloss et al., 1998), which is constitutively expressed (Kloss et al., 2001) and phosphorylates PER, which leads to degradation. TIM1 degradation by light (Kloss et al., 2001) and maybe also translational control of *per* and *tim* mRNA by Twentyfour (TYF) might also play a role (Lim et al., 2011). In addition to its role in phosphorylating and degrading PER, DBT also plays a role in translocation to the nucleus, by forming a complex with PER:TIM1, where TIM1 prevents degradation of PER. After further

phosphorylation of PER by Casein Kinase 2 (CK2) (Lin et al., 2002; Akten et al., 2003) and phosphorylation of TIM also by CK2 and Shaggy (SGG), a GSK3 orthologue (Meissner et al., 2008) to promote nuclear translocation, the PER:TIM1:DBT complex enters the nucleus around ZT19 (Curtin et al., 1995). It then represses the function of the CLK:CYC dimer by phosphorylating CLK from ZT18-ZT4 (under LD 12:12). Afterwards, TIM1 is degraded once the light phase begins (Kloss et al., 2001), leading to a subsequent degradation of PER mediated by phosphorylation through DBT. Once PER is degraded, CLK is not suppressed anymore, peaks and forms a heterodimer with CYC, to start the loop again.

A second feedback loop, which is interconnected with the main loop, is the "*clk*-loop". This loop regulates changing levels of *clk* expression throughout the day (Cyran et al., 2003) and contains the clock-genes *vrille* (*vri*) (Blau and Young, 1999), *par-domain protein 1* (*pdp1*) (Cyran et al., 2003) and *clockwork orange* (*cwo*) (Kadener et al., 2007; Lim et al., 2007; Matsumoto et al., 2007) . Figure 2 shows a schematic overview of the primary and secondary feedback loops. CLK binds to the E-Boxes of their transcription factors and activates their transcription at ZT 4 to 16, leading to a peak of *vri* and *cwo* mRNA levels at approximately ZT 14 (Blau and Young, 1999; Cyran et al., 2003; Kadener et al., 2007) and *pdp1* levels at ZT18 (Cyran et al., 2003) and a cycling in phase with *per* and *tim1* and in antiphase with *clk*. Both VRI and PDP1 bind to V/P boxes in the *clk* promoter region, but have different effects (Cyran et al., 2003; Glossop et al., 2003; Benito et al., 2007; Zheng et al., 2009). Whereas VRI acts as an inhibitor to *clk* expression (Cyran et al., 2003; Glossop et al., 2003), PDP1 acts as an activator to *clk* expression four hours later (Cyran et al., 2003; Benito et al., 2007; Zheng et al., 2009). This leads to cyclic changes in levels of *clk*. CWO on the other hand does not have an effect on expression of *clk*, but acts as a repressor of its own transcription by blocking E-Box activity in CLK:CYC mediated transcription, creating another feedback inhibition loop (Kadener et al., 2007; Lim et al., 2007; Matsumoto et al., 2007; Richier et al., 2008). Additionally, CWO can also act as an activator of circadian expression for *per*, *tim1*, *vri* and *pdp1* (Richier et al., 2008). *Vri, pdp1* and *cwo* thus have an effect on the regulation of amplitude, phase, and output of the core feedback loop. VRI and PDP1 also indirectly serve another purpose, which is the mediation of light-input into the central clock. Since the clock is able to entrain to light phases even if the ocelli and compound eyes are absent (Hu et al., 1978; Pearn et al., 1996; Ohata et al., 1998), a more direct way of receiving light-input is necessary. Once the blue-light

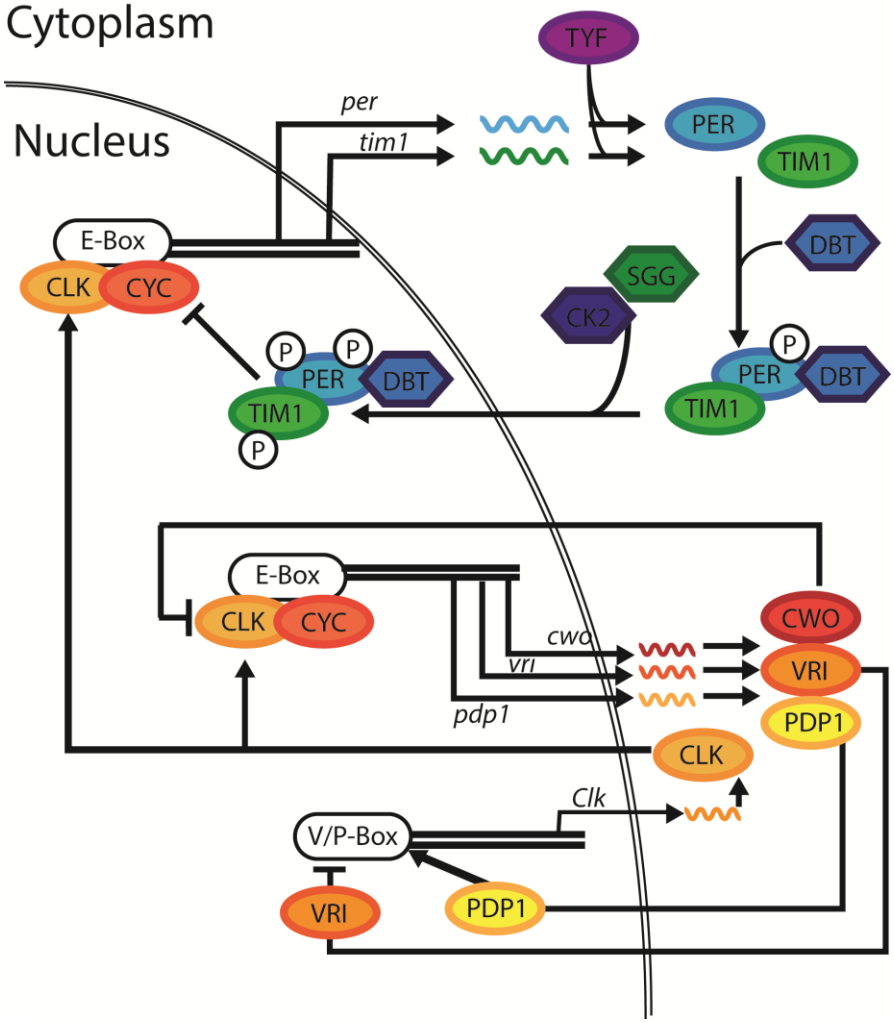

Figure 2: The transcriptional-translational feedback loops of *Drosophila melanogaster`s* clock. Oval shapes represent proteins, curly lines mRNA and double lines DNA. A detailed description of the feedback-loops can be found in Chapter 1.3.2.1. Abbreviations: CLK =Clock, CYC =Cycle, TYF = Twentyfour, PER = Period, TIM1 = Timeless 1, DBT = Doubletime, SGG = Shaggy, CK2 = Casein Kinase 2, CWO = Clockwork Orange, VRI = Vrille, PDP1 = Par Domain Protein 1, P = phosphate.

sensitive Cryptochrome (CRY1) (Emery et al., 1998; Cyran et al., 2003; Nitabach and Taghert, 2008) is activated by light, it mediates light-input into the clock by binding to TIM1 (Busza et al., 2004) which in itself is not light-sensitive. CRY1 expression is controlled by VRI and PDP1 and thus cycles in phase with CLK (Cyran et al., 2003). The binding of CRY1 to TIM1 enhances phosphorylation of TIM1, and makes TIM1 a high affinity target for the F-Box protein Jetlag (Jet) (Koh et al., 2006; Peschel et al., 2009) which mediates TIM1´s proteasomal degradation through the COP9 Signalosome (CSN) (Knowles et al., 2009). This CRY1 regulated degradation of TIM1 through light can trigger phase shifts when light pulses are present in the subjective night, and thus entrain the clock to changes in the light-dark cycle. A phase delay is triggered when the light pulse is present in the early night phase, since TIM1 levels are accumulating and degradation elongates the time-span until peak levels are reached. In the second half of the night TIM1 levels are declining, so a degradation event speeds up the process and leads to a phase advance. In the subjective day, TIM1 levels are constitutively low, so a further degradation does not have prominent effects on the phase.

1.3.2.2 The molecular feedback loop of hymenopteran species

The TTFL of the honeybee *Apis mellifera*, a social hymenoptera that is related to *C. floridanus*, is quite well characterized and differs from the TTFL of *Drosophila* in major points (Rubin et al., 2006). Major clock genes of the fire ant *Solenopsis invicta* have been characterized and resemble the honeybee feedback loop (Ingram et al., 2012). Firstly, neither the honeybee nor the fire ant express homologues to *Drosophila's* CRY1 or TIM1, but an orthologue of the mammalian Cryptochrome 2 (CRY2), that is not blue-light sensitive (Rubin et al., 2006; Ingram et al., 2012). The absence of CRY1 and TIM1 in both organisms resembles the mammalian clock, where mCRY1/2 replaces Tim 1 as a binding partner for PER (reviewed in (Ko and Takahashi, 2006)) and represses CLK:BMAL 1 function in the form of a PER1/2:CRY1/2 heterodimer. CRY2 acts as a transcriptional repressor (Yuan et al., 2007) and cycles in phase with PER in both *A. mellifera* and *S. invicta* (Rubin et al., 2006; Ingram et al., 2012). It also expresses domains necessary for core translocation and transcriptional inhibition and seems thus a likely binding partner for PER in the honeybee and fire ant. Additionally, the roles of CLK and CYC in the two hymenopteran species seem to be more similar to the mammalian CLK and BMAL1, than to *Drosophila's* CLK and CYC. First, CLK is not expressed in a cyclic manner, but constitutively expressed (Rubin et al., 2006; Ingram et al., 2012) and lacks the C-terminal binding domain which is responsible for transcriptional activation. Second, *cyc* expression does oscillate in antiphase to *per* and the CYC protein features a C-terminal transactivation domain which can also be found in the mammalian orthologue BMAL1 (Rubin et al., 2006; Ingram et al., 2012). The roles of CLK and CYC are switched in comparison to *Drosophila*, like it is the case in mammals. Figure 3 sums up the current state of knowledge on hymenopteran feedback loops. Furthermore, the interlocked feedback-loop containing *vri*, *pdp1* and *cwo* in *Solenopsis invicta* is different from *Drosophila's* (Ingram et al., 2012). Whereas *cwo* is constitutively expressed in *Drosophila*, it cycles in phase with *cyc* and antiphase to *per* and *cry* in *Solenopsis*. *Vri* seems to cycle in phase with *clk*, while *pdp1* is apparently constitutively expressed. Whereas *vri* and *pdp1* expression have not been tested for oscillations in *A. mellifera*, *cwo* was found to cycle in foragers, but not nurses, roughly in phase with *cyc* in (Rodriguez-Zas et al., 2012). Expression of these genes is controlled by the CLK:CYC heterodimer and concretely by the binding of CLK to their E-Boxes in *Drosophila*, so the different expression might be due to the structural differences of CLK:CYC (Bloch et al., 2004). A comparison of the cycling of clock gene mRNA can be found in Figure 4. Another difference between the honeybee TTFL and that of *Drosophila* is the differential expression of PER in honeybee nurses and foragers. Whereas *per* mRNA and PER protein are cycling and show high expression levels in foragers,

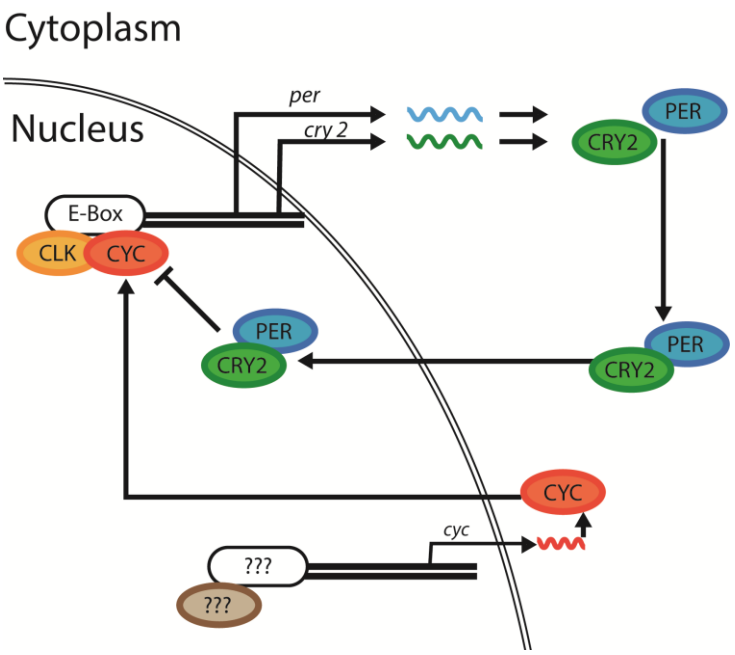

Figure 3: A schematic depiction of the hymenopteran feedback loops. Oval shapes represent proteins, curly lines mRNA and double lines DNA. A detailed description of the feedback-loops can be found in Chapter 1.3.2.2. Abbreviations: CLK =Clock, CYC =Cycle, PER = Period, CRY2 = Cryptochrome 2, ??? = unknown.

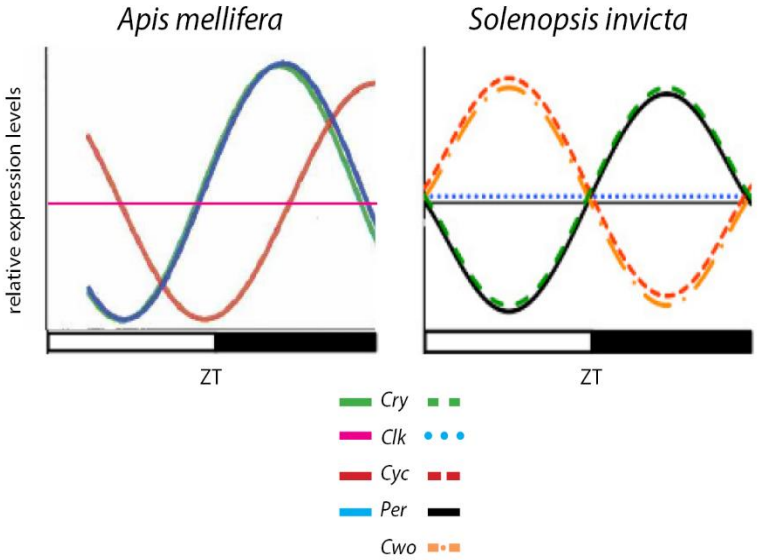

Figure 4: Clock gene mRNA cycling in *A. mellifera* and *S. invicta*. Detailed descriptions can be found in the text. Abbreviations: Cry =Cryptochrome, CLK = Clock, CYC = Cycle, PER = Period, CWO = Clockwork Orange. After (Rubin et al., 2006; Ingram et al., 2012)

which show robust circadian rhythms, the in hive-context arrhythmic nurses have either lower levels of per mRNA that show a weak cycling, or no *per* cycling at all (Toma et al., 2000; Bloch et al., 2001; Bloch et al., 2003; Bloch et al., 2004; Shemesh et al., 2007; Fuchikawa et al., 2017). Moreover, *cry* and *cyc* levels of nurses were also found to be attenuated when in contact to the brood (Shemesh et al., 2007). Still, the clock of nurses seems to be entrained and nurses removed from the brood show rhythmic behavior and clock gene cycling (Shemesh et al., 2010). These differences in *per* mRNA levels seem not be regulated by light, flight-experience or colony type, but related to development and task (Bloch et al., 2001; Bloch et al., 2004). Even though *per* mRNA levels seemingly do not cycle, or only weakly so, Fuchikawa et al. (2017) were able to show that protein levels of PER cycle in both, nurses and foragers, with a peak in the middle of the dark phase. This supports the hypothesis that behavioral rhythms can be uncoupled from a functional molecular clock and that the molecular clock can work in different ways in different organisms.

1.4 The anatomy of the circadian clock

The anatomy of the circadian clock has been characterized in a number of different insects, with *Drosophila melanogaster´*s again being one of the best characterized. The clock is divided into the central master clock, which resides in the brain, and several peripheral clocks in surrounding tissues, like the skin or gut.

1.4.1 The anatomy of the central clock in *Drosophila melanogaster*

*Drosophila melanogaster´*s central clock resides in the brain and consists of approximately 150 neurons, that express different clock genes, per hemisphere (reviewed in (Helfrich-Förster, 2005; Peschel and Helfrich-Förster, 2011)). These cells are necessary and sufficient for rhythmic locomotor activity (Kaneko and Hall, 2000; Hosokawa et al., 2011). They have been divided into seven major groups according to their anatomical location in the brain (reviewed in (Peschel and Helfrich-Förster, 2011)). Figure 5 depicts an overview of the groups of clock neurons of *Drosophila melanogaster*. These groups are not homogenous in clock gene, neuropeptide and neurotransmitter expression, hinting at functional division within the clusters. Three groups are located more dorsally, and thus termed Dorsal Neurons 1-3 (DN_1, DN_2, DN_3). They can be further sub-grouped by their size and expression patterns and consist of a total of approximately 58 cells, with the DN_3 being the largest group of approximately 40, the DN_1 being second with 16, and the DN_2 being the smallest, with only 2 cells. The other four groups of cell bodies are located more laterally and have thus been termed Lateral Neurons (LNs). They can be subdivided according to location and size into approximately 6 dorsal lateral neurons (LN_D), 2 lateral posterior neurons (LPN), 4 large ventro-lateral neurons (l-LN_V) and 5 small ventro-lateral neurons (s-LN_V). Additionally, a few hundred glial cells are also involved in the clock by expressing TIM and PER (reviewed in (Peschel and Helfrich-Förster, 2011)). All these groups have been shown to express the clock genes *per*, *tim*, *clk*, *cyc*, *vri* and *pdp1*, except for the LPN where only *tim* and *per* have been reported so far (reviewed in (Helfrich-Förster, 2005)). Of the main groups, all l-LN_V and 4 of the 5 s-LN_V express the neuropeptide Pigment-Dispersing Factor (PDF, see chapter 1.4.3-1.4.4). The only s-LN_V that does not express PDF is the so-called fifth s-LN_V, which is located more dorsally than the others (Helfrich-Förster, 2005). An antibody against this neuropeptide can be used to detect the whole arborization pattern of the pdf-positive fibers of the clock network. The fibers protruding from all clusters project towards the dorsal protocerebrum, where the neurosecretory center of the brain is located, except for

those of the l-LN$_V$ and the LPN (Helfrich-Förster, 2005; Helfrich-Förster et al., 2007b). Fibers protruding from the LPN could not be stained yet. Additionally, the LN$_D$, s-LN$_V$, l-LN$_V$, DN$_1$ and DN$_3$ all send fibers towards the accessory medulla (Helfrich-Förster, 2005; Helfrich-Förster et al., 2007b) which is regarded as the main pacemaker center of many insects) (Helfrich-Förster et al., 1998). A more detailed description of the accessory Medulla can be found in 1.4.3.3. Fibers from the l-LN$_V$ also project into the optic lobes and arborize on the surface of the medulla, as well as travelling towards the other hemisphere´s accessory medulla. The l-LN$_V$ thus seem to be relevant for mediating light input from the eyes as well as for the coupling of the clock neurons in both hemispheres (Helfrich-Förster, 2005; Helfrich-Förster et al., 2007b). A more detailed description of the network revealed by PDF can be found in chapter 1.4.3.

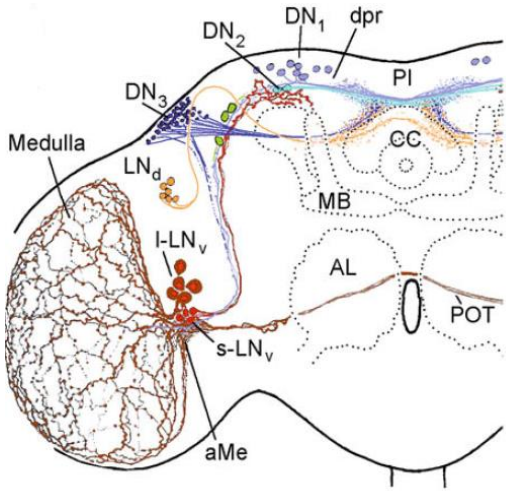

Figure 5: The anatomy of *D. melanogaster´s* clock. Abbreviations used: aMe = accessory medulla; AL= antennal lobe; MB = mushroom body; CC = central complex; dpr = dorsal protocerebrum; PI = pars intercerebralis; DN1 = Dorsal Neurons 1; DN2 = Dorsal Neurons 2; DN3= Dorsal Neurons 3; LNd= dorsal lateral Neurons; s-LNv= small ventral lateral Neurons; l-LNv= large ventral lateral Neurons; POT = posterior optic tract. The PDF-network and PDF expressing cell clusters are depicted in red. After (Helfrich-Förster, 2004)

1.4.2 The anatomy of the central clock in *Apis mellifera*

Though not as well characterized as the fruit fly *Drosophila melanogaster*, the honeybee`s central clock has also been the subject of anatomical studies. Especially the distribution of PER-positive cells and the PDF-network have been extensively studied (Bloch et al., 2003; Závodská et al., 2003; Fuchikawa et al., 2017). Though Závodská et al. (2003) found only three PER-positive cells in the lateral part of each hemisphere, (Bloch et al., 2003) already reported two distinct clusters of PER cells. These clusters are the four anterior PER-ir lateral neurons (APER-L) in the pars lateralis of the protocerebrum, between the pedunculus and the calyces of the mushroom bodies, and the two deep PER-ir lateral neurons (DPER-L) located more posteriorly between the mushroom body calyces. (Fuchikawa et al., 2017) were later able to show that even more PER-positive cells can be found in the bee brain. Figure 6 gives an overview of the location of PER-positive clusters in the brain. Four distinct clusters of neurons

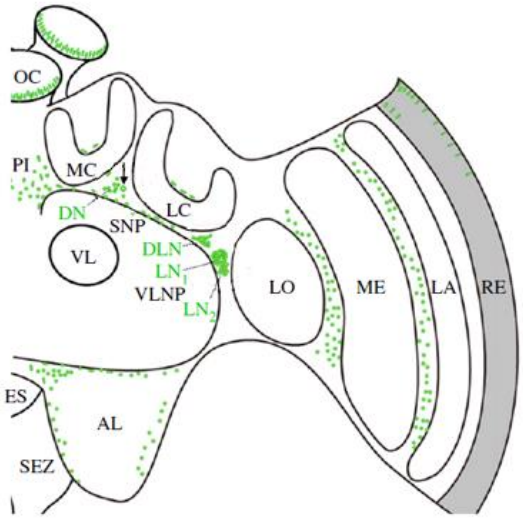

Figure 6: The location of Per-positive cell clusters in the honeybee-brain. Abbreviations: AL= antennal lobe; ES = esophageal foramen; LA= lamina; LO = lobula; LC= lateral calyx; MC = median calyx; ME = medulla; OC = ocelli; PI = pars intercerebralis; RE = retina; SEZ = subesophageal zone; SNP = superior neuropils; VLNP= ventrolateral neuropils; VL =n vertical lobe; DN= Dorsal Neurons; DLN = Dorsolateral Neurons; LN_1 = Lateral Neurons 1, LN_2 = Lateral Neurons 2. All Per-positive neurons are depicted in green, a description can be found in the text. After (Fuchikawa et al., 2017).

were observed and named according to their location, 105-120 cells located between the anterior ventrolateral protocerebrum and the optic lobes were termed lateral neurons 1 (LN_1), a second cluster of approximately 15 cells just ventrally of the LN_1 lateral neurons 2 (LN_2). Furthermore, a cluster of 60-75 neurons was located dorsally of the LN and spread from anterior to posterior, the dorsal lateral neurons (DLN). A last distinct cluster of 15 cells was found in the dorsal protocerebrum between the medial and lateral calyces, the dorsal neurons (DN). Also, a large number of nuclear stained cells was found in various locations in the cell body layer of the antennal lobes, as well as in the optic lobes. AmPER-ir cells in the optic lobes were concentrated mainly between the lobula and the medulla and between the medulla and the lamina. More nuclei were found above the calyces, in the compound eyes, in the ocelli and along a line passing ventrally to calyces of the MB, just above the dorsal protocerebrum. Lastly, two cells that might be the DPER-L were cytoplasmatically, but not nuclearly stained. Of these cells, only the LN_2 cluster showed cytoplasmatic co-expression of PDF (Fuchikawa et al., 2017). Though (Závodská et al., 2003) and (Bloch et al., 2003) had also found 10 to 20 PDF-positive cell bodies per hemisphere, they were not able to find co-localized PER in these cells. The PDF-network of the honeybee also features an accessory medulla, innervations in the optic lobes and the protocerebrum (Beer, accepted), and will be discussed in detail in chapter 1.4.3.4.

1.4.3 The PDF-network

1.4.3.1 The Pigment-Dispersing Factor

The pigment-dispersing hormone (PDH) is a octadecapeptide that was first reported to play a role in control of integumental color change and eye pigment movements in crustaceans (reviewed in (Rao, 2001)). Together with the octapeptide red pigment-concentrating hormone (RPCH), it belongs to the pigmentary effector-hormones of crustaceans, and can be subdivided into α- and β-PDH, which differ in six aminoacids. The β-PDH is the major form found in the eyestalks of *Uca pugilator*. Dircksen et al. (1987) used a glutaraldehyde conjugate of synthetic PDH of *Uca pugilator* to immunize rabbits and thus produce an antiserum against β-PDH. This antiserum is able to stain insect-homologues to PDH, for example in *Drosophila melanogaster* (Helfrich-Förster and Homberg, 1993; Park and Hall, 1998), *Leucophea maderae* (Stengl and Homberg, 1994) or *Apis mellifera* (Bloch et al., 2003; Závodská et al., 2003). This homologue has been called Pigment-Dispersing Factor, due to its ability to disperse pigments in crustacean chromophores (Dores and Herman, 1981; Rao, 2001). Insect PDF, just as its homologue PDH, is a neuropeptide consisting of 18 aminoacids with conserved endings, partly conserved residues and a high sequence similarity (reviewed in (Rao, 2001). In endogenous clocks, neuropeptides are mostly employed in signal transduction (Maywood et al., 2006; Nässel and Homberg, 2006), relaying input to the clock as well as information to the output regions of the brain (Helfrich-Förster, 2005). Genetically coded precursorproteins of neuropeptides are synthesized in the cytoplasm and may give rise to different neuropeptides, which are then stored in vesicles, transported to their release sites and released by fusion of the vesicles to the membranes of synapses or varicosities (Nässel and Homberg, 2006). It has been shown for *Drosophila melanogaster* (Miskiewicz et al., 2004; Miskiewicz et al., 2008) and *Leucophea maderae* (Reischig and Stengl, 2003b) that PDF is stored in densecore vesicles and released in a paracrine fashion from the varicosities. PDF levels change in a cyclical manner in the terminals of the s-LN_v, and it seems to be released rhythmically under control of the clock (Park and Hall, 1998; Blau and Young, 1999). The PDF-receptor, which binds PDF at its target membrane, has been identified as a G-protein-coupled receptor (GPCR) belonging to the classical hormonal receptors (Hyun et al., 2005; Lear et al., 2005; Mertens et al., 2005). Binding of PDF to its receptor leads to activation of an adenylate cyclase and a rise in cAMP levels (Hyun et al., 2005; Mertens et al., 2005; Nässel and Homberg, 2006). PDF-receptors in the brain of *Drosophila* can be found on the s-LN_v, not or only in low abundance on the l-LN_v and about half of the non-PDF expressing clock neurons, as well as on some non-circadian, non-neuronal cells in the visual system of *D. melanogaster* that seem to be targeted by the l-

LN_vs (Im and Taghert, 2010). To end PDF signaling, the neuropeptide is either degraded or internalized with the receptor (Nässel, 2002).

Ectopic expression of PDF in the dorsal brain alters behavioral rhythms (e.g. to hyperactivity or arrhythmicity) in *Drosophila melanogaster* (Helfrich-Förster et al., 2000), whereas injections in *Leucophea maderae'*s accessory medulla lead to a phase shift of activity rhythms (Petri and Stengl, 1997), hinting at a role of PDF in output as well as input of the clock. PDF seems to stabilize TIM (Seluzicki et al., 2014) and PER (Li et al., 2014), and also influences PER levels together with CRY (Cusumano et al., 2009; Im et al., 2011).

1.4.3.2 The PDF-network in *Drosophila melanogaster*

In *Drosophila*, the PDF expressing cells are the four l-LN_v and four of the s-LN_v, while the fifth s-LN_v is PDF negative (Helfrich-Förster and Homberg, 1993; Helfrich-Förster, 1995; Kaneko et al., 1997). A depiction of the PDF-fiber network in *Drosophila melanogaster* can be seen above, in Figure 5 (Chapter 1.4.1). They are located at the anterior base of the medulla (Helfrich-Förster and Homberg, 1993). The s-LN_v project ipsilateral into the central accessory medulla (aMe) and the dorsal protocerebrum, where they terminate in close proximity to the DN_2 and the mushroom body calyx (Helfrich-Förster et al., 2007a). The PDF fibers arising from the l-LN_v on the other hand, form a thick bundle, which runs towards the ipsilateral accessory medulla, and thickens there (Helfrich-Förster et al., 2007a). From this bundle, several fibers split off and invade the central accessory medulla, and arborize on the ipsilateral surface of the medulla (Helfrich-Förster, 1997; Helfrich-Förster et al., 2007a). A number of thin fibers separate from the large fibers to form the ventral elongation of the accessory medulla, which travels ventrally before turning posteriorly and extending to the posterior surface of the medulla in the serpentine layer, where it approaches the varicose fibers on the distal surface of the medulla (Helfrich-Förster et al., 2007a). Another part of fibers originates from the bundle and enters the posterior optic tract (POT), travelling towards the contralateral accessory medulla. In the POT, the fibers tend to fasciculate, but they split up into two bundles before invading the central contralateral accessory medulla and arborizing on the surface of the contralateral accessory medulla. The fibers originating from the l-LN_v of both hemispheres contribute equally to the arborizations on the surface. In summary, the fibers arising from the l-LN_v contribute to the arborizations on the anterior surface of the ipsi- and contralateral medullae, but only the ipsilateral ventral elongation of the accessory medulla (Helfrich-Förster et al., 2007a).

1.4.3.3 The PDF-network in *Leucophea maderae*

Another insect with a very well characterized clock network is the cockroach *Leucophea maderae.* Lesion experiments have proven that its clock is located in the accessory medulla, a small neuropil located in the ventral region between lobula and medulla (Petri et al., 1995; Reischig and Stengl, 2003a). The accessory medulla of the cockroach has been characterized as a pear-shaped neuropil at the base of the proximal anterior part of the medulla (Reischig and Stengl, 1996; Reischig and Stengl, 2003b), which consists of a shell, a core and an anterior neuropil that is connected to the shell neuropil. It is associated with approximately 300 cells, of which approximately 20 express PDF (Petri et al., 1995; Reischig and Stengl, 1996; Reischig and Stengl, 2003b). Other neuropeptides that have been identified in the densecore vesicle packed accessory medulla are allatostatin, allatotropin, corazonin, gastrin/cholecystokinin, leucokinin (Petri et al., 1995), FMRFamid related peptides (Petri et al., 1995; Sohler et al., 2007; Soehler et al., 2008), baratin (Nässel et al., 2000), several myoinhibitory peptides (Schulze et al., 2012) and orcokinin. Thus, peptide-based neuromodulation seems to play an important role of the workings of the accessory medulla as central clock.

Figure 7 depicts a reconstruction of the PDF-network in *Leucophea maderae*. The 20 PDF cell bodies in the accessory medulla can be split into the 12 anterior PDF medulla neurons (aPDFMe) and 8 posterior PDF medulla neurons (pPDFMe), which can be sub-grouped according to their size, location and staining intensity (Wei et al., 2010). The aPDFMe consist of three groups of four cells each, large and intense (containing one very large and intense stained cell), medium and less intense and small and faint, the pPDFMe of two groups of five large and intense and three smaller and faint stained cells. Additionally, two clusters of approximately 50-70 somata can be found proximal of the posterior edge of the lamina, the dorsal and ventral lamina neurons (dPDFLa, vPDFLa). These somata project primarily to the first optic chiasma. (Wei et al., 2010) provides a comprehensive overview of the complete network revealed by PDF-staining.

All PDF-somata contribute to the fibre-network in the accessory medulla. The aPDFMe link the aMe to the lamina and medulla of both optic lobes through the anterior fiber fan in the most distal layer of the medulla, and the median layer fiber system of the medulla. Some fibers from the anterior fiber fan run perpendicularly into a median layer to arborize there, while others cross the first optic chiasma to innervate the lamina. They run anteriorly across the proximal edge of the lamina to form a dense fiber network, as well as entering the distal lamina. Several large fibers from the ipsi- and contralateral aMe run posterior to the aMe in the lobula valley

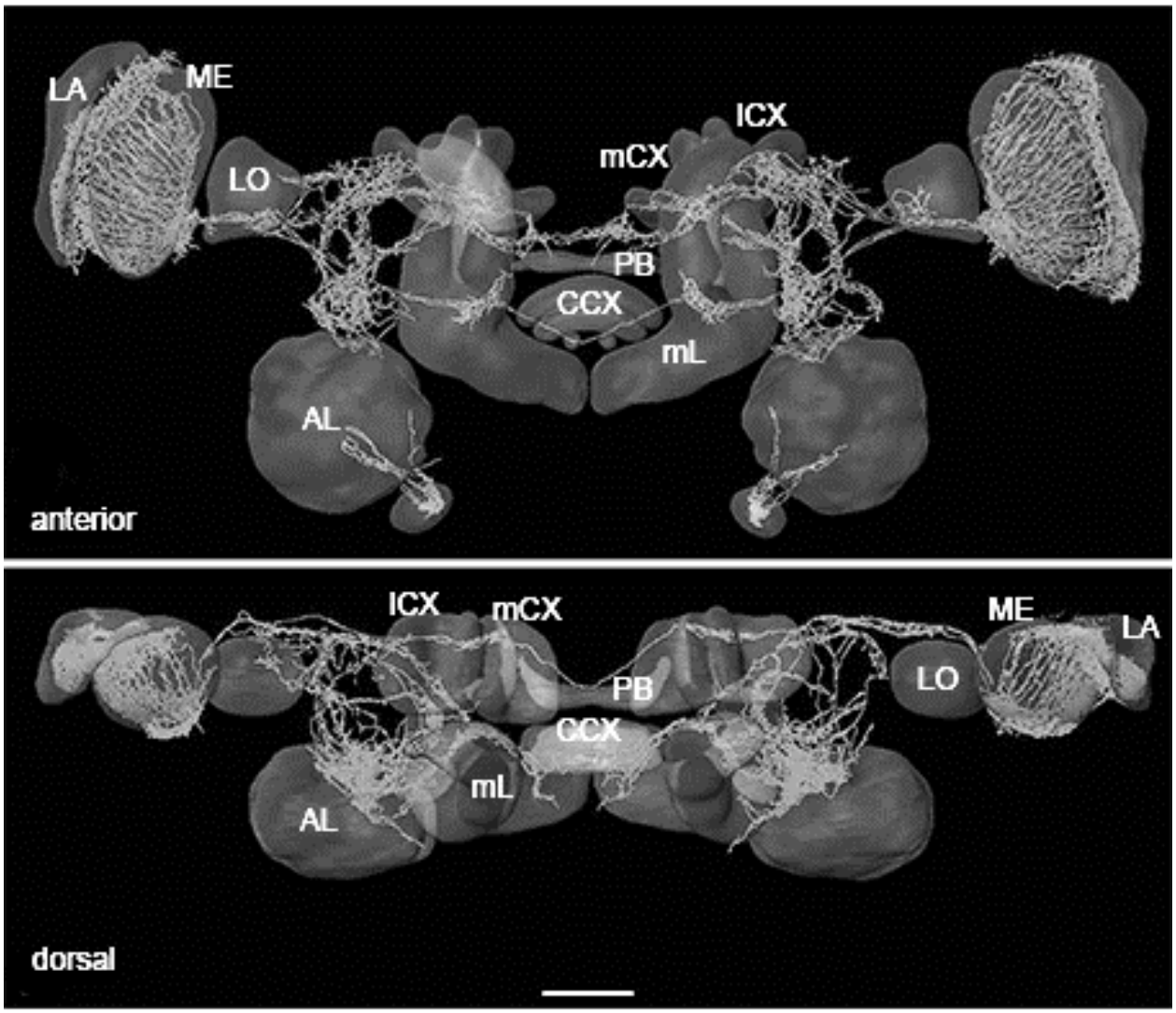

Figure 7: A reconstruction of the PDF network of *Leucophea maderae*. Abbreviations: AL = antennal lobe; CCX = central complex; LA= lamina; LO = lobula; lCX= lateral calyx; mCX = median calyx; mL= median lobe; ME = medulla; PB = protocerebral bridge. PDF-fibers are depicted in orange. A detailed description can be found in the text. After (Wei et al., 2010)

tract (LVT), fasciculate und form a dense bundle running along the posterior surface of the lobula. This bundle bifurcates between the lobula and the distal median protocerebrum, splitting into the anterior optic commissure (AOC) and posterior optic commissure (POC). A small plexus, which is directly linked to the accessory medulla by a fiber running through the lobula, can be found near the bifurcation site. Four to six fibers form the AOC, crossing the midline of the brain and giving rise to several plexi and arborization sites. The AOC bypasses the mushroom body peduncle anteriorly and arborizes between the peduncle and the vertical lobe. Some fibers of this arborization site reach towards the anterior fiber plexus (AFP, see below), some others travel further towards the midline, arborizing in a second site in the superiomedial

protocerebrum, medial of the vertical lobe, and merging with the main strand of fibers. Three plexi rise from the main branches of the AOC, a first one next to the plexus near the lobula, a second one near the first arborization site and a third one between those two. All plexi form overlapping arborization anterio-posteriorly, in the superior lateral protocerebrum (SLP). The second main strand of fibers originating from the bifurcation, the POC, connects both accessory medullae. It innervates the posterior optical tubercles (POT-u) posterior of the medial lobe of the mushroom bodies, and also some smaller plexi and a large arborization site. The smaller plexus is located between the first plexus and the POT-u. It gives rise to several fibers travelling parallel to the POC and connects it to the POT-u. Two fibers from the first plexus travel towards this plexus. One extends into it, the other projects anteriorly through the inferior lateral protocerebrum (ILP) and the ventrolateral protocerebrum (VLP), giving rise to the anterior fiber plexus (AFP) lateral to the vertical lobe of the mushroom body. The fibers in the AFP ramify extensively, extending towards the frontal surface of the protocerebrum and forming a layer lateral of the vertical lobe. Additionally to the fibers from the first arborization site, the AFP is innervated by two fibers, originating from one fiber in the accessory medulla that runs anteriorly through the lobula, bifurcates and enters the AFP. Furthermore, some fibers from an unidentified soma can be found in the tritocerebrum (Wei et al., 2010). Thus, the PDF-network of the cockroach is similar to that found in the fruit fly, connecting the accessory medullae of both hemispheres with each other as well as with the optic lobes and the central brain.

1.4.3.4 The PDF-network in *Apis mellifera*

The closest related species to *Camponotus floridanus* whose PDF-network has been characterized is the honeybee *Apis mellifera*. First descriptions can be found in (Závodská et al., 2003), where 10 PDF-positive somata were found at the base of the optic lobe and fibers were reported in the protocerebrum, deutocerebrum and subesophageal ganglion. (Bloch et al., 2003) published a more detailed description in the same year, reporting the number of somata to be 20 per hemisphere, which were not co-localized with Per. Projections of fibers in the optic lobes were found in the lamina, tangential to the serpentine layer of the medulla and in the lobula. The fibers entering the medulla were reported to enter via Cuccati`s Bundle, which was described for *Drosophila* in (Fischbach and Dittrich, 1989). In the protocerebrum, a number of fibers travelled as an anterior commissure along the dorsal boundary of the superior protocerebrum below the calyces and between the vertical lobes of the mushroom bodies (Bloch et al., 2003). Varicose PDF fibers were reported for the lateral margin of the protocerebrum and around the cells of the pars intercerebralis. Moreover, fibers could be found

in the ventrolateral protocerebrum but not entering the optic tubercles, in a posterior plexus between the medial lobe of the mushroom bodies and the dorsal margin of the deutocerebrum and in a posterior tract linking the two optic lobes. The fibers entering the anterior and posterior commissures as well as those in the optic lobes were reported to derive from a tract similar to the LVT described in the cockroach (Reischig and Stengl, 2002; Bloch et al., 2003). Moreover, many fibers were detected around the central complex. (Beer, accepted) recently provided an even more elaborate description of the network. Esther Kolbe, a co-author of Beer (accepted) provided a 3D-reconstruction of the honeybee PDF-network in her Doctoral Thesis, which can be found in Figure 8 (Kolbe, 2014). These authors not only found approximately 15 PDF-positive somata proximal to the medulla, those somata also belonged to the LN_2 cluster co-expressing the PER protein. A small neuropil in front of the medulla is innervated by PDF and might be a homologue to the accessory medulla of other insects (Beer, accepted). The LVT-like structure described in (Bloch et al., 2003) was also decribed in Beer (accepted). Fibers on the surface of the lobula are reported to turn posteriorly into a tract connecting the aMe with the protocerebrum and the ipsi- and contralateral hemispheres. A very conspicuous feature of the *Apis mellifera* LVT is the so-called loop, a structure formed after the fibers reach the posterior rim of the lobula, in which they turn back to the anterior lobula and disperse into smaller fibers innervating the protocerebrum. Fibers running into the posterior optic commissure (POC) leave or enter the LVT just before this loop, other fibers from the ventral protocerebrum join the loop. The fibers in the distal medulla leave the medulla mostly at the distal and ventral rim area, travelling towards the lamina. Additional to this innervation of the medulla, a loose fiber fan is stretched over the anterior surface of the medulla, innervating the proximal medulla and the distal medulla in its most dorsal region. The network in the protocerebrum described in Beer (accepted) is similar to that of Bloch et al. (2003). A huge number of fibers forms a dense network on the surface of the protocerebrum, with a very prominent tract in the dorsal protocerebrum, between the vertical lobes and the mushroom body calyces (Beer, accepted). Two PDF fibers were found to leave the bundle between the medial and lateral calyx and cross towards the posterior protocerebrum, running close to the PER-positive DN. Some of the fibers running medially between the vertical lobe and calyces run into the median bundle, while others form an anterior dorsal commissure running to the contralateral hemisphere. A part of the fibers in the median bundle innervate the antennal lobes ventroposteriorly, not entering the glomeruli. Posterior to the antennal lobes, fibers also enter the tritocerebrum by surrounding the oesophageal foramen. The anterior optic tubercles, though surrounded by PDF fibers, are not innervated. A second anterior commissure is found

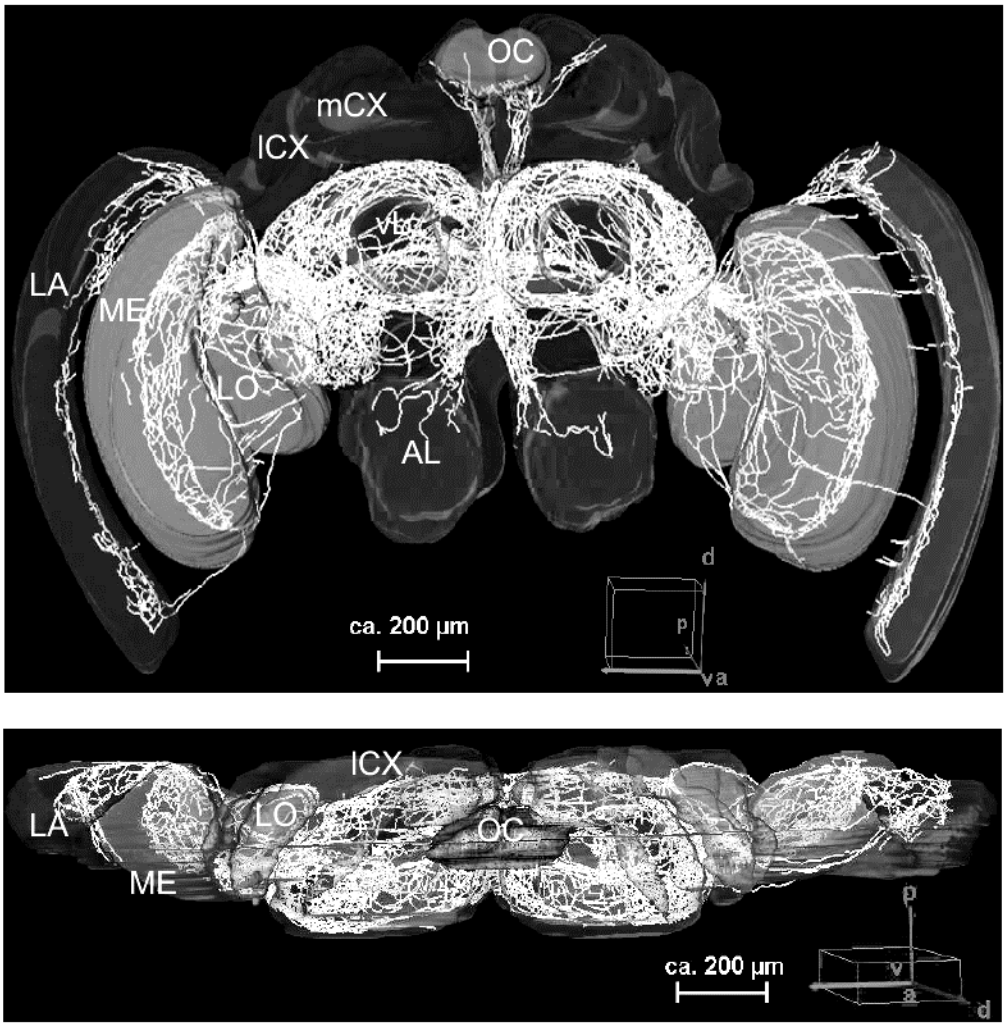

Figure 8: The PDF network in *Apis mellifera*. Abbreviations: AL = antennal lobe; LA= lamina; LO = lobula; lCX= lateral calyx; mCX = median calyx; mL= median lobe; ME = medulla; OC = ocelli; vL = verticall. PDF-fibers are depicted in white. A detailed description can be found in the text. After (Kolbe, 2014).

ventrally of the ventral lobes of the mushroom bodies. In the medial brain, fibers originating from the surface and the LVT form a ring-like structure around the vertical lobe and the peduncle, as well as a triangle behind the medial lobes of the mushroom body. The dorsal and ventral double commissures are a part of this triangle and arborize anterior and posterior of the central complex, not innervating but closely surrounding it. A last commissure stemming from the LVT is the posterior optic tract (POC), connecting the PDF neurons of both hemispheres and running posterior of the double commissures of the triangle. A number of fibers from the POC run dorsally innervating the ocelli, others innervate the Posterior Optic Tubercles (POTUs) or arborize closely to the protocerebral bridge (Beer, accepted). In summary, the network in the honeybee shares many similarities with the PDF-network of the cockroach and fruit flies, but deviates in others, such as the number of fibers and arborizations.

1.5 Study Aims

This study aims to provide first insights into the workings of the circadian clock of the worker-caste of the Carpenter Ant *Camponotus floridanus*. Three aspects of the clock have been examined: endogenous rhythmic behavior in response to light, oscillations of components of the molecular feedback loop and the anatomy of the central clock in the brain.

The first aspect, endogenous rhythmic behavior, was tested in the form of locomotor behavior. To verify whether an entrainable clock was involved in locomotor output, the ability to entrain to different LD phases (8:16, 12:12, 16:8) as well as the persistence of rhythmic behavior under constant conditions (constant darkness) was tested. Two different temperatures were used to check for temperature compensation and other effects of temperature on locomotor behavior.

The second aspect, oscillations of components of the molecular feedback loop, was examined by evaluating the changes of PER protein in the brain throughout the day. PER-positive cells were stained immunohistochemically and the staining intensities at different timepoints served as an approximation of the daily change in protein concentration levels.

The third aspect, anatomy of the central clock, was examined in two facets, the location and properties of the PER-positive cell clusters, and the patterns of the PDF-network and its connected cell-bodies. The data on PER was gained from experiments on its protein level cycling, additional PDF labelling of these brains provided insights on the spatial relationships of PER and PDF. Further PDF staining in minor and major brains was used to reconstruct the PDF-network and compare the networks of the two size-castes with each other and to other insects.

2. MATERIAL AND METHODS

2.1 Experiments:

All experiments conducted for this thesis were conducted at the University of Würzburg with workers of the Carpenter Ant *Camponotus floridanus* and can be found in the table below.

Table 1: Content of experiments

Experiment	Components	Colony
Preliminary tests for Experiment 2,3&4	Conducted before thesis by Pamela Menegazzi and I, Test staining and protocol optimization	C79
Experiment 1	Locomotor recordings at • LD12:12 (25°C) • LD 8:16 (25°C) • LD 16:8 (25°C)	C79
Experiment 2	Locomotor recordings at • LD12:12+DD (25°C) • LD12:12+DD (30°C)	C79
Experiment 3	Locomotor recordings at • LD12:12+DD (25°C) • LD12:12+DD (30°C)	C152
Experiment 4	Staining of wholemount brains of minor and major workers with PDH/SYN	C152
Experiment 5	Staining of sections of minor and major worker brains with PDH/HRP	C152
Experiment 6	Staining of wholemount brains of minor workers with PDH/PER	C79
Experiment 7	Staining of wholemount brains of minor workers with PDH/PER	C90

2.1.1 Locomotor behavior in response to light at different temperatures

To establish whether entrainment by light was possible for *C. floridanus*, in Experiment 1, the locomotor behavior of individuals of Colony C79 was tested at different light-dark ratios at the same temperature. Further characteristics of the circadian clock (free-run in constant conditions, period length, temperature compensation) were established in Experiment 2 (C79) and 3 (C152), where individuals were also recorded in constant darkness, after they had been entrained to a LD 12:12 hour day at either 25°C or 30°C. For experiments 1 and 2, the feeding devices by Steffi Mildner and Flavio Roces were used (Mildner and Roces, 2017), for Experiment 3 new feeding devices were designed. Experiments 1 and 2 also served to establish the optimal experimental parameters for pre-entrainment, entrainment and constant phase, as well as feeding and duration of the phases. After the unfortunate death of the queen of Colony C79, Experiment 3 was performed with Colony C152. Following the conclusion of the experiments, live ants were released back into the mother colony.

2.1.2 The PDF-network in minor and major workers of *Camponotus floridanus*

To fully characterize the anatomical properties of the PDF-network in minor and major ants of *C. floridanus*, staining on wholemount brains (Experiment 4) and sections of brains (Experiment 5) collected at ZT 4 from the mother colony C152 was performed. The staining protocols were optimized by Pamela Menegazzi before I started the work on my doctoral thesis and additionally by me during my Bachelor and Master internships. Brains for Experiment 4 and 5 were stained with the anti-PDH antibody of Heinrich Dircksen (Dircksen et al., 1987), kindly provided by him. This polyclonal antibody, though raised against crustacean pigment dispersing hormone, stains the Pigment-Dispersing Factor (PDF) in numerous insects, and also this ant. In Experiment 4, anti-Syn, the monoclonal antibody 3c11 from the Hofbauer-Buchner Hybridoma Library, which recognizes the Synapsin (SYN) protein and thus labels all synaptic endings, was used to stain all surrounding neuropils. Confocal scans of the stained brains were used to generate a 3D-reconstruction of the PDF-network and the neuropils of the brain.

Additional staining on sections of brains was produced to verify the 3D reconstructions (Experiment 5). The antibody Cy™3 AffiniPure Goat Anti-Horseradish Peroxidase (Jackson ImmunoResearch, # 123-165-021) was used for neuropil staining in this experiment. It labels all membranes and thus also reveals the neuropils of the brain.

Additionally, PDF-staining from Experiments 6 and 7 (see below) was evaluated for number of PDF-somata at different time points.

2.1.3 The localization and cycling of the Period protein in *C. floridanus*

To establish whether PDF and PER co-localize in the ant brain, and whether PER staining intensities varied throughout the day, staining of brains of nocturnal minor individuals of *C. floridanus* was performed. Entrained ants were collected from monitors at the ZTs 0, 3, 6, 9, 12, 15, 18 and 21 (Experiment 6) and the ZTs 0, 6,12 and 18 (Experiment 7). The PER antibody used is the polyclonal anti-Period antibody, which is raised against a part of the period protein in rabbits (Fuchikawa et al., 2017) and was kindly provided by Eva Winnebeck. Confocal scans of Experiment 6 were evaluated qualitatively and quantitatively for the location of cell clusters and number of cells per cluster at ZT 0 and 3. After the categorization of clusters, the staining intensity of PER cells in Experiment 6 and 7 was established for all timepoints.

2.2 Animal rearing:

Minor and Major workers of the species *Camponotus floridanus* used for this dissertation were provided by the Department for Zoology II, situated in the Biocenter of the Julius-Maximilians-University Würzburg. The founding queens of the colonies were captured on the Orchid Islands, Florida on 30.08.2001 (C79 and C90) and 09.07.2002 (C152), and reared in artificial plaster nests in an ambient-controlled room in Würzburg. The colonies are kept in plastic boxes with fluon-coated walls, containing plaster nests, at an ambient temperature of 25°C, relative humidity of 50% and twelve hours of illumination daily (LD 12:12, light phase from 6.00 a.m. to 6.00 p.m., CET, 300lux). Colonies were fed with water, diluted honey and freshly killed cockroaches ad libitum. Ants used for the experiments were taken randomly from all areas of the nest. Minor and major workers were distinguished by eye, since body size was very different (see (Simola et al., 2016)). Only ants of the lowest and highest range of body size were used, to avoid mislabeling of morphological caste. This study complies with the ethical guidelines of the country where the research was carried out.

2.3 Monitoring of Locomotor Behavior:

Locomotor behavior of minor individuals of *Camponotus floridanus* in response to light and temperature was monitored in social isolation in TriKinetics LAM monitors. Minor ants were selected randomly from the colonies C79 or C90 (Experiments 1,2,6,7) or C152 (Experiments 3,4,5) and pre-entrained to the LD cycle as a subcolony (see 2.3.1). After pre-entrainment, ants were transferred to monitors and monitored individually in a light-dark-cycle (LD) at constant temperature and humidity (see 2.3.2). After the LD phase, they were either released from the

monitor (Experiment 1) monitored in ensuing constant darkness and then released (Experiments 2,3) or sacrificed for staining of the brain (Experiments 6,7).

2.3.1 Pre-entrainment in sub-colonies

The pre-entrainment of ants in subcolonies was performed to minimize stress and ensure acclimatization to the new environment before monitoring started. Ants were taken randomly from their colonies and put in plastic boxes (19.9x19.9x9.3cm) with fluon coated walls and lids with ventilation holes. Sugar water (5%) was offered *ad libitum*. Boxes were placed inside an incubator (see 2.9) with controlled lighting (LED-strips, IKEA, 300lux) and temperature. Humidity was controlled with bowls of saturated saline-solution and monitored with an environmental monitor, to ensure relative humidity between 50-60%. The light-cycle was chosen according to the experiment, temperature and humidity stayed constant throughout pre-entrainment. See point 2.3.5 for length of pre-entrainment.

2.3.2 Entrainment in TriKinetics LAM (LD-phase)

After Pre-entrainment, single ants were transferred to glass-tubes (10x1.6cm), which were stoppered with feeding devices (see 2.3.3 Feeding) at each end, with a pair of live animal forceps. These glass tubes were then set into the TriKinetics Locomotor Activity Monitors (LAM; TriKinetics, Waltham, MA) monitors used for recording activity (see 2.3.4 Activity Recording) and secured with rubber bands, to minimize sliding and thus disturbing the animals. The monitors were transferred back into the incubator used for pre-entrainment, keeping the pre-entrainment conditions indicated in 2.3.5 Monitoring Protocols. See Table 2 in chapter 2.3.5 for the length of the Entrainment/LD-phase.

2.3.3 Feeding

Ants were fed on both ends of the glass tubes. The feeding devices used for Experiment 1, 2, 6 and 7 were those described by Stephanie Mildner and Flavio Roces in (Mildner and Roces, 2017) and can be seen in Figure 9A,B. They consist of a plastic capsule, containing a sponge for sugar water, which is connected to a mesh wire ring for air ventilation which is plugged into the glass tube. A wider mesh separates the sponge from the mesh ring, so ants can drink but not crawl into the sponge. These feeding devices were refilled with a syringe at least every second day, to ensure they stay humid at all time and animals do not desiccate. Though they were easy to handle and well suited for collecting animals from the monitors individually, novel

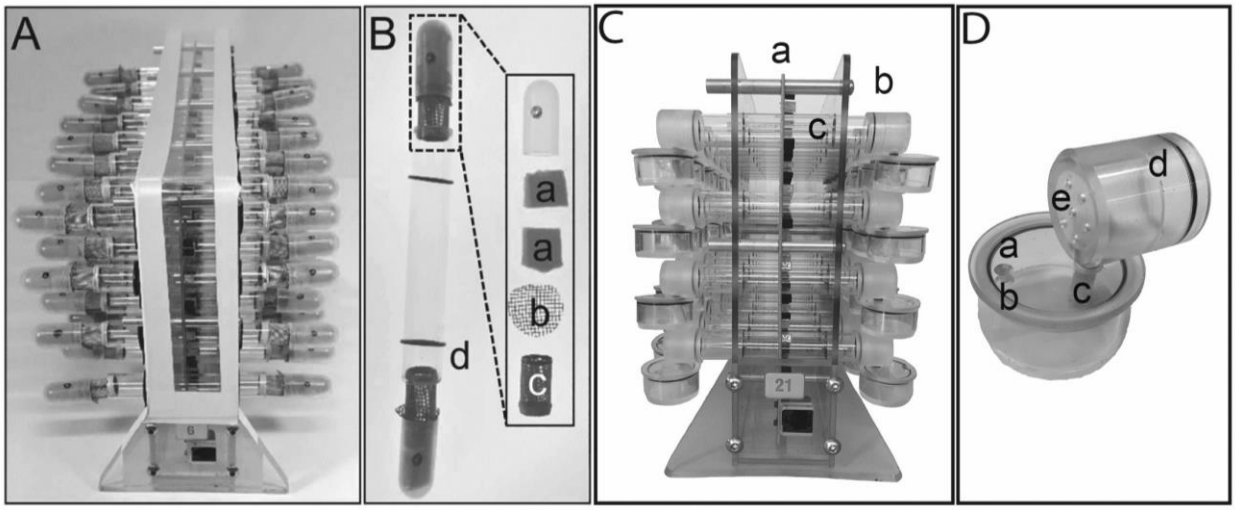

Figure 9: The feeding devices. A,B) The Mildner -Roces Devices, pictures after (Mildner and Roces, 2017) C,D) The new Devices A) The Mildner-Roces devices in use in a LAM-Monitor. B) The design of the devices, a) sponge b) mesh grid c) mesh wire ring d) glass tube. C) The new devices in use in a LAM monitor. a)Platine holding the infrared lights b) feeding device c)Glass tubes D)The design of the devices, a) reservoir b) Refilling-Hole c) Sponge d) Capsule e) Ventilation Holes.

devices were designed for Experiment 3 for two reasons: First, survival was sometimes low with these feeding devices (reasons unclear), resulting in difficulties when recording over longer time-periods. Second, these devices had originally been designed to facilitate pulse-like feeding, leading to a small volume of food-storage and thus resulting in frequent disturbances by opening the incubator and refilling the device. Because of this, the new feeding devices depicted in Figure 9D,E were designed. These feeding devices consist of a larger reservoir (3x1.5cm) made of plexi-glass, which is connected to a Plexiglas capsule with ventilation holes that plugs onto the glass-tube. A piece of sponge is stuck through the screw thread connecting reservoir and plug, sucking up the sugar water in a torch-like fashion. The volume of sugar-water that can be held by this reservoir is approximately 5ml, thus elongating the feeding schedule from every two days to every seven days.

2.3.4 Monitoring Protocols

In Table 2, the individual number of days in Pre-entrainment, Entrainment and Constant Conditions, as well as the colony the tested animals originated from, the temperature at which the experiment was conducted, and the length of the light and dark phase in hours, can be found, sorted by experiment. The humidity was kept constant in all experiments (~50-60% rH).

Table 2: Conditions and parameters of the Experiments

Experiment	Colony	LD	Pre-entrainment	Entrainment (LD-Phase)	Constant Darkness	Temperature
Experiment 1	C79	8h:16h	1 day	10 days	-	25°C
Experiment 1	C79	16h:8h	1 day	10 days	-	25°C
Experiment 1	C79	12h:12h	1 day	7 days	-	25°C
Experiment 2	C79	12h:12	1 day	4 days	10 days	25°C
Experiment 3	C152	12h:12h	7 days	8 days	12 days	25°C;30°C
Experiment 6	C79	12h:12h	1 day	5 days	-	25°C
Experiment 7	C90	12h:12h	1 day	5 days	-	25°C

2.3.5 Activity Recording

Locomotor activity was recorded using a TriKinetics Locomotor Activity Monitor (LAM). These monitors consist of a platine with holes, referred to as channels, for the glass-tubes described above, surrounded by three infrared beam-arrays. Each platine can hold up to 32 glass-tubes, and records disturbances of the infrared beam of each channel. The data collected from the beam-crosses of the animals, in this case the ants, is then periodically uploaded to a connected computer und stored in the form of numeric data in a text-file by the DAM-System Collection Software (TriKinetics; Waltham, MA). This text-file contains all channels of the monitor and the number of beam crosses for each channel binned per minute and assorted by date and time.

2.3.6 Data analysis

The data generated by the DAM-Collection Software was used to visualize and analyze different aspects of circadian behavior, like average days and period length, and general information on the animals, like survival and distribution of activity types.

2.3.6.1 Actograms

As a first step, Actograms were generated using the ActogramJ- Plugin (Schmid et al., 2011) in FiJi (Schindelin et al., 2012), to gain a general visualization of locomotor rhythms in the 24-hour context. All Actograms were generated from the text-files recorded from the DAM-System,

with the starting point at ZT18 (0.00 CET), in the middle of the dark phase. The actograms were double plotted, meaning two consecutive days were depicted in one line, then the second of the two days repeated and followed by the third consecutive day in the next line, and so on. This way of plotting facilitates the identification of patterns that are located at the transition between two days while retaining effects that might occur in the middle of the dark phase. Black bars indicate the number of beam crosses per minute, with the upper limit set to an empirically established value that allowed the best resolution of daily activity, which means all values equal and higher than the limit are depicted as a full bar. This "upper limit" is indicated in chapter 3.1. After generation, actograms were used to identify patterns of locomotor behavior in the LD phase and calculate the percentage of entrained animals. Entrained animals were defined as synchronized to the period length of the LD cycle (24h), all others as arrhythmic. These patterns were categorized after their preference for a distinct phase of the LD, either as dark or light preferring, or as both if they had defined activity bouts in both phases. Animals that changed their preferred phase during recording were defined as switching, those active during the whole day with no clear preference for any phase or distinct activity peaks as arrhythmic.

Additionally, actograms were used for qualitative and quantitative analysis of the ant`s behavior under constant darkness. Their rhythmicity and period length were calculated (see 2.3.6.3 and 2.3.6.4) and it was determined whether the start of their activity in constant conditions continued from the start of activity during the LD-cycle. The activity type was defined by this behavior, ants starting their activity from the dark phase were defined as nocturnal, those starting from the light phase as diurnal and ants that showed no measurable period length as arrhythmic.

Actograms also facilitated the determination of when an individual died for calculation of survival.

2.3.6.2 Average Day

Average Daily activity profiles show the average daily activity of all individuals averaged over several days in the form of a graph. This serves to eliminate unique artifacts and daily fluctuations and to indicate long-term, stable circadian patterns of behavior integral to the whole colony.

To generate average daily activity profiles, data of as many days as possible from the cropped text-file was averaged for each individual ant of each temperature condition, then averaged for all ants. This method has been reviewed in Schlichting and Helfrich-Förster (2015a). Days that showed increased bouts of activity at the beginning or end of recording were excluded from calculations, since they are due either to adaptation to the new surroundings (beginning) or to

dying (end) and do not represent normal behavior during the LD. To smooth the raw datasets and thus remove short term fluctuations, a moving average of 11 was applied, i.e., each group of 11 consecutive data points was averaged to a new value. These new values were then plotted over time using Qti-Plot (Vasilef, 2011), starting at ZT 18 and ending at ZT18, to better depict effects at the transition between light and dark phase. Paint (Microsoft) was used to color the areas below the graph, for visualization of light (light gray) and dark (black) phase. In Experiments 2 and 3, average days were only calculated for individuals that were also used for period-length analysis.

2.3.6.3 Period length

Period length was measured automatically with the ActogramJ Plugin for FiJi. The period lengths in Experiments 2 and 3 were calculated from the onset of constant darkness, e.g. the beginning of the dark phase on day eight (Experiment 3), to the end of the light phase on day 18, ten full days. The Method chosen was the Chi^2-Analysis. Only period lengths whose power is above the significance level were considered. These period lengths were filed in an excel sheet and the mean period length of all individuals in an environment of a given temperature was calculated.

2.3.6.4 Additional data analysis

Additional information that was taken from the locomotor monitoring data is the number of animals that survived up until a certain amount of days. Furthermore, the average of daily, light and dark activity, in beam crosses per minute of the single animals, was used to calculate the mean activity of all animals during one day, the light and dark phase, to determine whether temperature or LD cycle can influence the preference for a day phase. The percentage of preference for a certain LD phase and type of activity, as well as the percentage of ants with consistent preference for a phase between LD and DD (meaning nocturnal ants that were entrained to the dark phase, etc.), were calculated and plotted.

2.4 Pre-processing of brain-samples

2.4.1 Collection of animals

2.4.1.1 Collection from monitors

Only clearly rhythmic ants preferring the dark phase of the LD cycle were used for Experiments 6 and 7. This was evaluated by monitoring individual ants in TriKinetics LAM monitors, as described in chapter 2.3. Six animals were collected at each of the eight consecutive time-points, ZT 0, 3, 6, 9, 12, 15, 18, 21, starting with ZT 0 at 9.00am MET for Experiment 6 or ZT 0, 6, 12, 18, starting with ZT 0 at 9.00am MET for Experiment 7. They were taken directly from the glass-tubes inside the monitor and quickly decapitated in constant darkness. To ensure that no protein was degraded during preparation, all head-capsules were perforated with a pair of sharp forceps under a binocular-microscope and immediately transferred to a fixative solution (Paraformaldehyde (PFA, Sigma) 4% in Phosphate Buffered Saline (PBS, Sigma)). See 2.7.4 for details. After pre-fixation, the heads were washed several times with PBS and stored at 4°C until preparation (see 2.4.2).

2.4.1.2 Collection from colonies

Ants that were used for Experiments 4 and 5 were collected directly from the mother colony C152 at ZT 4. They were immediately decapitated with a scalpel and the brains prepared from the head-capsule according to 2.4.2.

2.4.2 Preparation of brains:

All brains were prepared from the head capsule, using a scalpel, a pair of sharpened forceps, and a petri-dish with a waxed floor, a soldering iron and a binocular. Head capsules were transferred to the petri dish, the wax melted with the soldering iron, and the head embedded facing upwards (see Fig. 10). The antennae were removed and the whole head quickly covered with PBS. A window was cut with a very fine scalpel (see Fig. 10, dotted line) along the dorsal rim of the head, ventral through both eyes and then directly above the antennae. The cuticula was removed, as well as the air

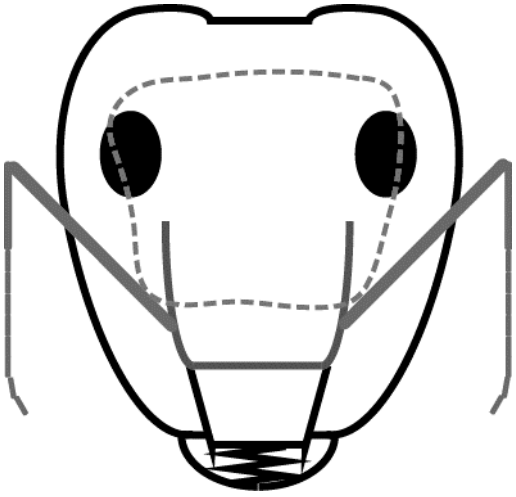

Figure 10: Schematic depiction of the ant head. The gray dotted line indicates the cutting line for the scalpel.

cushions directly below it, to provide full access to the brain. The brain was then freed from trachea and remaining retinae with the help of the forceps and gently lifted from the head capsule. Brains were immediately transferred to the fixative solution.

2.4.3 Fixation

Since the structure of cells, proteins and the brain itself quickly deteriorate on their own once the organism dies, it is necessary to fix them with a crosslinking chemical, like Formaldehyde. The fixative used depended on the experiment and can be found in 2.5.4. Both chemicals used (Zamboni´s Fixative and PFA, see 2.8.1 Chemicals) were tested prior to experiments by Pamela Menegazzi and I (Bachelor Thesis, Master Thesis) for their suitability for the respective experiments. During these tests, PFA proved to be the best choice for labelling of the PER protein, while brains fixated in Zamboni´s Fixative yielded better results for PDF staining.

2.4.4 Embedding and Vibrating Blade Microtome Sectioning

Brains for Experiment 5 had to be cut into thin sections of 60 µm. These brains proved that no staining of fibre tracts of the PDF-network were lost due to the thickness of the wholemount brain. After fixation, the brains were washed with PBS several times, prior to embedding. The whole brains were embedded in 7% Agarose (Low EEO, Sigma) blocks. The agarose powder was diluted in desalinized water and heated to the point of boiling in a microwave, then stirred on a heating plate at ~150°C until use, to eliminate bubbles. The brains were individually transferred to small silicone forms in a droplet of water, then dried with filter paper and lifted from the form with the tip of a brush handle. Agarose was poured into the form bubble-free, and a single brain pushed into the agarose quickly. After cooling blocks were trimmed, and one corner of the block was cut off, to enable identification of the orientation of the sections after staining. The block was then glued to the sample plate of a vibrating blade microtome (Vibratome, Leica VT 1000 S) and the sample plate screwed tightly into the microtome bath, filled with PBS. A vibrating blade was then used to cut 60µm sections of the embedded brain, sections were immediately transferred to individual wells of a 48-well-plate containing PBS.

2.5 Immunohistochemistry

Immunohistochemistry is a method designed to detect proteins of interest in histological samples with the help of specifically designed antibodies. To start the process, a primary antibody directed against an epitope of the protein in question is applied to a histological

sample, which can range from whole animals, over whole organs, to sections of either. In the simplest case, the primary antibody is directly coupled to an enzyme or fluorophore. These can then be detected using either a substrate the enzyme can turn into a precipitation, or a fluorescence microscope. Though this is very simple and robust, the signal gained may not be very strong, since it is not amplified in any way. Also, one is bound to the detection method (e.g. a certain wavelength) dictated by the already coupled enzyme or fluorophore. Thus, a common way of staining is the employ of a non-coupled primary antibody and a secondary antibody which specifically binds to the primary antibody, allowing for a choice of labelling. This secondary antibody is directed against an epitope of the animal the primary antibody was raised in. The secondary antibody can again either be coupled to an enzyme or a fluorophore. The immunohistochemical experiments at hand were conducted with fluorophores as labels. The fluorophores where then excited using a laser-beam set to the excitation-maximum provided by the supplier in a confocal laser microscope (see 2.6) and detected. The images detected by the microscope where then stored and processed as detailed in 2.7

2.5.1 Immunofluorescent labelling

The staining in all experiments was performed using the same basic principle, which is described here. Details of the antibodies used, incubation times and other deviations can be found in chapters 2.5.2 to 2.5.4, which give detailed information on the protocols used for each experiment.

Directly after cutting with the vibratome (sections) or fixation (wholemounts), the samples were washed several times with PBS. After these initial washes, the samples were washed again, this time with PBST (PBS containing 0.5% Triton X100, see 2.8), which amplifies the permeability of the membranes and thus allows for better penetration by the antibodies.

Subsequently, the samples were blocked in a solution containing serum of the animal the secondary antibody was raised in (pre-incubation). This step is necessary to block unspecific epitopes contained in the sample and prevent unspecific staining. All secondary antibodies used were raised in goats, thus the blocking serum used was Normal Goat Serum (NGS).

After pre-incubation, samples were incubated in the primary antibody or antibodies. Though antibodies have their highest binding rates at higher temperatures (natural binding temperature would be the body temperature of the specific animal), incubation at 4 °C is more specific albeit slower. To obtain the best staining, both were combined by first incubating at room temperature, followed by several days at 4°C and additional hours at room temperature. Sodiumazide was added to the primary antibody solution to prevent samples from being infested by funghi.

After incubation in the primary antibody, samples were thoroughly washed in PBST to remove all unbound primary antibody before the incubation in the secondary antibody.
Incubation in the secondary antibody was performed at 4°C for several hours. The secondary antibody needs to be raised in a different animal than the primary, but be directed against the epitopes of the animal the primary was raised in (E.g. Goat- anti-rabbit). Since the secondary antibody is labeled with a fluorophore, samples need to be shielded from light exposure to avoid bleaching from this step on. Afterwards, the samples were washed with PBST and subsequently PBS to remove all traces of un-bound secondary antibody.
If a double-labelling with a primary antibody raised in the same animal as the first primary antibody was necessary, brains were fixed again and the protocol started from the top unto this point (see 2.5.2 for details).
In some samples, a staining of the background structures was necessary to provide orientation in the brain. If this had not been done with anti-SYN in the first step, it was performed with anti-HRP directly labelled antibody (see 2.5.4 for details).
When all desired staining was finished, samples were embedded in Vecta-Shield. Sections were arranged on glass slides in their cutting order and covered with a cover slip, while whole-mounts were placed between two coverslips. They were put in wells made of several reinforcement rings (self-adhesive, office supply) serving as spacers, on top of a cover slip and covered by a second coverslip to facilitate the permeation of the microscope laser from both sides. Some wholemount brains were compressed slightly in this procedure, those meant for reconstruction were not. For both mounting techniques, the slides were sealed with fixo-gum to avoid evaporation of the VectaShield embedding solution. All slides were stored in the fridge at 4°C for conservation.

2.5.2 PDH staining in wholemounts

The staining protocol for PDF and SYN staining in wholemount brains can be found in table 3 and complies largely with the basic principle. The antibodies used are the anti-PDH antibody by Heinrich Dircksen (see 2.9) and the anti-SYN antibody 3c11 from the Würzburg Hybridoma Library (see 2.9).

Table 3: Staining protocol for PDH/SYN double-labelling on wholemounts

Step	Details	Duration/Temperature
1. Sampling	• From the colony • At ZT 4	
2. Preparation	• Embedding in wax • Preparation in PBS	
3. Fixation	• In Zamboni´s Fixative	Overnight at 4°C
4. Washing	• In PBS	2x15m at RT
5. Washing	• In PBST	2x15m at RT
6. Pre-incubation	• In 5%NGS in PBST	Overnight at 4°C
7. Primary Incubation	• In Primary AB: 1:500 anti-PDH, 1:300 anti-SYN, 5% NGS, 0.02% NaN_3 in PBST	24h at RT; 3d at 4°C; 24h at RT
14.Washing	• In PBST	6x15m at RT
15. Secondary Incubation	• In Secondary AB: 1:300 Alexa Goat anti-rabbit 635, 1:300 Alexa Goat anti-mouse 555, 5%NGS, 0.02% NaN_3, in PBST	5d at 4°C
16. Washing	• In PBST	3x15m at RT
17. Embedding	• In Vecta-Shield • Between cover slips with reinforcement rings as spacers	
18. Detection	• With Leica DM5500Q	

2.5.3 PDH staining on sections

For staining with antibodies against PDH and HRP, the staining protocol needed to be altered, since HRP is directly conjugated with a flourophore. This can be seen in table 4. The antibodies

used are the anti-PDH antibody by Heinrich Dircksen (see 2.9) and Cy™3 AffiniPure Goat Anti-Horseradish Peroxidase (Jackson ImmunoResearch, # 123-165-021).

Table 4: Staining protocol for PDH/HRP double-labelling on sections

Step	Details	Duration/Temperature
1. Sampling	• From the colony • At ZT 4	
2. Preparation	• Embedding in wax • Preparation in PBS	
3. Fixation	• In Zamboni´s Fixative	Overnight at 4°C
4. Washing	• In PBS	6x15m at RT
5. Embedding	• In 7% Agarose • With anterior side of the brain facing the top of the block	
6. Cutting	• With vibratome • 60µm section • Transfer to well-plate in order of cut	
7. Washing	• In PBS	2x15m at RT
8. Washing	• In PBST	2x15m at RT
9. Pre-incubation	• In 5%NGS in PBST	Overnight at 4°C
10. Primary Incubation	• In Primary AB: 1:500 anti-PDH, 5% NGS, 0.02% NaN_3 in PBST	24h at RT; 3d at 4°C; 24h at RT
14.Washing	• In PBST	6x15m at RT
15. Secondary Incubation	• In Secondary AB: 1:300 Alexa Goat anti-rabbit 635, 5%NGS, 0.02% NaN_3, in PBST	5d at 4°C
16. Washing	• In PBST	3x15m at RT
17. Pre-incubation	• In 5%NGS in PBST	Overnight at 4°C

18. Incubation	• In 1:250 anti-HRP, 5% NGS, 0.02% NaN_3 in PBST	12h at RT, 2 days at 4°C, 2h at RT
19. Washing	• In PBS	3x15m at RT
20. Washing	• In PBST	3x15m at RT
17. Embedding	• In Vecta-Shield • Between cover slips with reinforcement rings as spacers	
18. Detection	• With Leica TCS SP8	

2.5.4 PER/PDH double-labelling

The protocol for double-staining of the PERIOD protein and the neurotransmitter PDF in Experiment 6 and 7 can be found in table 5 and is altered from the basic principle in a number of ways. These alterations were established by Dr. Pamela Menegazzi in preliminary tests before the start of this work. First, brains that were to be stained with anti-PER antibody were dehydrated with a methanol series directly after the fixation and stored at -20°C until all time points had been sampled. This improved the staining quality of PER. Then all time-points were rehydrated at once and stained in one assay to minimize differences in staining intensity due to handling. Furthermore, brains were cooked in Sodium citrate prior to pre-incubation to amplify the permeability of the membranes. Since the PER and the PDH antibody were both raised in rabbits, it was not possible to use both antibodies in one incubation step. Thus, samples were first incubated in anti-PER and after the staining process was finished samples were fixated again and the staining process repeated with anti-PDH. Table 5 provides an overview of the complete staining procedure. The antibodies used are the anti-PDH antibody by Heinrich Dircksen (see 2.9) and the PER antibody raised by Eva Winnebeck (see 2.9).

Table 5: Staining Protocol for PER/PDH double-labelling

Step	Details	Duration/Temperature
1. Sampling	• From monitors • ZT 0,3,6,9,12,15,18,21	
2. Prefixation	• Through hole in head-capsule	6h at 4°C

	• Whole heads including cuticula	
3. Preparation	• Embedding in wax • Preparation in PBS	
4. Fixation	• In 4% PFA in PBST	45m at RT
5. Washing	• In PBS	3x15m at RT
6. Dehydration	• In Methanol in PBS • 30,50,70,90,95, 3X100%	15m per dilution at RT, store at 20°C
8. Rehydration	• In methanol in PBS • 95, 90, 70, 50, 30, 0%	15m per dilution at RT
9. Washing	• In PBS	3x15m at RT
10. Cooking	• In Sodium citrate	40m at 80°C
11. Washing	• In PBS	3x15m at RT
12. Pre-incubation	• In 5%NGS in PBST	Overnight at 4°C
13. Primary Incubation	• In Primary AB: 1:1000 anti-PER , 5% NGS, 0.02% NaN_3 in PBST	24h at RT; 5d at 4°C; 24h at RT
14.Washing	• In PBST	6x15m at RT
15. Secondary Incubation	• In Secondary AB: 1:300 Alexa Flour Goat anti-rabbit 488, 5%NGS, 0.02% NaN_3, in PBST	24h at 4°C
14. Washing	• In PBST	10x1h at RT
15. Washing	• In PBS	Overnight at 4°C; 2x15m at RT
16. Re-fixation	• In 4%PFA in PBST	2h at RT
17. Washing	• In PBS	3x15m at RT
18. Primary Incubation	• In Primary AB: 1:1000 anti-PDH , 5% NGS, 0.02% NaN_3 in PBST	24h at RT; 5d at 4°C; 24h at RT
19. Washing	• In PBST	6x15m at RT
20. Secondary Incubation	• In Secondary AB: 1:300 Alexa Flour Goat anti-rabbit 635, 5%NGS, 0.02% NaN_3, in PBST	24h at 4°C
21. Washes	• In PBS	3x15min at RT

22. Washes	• In PBST	3x15m at RT
23. Embedding	• In Vecta-Shield • Between cover slips with reinforcement rings as spacers	
24. Detection	• At Leica TCS SP8	

2.6 Confocal Laser-Scanning Microscopy:

All immunohistochemically stained samples were analyzed with a confocal laser-scanning microscope (CLSM), either the Leica DM5500 Q or the Leica TCS SP8. This is a special type of microscope with a number of advantages: first, it employs lasers which can be set to very specific wavelengths to excite the flourophores used in the staining, second, several channels (=dyes) can be recorded in one image, third, it minimizes light scatter, and thus blurring, due to its special recording properties and fourth, it is able to record 3-dimensional projections of the samples scanned. The lasers in the microscopes used are single wavelength lasers of 532nm and 635nm (Leica DM5500 Q) and a white light laser (Leica TCS SP8). The white light laser consists of a photonic crystal fiber that is fed by a high-energy pulsed IR-fiber laser and generates a spectral continuum. This spectral continuum is then selected for small bandlets of wavelength by an acousto-optical tunable filter, thus enabling the excitation of several distinct wavelengths at once, with only one light-source. The single wavelength lasers and the white light laser both facilitate specific excitation of the used flourophores (see table 6 for excitation and emission wavelengths used) and the recording of both channels of the double-staining in one image. Two principles are working to reduce light scatter: the excitation of only a single point of the sample by the laser, and the detection pinhole. In confocal microscopy, as opposed to bright field microscopy, only a single focal point is illuminated by the laser, limiting the emission of scattered light from adjacent areas. Additionally, an aperture called pinhole prevents scattered light that might radiate from planes below or above the focal point in thick samples from being detected, by shielding them from the detector. Only light emitted from the focal plane, which is set by the diameter of the pinhole, is able to pass this aperture and proceed to be detected by a color-selective detector. The table below shows the wavelengths at which each secondary antibody was recorded, their absorption and emission maxima, and the color of the channel they were recorded in.

Table 6: Recording specifics of the Secondary Antibodies

Experiment	Secondary Antibody	Absorption-Maximum	Emission-Maximum	Channel
2: PDF/SYN Leica DM5500 Q	PDF: Alexa Flour 635nm	633nm	647nm	Far red
	SYN: Alexa Flour 555nm	555nm	565nm	Orange
3: PDF/HRP Leica TCS SP8	PDF: Alexa Flour 635nm	633nm	647nm	Far red
	SYN: Alexa Flour 555nm	555nm	565nm	Orange
4: PDF/PER Leica TCS SP8	PDF: Alexa Flour 635nm	633nm	647nm	Far red
	PER: Alexa Flour 488nm	496nm	519nm	Green

Since the whole sample, and not only a single focal point needs to be scanned, the laser-beam is redirected by mirrors, which move it in a grid-like fashion through every plane of the sample. Each plane is recorded as a xy picture (slice). Slices are arranged as a z-stack, thus forming a 3D representation of the stained sample.

Both microscopes also feature a moving specimen-table which allows for automatic recording of several image-tiles in brains that were too large to be recorded in a single image. The number of image tiles was chosen according to the size of the brain, the software later stitched the stacks of the single tiles together automatically to form a single picture.

Images that were recorded for the purpose of staining intensity evaluation (Experiments 6 and 7) were recorded with fixed settings for gain, laser intensity, amplifier offset and slice thickness (2µm) so as not to influence the intensity of the signal with different settings and recorded with a 10x objective. All other images were manually set to the optimal settings for signal-to-noise ratio. Whole-mount brains for PDF-network reconstruction and images of the whole brain slices were recorded with a 10x objective, detail images of brain slices with a 20x objective.

Due to technical problems with the faster and more precise Leica TCS SP8, wholemount samples of PDF/SYN staining form experiment 4 had to scanned at the older and less precise Leica DM5500 Q.

2.7 Data Processing

2.7.1 Image processing in FiJi

All Image stacks were opened in FiJi, an Image J distribution (Schindelin et al., 2012) for visual evaluation of the staining, using the Bioformats plugin (Linkert et al., 2010). Images were first evaluated qualitatively, and stained structures identified. Brightness and Contrast were adjusted in all images not intended for staining intensity measurements. Z-stacks were then used to generate so-called projections, which are overlays of the different slices calculated by maximal staining intensity. The number of slices overlaid for each picture was chosen empirically according to the best depiction of the structure in question and is stated in chapter 3 for each projection shown. The two channels of staining were subsequently merged to show the relation of the stained structures, e.g. the course of a fiber through a certain neuropil or whether a cell stained with two different antibodies was double-labelled. Different colors were chosen for the different structures stained, to emphasize double-labelling and optimize visibility. Magenta was chosen for PDF, green for neuropils (SYN or HRP) or PER staining.

2.7.2 Identification of PER cell clusters

To quantify the staining intensities of PER cell bodies, their location had to be identified first. This was done as described in 2.7.1 by qualitative visual assessment of the PER channel z-stack in the staining of PER at ZT0. The clusters found were then categorized and named according to their location. Cell numbers were counted and the mean number of cells per cluster was calculated. A schematic overview of the brain and the PER cell clusters was drawn and digitalized with the help of a scanner and Adobe Illustrator, due to high noise in the background which prevented the generation of an complete overview by projection.

2.7.3 Quantification of PER staining intensity

Pictures used for Quantification of PER staining were opened in FiJi and changed into 8-bit greyscale format for intensity measurements. PER cells in five hemispheres were measured (n=5). For each of the five clusters chosen for quantification, a fixed number of cells were chosen (according to the average number of cells per cluster) and measured with the free form tool, by drawing around the shape of a single cell then measuring the average greyscale value inside the shape. If there were more cells, only the brightest ones were measured, if there were less, the background was measured until the relevant number was reached. This was done to correct for cells that might not be visible at some time points due to their low staining intensity.

For each cell measured, the background was measured in its´ close vicinity and subtracted from the measurement to correct for background staining. This corrected measurement was then saved in Excel and the Average Staining intensity of all measurements was calculated individually for each time-point and cluster. These averages were depicted in the form of a line-graph (one line per cluster), with the staining intensity plotted over the time points sampled, starting at ZT18. This starting point in the middle of the dark phase was chosen to visualize the transition points between the dark and light phase. The value of ZT 18 was then plotted once more at the end of the graph, so that the transition from ZT15 to ZT18 is also depicted. Additionally, a detail picture of each measured cluster was generated at each measured time-point and corrected for background-staining intensity by subtracting the fixed measure background intensity measured beforehand from the whole picture.

2.7.4 Reconstruction of the PDF network:

The PDF and its surrounding neuropils were reconstructed in FiJi from the wholemount staining performed in Experiment 4. Staining was scanned from both sides (anterior and posterior), as the brains were too thick for the laser to penetrate from one end of the sample to the other, then merged in FiJi.

2.7.4.1 Neuropil Reconstruction

Neuropils were reconstructed using the Segmentation Editor Plugin (Schindelin et al., 2012) implemented in FiJi. To generate a 3D-model of the neuropil, the SYNAPSIN channel of the staining was opened in FiJi and the Segmentation Editor was started. In the new segmentation window, the neuropil staining is depicted, in a second window, the “labels” that are generated from the staining are depicted and saved in the form of a picture stack. Each neuropil is assigned a label with a specific color, then the neuropil in question is encircled with the freehand tool in a number of slices. The program then interpolates the form in the slices in which the neuropil was not marked. Inaccurate extrapolation is now corrected manually and the complete form assigned to the labelfield of the correct neuropil. When all neuropils are segmented into the different labels, the .label file is saved and the command “Create Surfaces” is used to generate a 3D-rendering of the structures. Since this command did not work, the labelfield-data was loaded into Amira (FEI Visualization Sciences Group, Thermo-Fisher Scientific), rescaled, a surface generated and a surface view generated.
Figure 11 depicts a screenshot of the Segmentation Editor and the linked labelfield data.

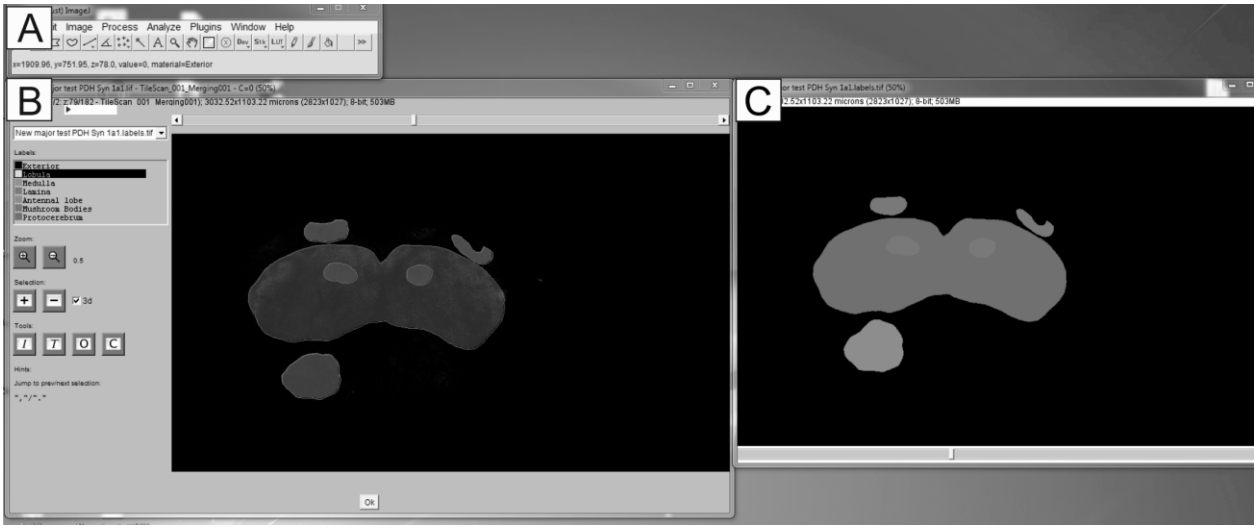

Figure 11: The Segmentation Editor. A) The Fiji command line B) The Segmentation Editor with the embedded confocal image stack of Synapsin-Staining. C) The generated labelfield.

2.7.4.2 PDH cell body reconstruction

The PDH cell bodies were reconstructed in the same way the neuropils were reconstructed, with the Segmentation Editor and Amira. The sole exception was that the PDF-channel of the staining had to be used for this reconstruction. See 2.7.4.1 for details.

2.7.4.3 PDH network reconstruction

To reconstruct the PDF network, the PDF channel of the wholemount scans from Experiment 4 was opened in FiJi and the plugin Simple Neurite Tracer was started (Longair et al., 2011). Simple neurite tracer automatically transforms the image stack to greyscale (8-bit). Each neuron is traced by hand with the application. A starting point for a neuron is chosen by clicking on the image and further points along the path can be chosen in the same fashion. The program then extrapolates the course of the neuron according to the grey-values of the image-stack. Each new section then needs to be confirmed, if the program does not extrapolate correctly the new part of the path is abolished and a point closer to the already existing path needs to be chosen. In this fashion the main branch of the path is traced until it is completed by pressing the “complete path” button. Further fibers branching off the main fiber can now be added until the complete network is traced. Fibers that have been traced already are marked in a chosen color. When all fibers are marked, the paths are selected in the path list and a fill is calculated with the command “fill out”. The fill is calculated from the gray-values surrounding the chosen path, its thickness depends on how long the program is allowed to fill out. The optimal time for

this needs to be tested empirically, by generating several fills with different calculation times and comparing the generated fills with the fibers in the original scan. Once an optimal fill is calculated, the result is exported by generating an image stack of it with the button “Create Image Stack from Fill”. This image stack contains the fill in the form of a labelfield and can now

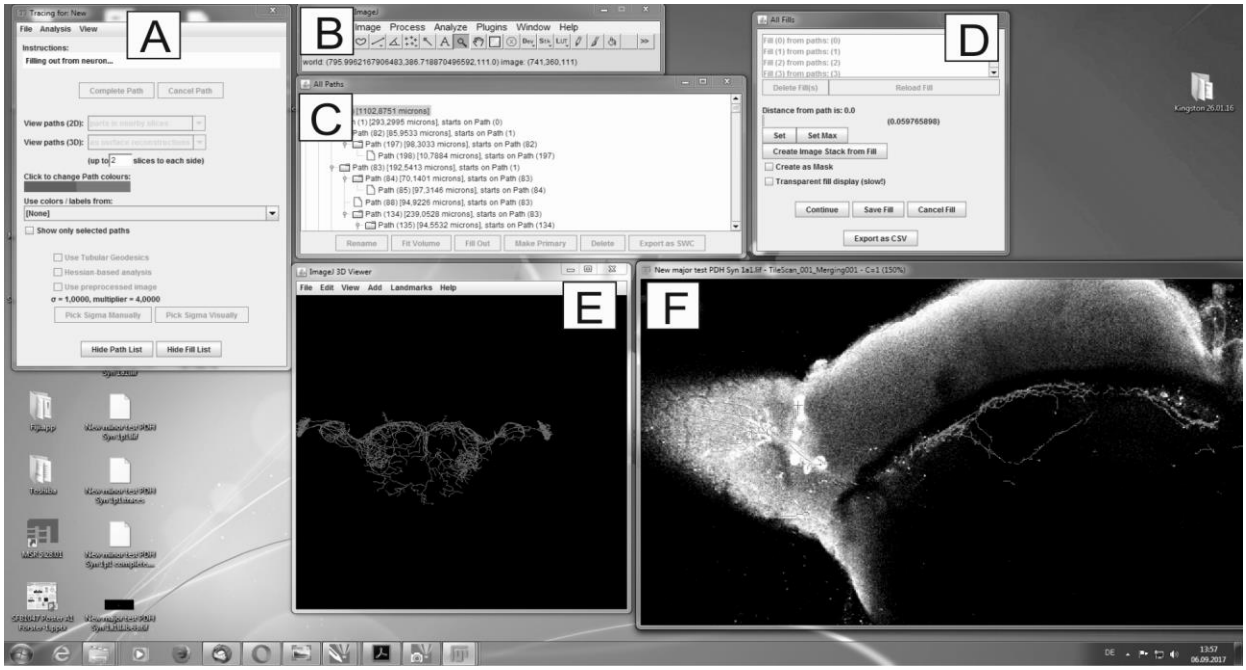

Figure 12: The "simple neurite tracer" add-in. A) The main “simple neurite tracer” window B) the Fiji command line C) the paths generated with simple neurite tracer D) The filling tool E) The 3D-Viewer F) The original image stack of PDH-staining, with the reconstructed paths.

be loaded into the 3D-viewer for rendering. All necessary windows can be seen in Figure 12.

2.7.4.4 Generation of the 3D-model

After the neuropils, cell bodies and the PDF network were reconstructed, all files were loaded into Amira, starting with the neuropils and cell bodies as described in 2.7.4.1. Then the PDF network picture stack was added and recalculated for Amira using the skeletonize tool. The reconstructed PDF network was then automatically added to the reconstructed neuropils and cell bodies. The relation of the different components to one another was checked for mis-alignments and the reconstruction was compared to the original scans.

2.8 Statistics

All statistics were performed using R-Studio (Version 1.0.136). Chi^2 tests were performed to compare the percentage of survival, entrainment, rhythmicity, preference for LD phases and activity type in Experiments 1-3. All other data was tested for normal distribution using shapiro-wilkes test. If data was normal distributed and only one grouping variable applied, a one-way ANOVA was calculated. In case of significant differences, a Tukey post-hoc test with Bonferroni correction was performed. If data was not normal distributed and only one grouping variable applied, a Kruskal-Wallis test was calculated. In case of significant differences, a pairwise Wilcox test with Bonferroni correction was performed as post-hoc test. If two grouping variables applied, a two-way ANOVA was calculated, if the data was not normal distributed the significance values were adjusted with the method proposed by Glaser on pages 111 and 112 of his book "Varianzanalyse" (Glaser, 1978). In case of significant differences, a Tukey post-hoc test with Bonferroni correction was performed

2.9 Materials

The following tables compile all used Materials and machines as well as their composition and manufacturer.

Table 7: Solutions

Solution	Ingredients/Specifications	Manufacturer
Sugar Water	5% Saccharose in H2O	Südzucker GmbH, Ochsenfurt
Phosphate Buffered Saline (PBS)	1 M, diluted from 10x Stock, pH 7.8	Sigma-Aldrich, St. Louis, MO
Phosphate Buffered Saline with Triton X (PBST)	1M PBS, 0.5% Triton X100	Sigma-Aldrich, St. Louis, MO
Fixation Reagent (PFA in PBST)	4% Paraformaldehyde in PBST	Thermo-Fisher Scientific, Carlsbad, CA
Fixation Reagent (Zamboni´s Fixative)	4% Paraformaldehyde, 7,5 % saturated picric acid solution 0.1 M phosphate buffer, pH 7.4	(Stefanini et al., 1967) Sigma-Aldrich, St. Louis, MO

VectaShield	Embedding medium for fluorescently labelled preparations	Vector Laboratories, Burlingame, CA
7% Agarose-Gel	7% Agarose (low EEO) in H2O (desalinated)	Sigma-Aldrich, St. Louis, MO
Sodium Citrate	10mM, pH=48.5	Sigma-Aldrich, St. Louis, MO

Table 8: Antibodies

Primary Antibodies		
Anti-PDH	Polyclonal, raised in rabbit, recognizes ß-PDH	(Dircksen et al., 1987)
Anti-SYN (3c11)	Monoclonal, raised in mouse, recognizes the SYNAPSIN protein	(Hofbauer et al., 2009)
Cy™3 AffiniPure Goat Anti-Horseradish Peroxidase	polyclonal, raised in rabbit, recognizes Horseradish peroxidase, secondary AB included (Cy™3)	Jackson ImmunoResearch, # 123-165-021, West Grove, PA
Anti-PER	Polyclonal, raised in rabbit, recognizes part of the PERIOD protein	(Fuchikawa et al., 2017)
Secondary Antibodies		
Alexa Fluor 488	Goat anti-rabbit	Invitrogen, Thermo-Fisher Scientific, Carlsbad, CA
Alexa Flour 555	Goat anti-mouse	Invitrogen, Thermo-Fisher Scientific, Carlsbad, CA
Alexa Flour 635	Goat anti-rabbit	Invitrogen, Thermo-Fisher Scientific, Carlsbad, CA

Table 9: Other Chemicals

Normal Goat Serum	Invitrogen, Thermo-Fisher Scientific, Carlsbad, CA
NaN3	Sigma-Aldrich, St. Louis, MO

Table 10: Machines

Incubator	MIR-553	Sanyo, Osaka
Tilting Table	Polymax 1040	Heidolph, Schwabach
Locomotor Activity Monitors	LAM	TriKinetics, Waltham, MA
Vibratome	Leica VT 1000 S	Leica, Wetzlar
LED-Strips	White-light LED strip LEDBERG	IKEA
Confocal Microscope	TCS SP8, Microsystems LAS AF – TCS SP8 Software: LAS AF Objectives: 10x: ACS APO 10.0 x 0.30 DRY 20x: HC PL APO CS2 20x/0.75 IMM	Leica, Wetzlar
Confocal Microscope	DM5500 Q, Microsystems LAS AF – TCS SPE Software: LAS AF Lite Objective: ACS APO 10.0 x 0.30 DRY	Leica, Wetzlar
Incubator	MIR-154	Sanyo, Osaka
Soldering Rod	WTCP-51	Weller, Besigheim

Table 11: Software

FiJi	Version: 1.47t	Wayne Rasband, www.rsb.info.nih.gov/ij
Leica Software LAS AF	2.7.3.9723	Leica, Wetzlar
Microsoft® Office Excel	Version: 2013	Microsoft®

R-Studio	Version 1.0.136	RStudio, Inc.
Amira	Version: 6.0.0	FEI Visualization Sciences Group, Thermo-Fisher Scientific
Qti-Plot	Version: 0.9.8.10	(Vasilef, 2011)

Table 12: Other Materials

Microscope slides	Superfrost Menzel-Gläser, 76 x 26mm	Thermo-Fisher Scientific, Carlsbad, CA
Cover slips	24 x 32 mm	Hartenstein, Würzburg
Sealing Fluid	Fixogum	Marabu, Bietigheim-Bissingen
Spacer	Reinforcement Rings, self adhesive, No. 5898	Herma, Filderstadt
Feeding Devices (Mildner)		(Mildner and Roces, 2017)
Feeding Devices (Kay)		(Kay et al, 2017)
48 Well-Plate	Nunc 48 well-plate	Thermo-Fisher Scientific, Carlsbad, CA

3. RESULTS:

3.1 The endogenous Locomotor Behavior of *C. floridanus*:

3.1.1 *C. floridanus* is able to entrain to different light phases

In Experiment 1, the behavior of *C. floridanus* in response to different light phases was examined at 25°C. Figure 13 gives an overview over survival and entrainment of all ants tested in this experiment. Survival was determined after seven days, since the shortest recording (LD 12:12) ended after this period. Survival rates were significantly different across all conditions (Chi^2=47.6, p<0.0001). The lowest survival-rate at LD 8:16 of 47% differed highly significantly from the highest at LD 12:12 of 87% (Chi^2=45.81, p<0.0001) but also from the survival rate at LD 16:8, of 71% (Chi^2=15.5, p<0.001). The difference in survival between LD 12:12 and LD 16:8 was also significant (Chi^2=9.4, p=0.002). The percentage of entrained individuals ranged from 86% at LD 12:12, over 87% at LD 8:16 to 91% at LD 16:8 and was not significantly different between the LD conditions (Chi^2=2.1, p=0.35), indicating that the majority of ants is able to entrain to different LD cycles. Some of the actograms evaluated to generate the data on entrainment can be found in Figures 14-16. Figure 14 shows typical actograms of individuals kept at 25°C and a LD of 8:16, Figure 15 those of individuals kept at 25°C and a LD of 12:12 and Figure 16 those of individuals kept at 25°C and a LD of 16:8. Figure 14A-C; 15A-C and 16A-C show typical examples of the most common preferences, entrained to the dark (A) the light (B) or no phase (arrhythmic, C). Even though the individuals in Fig. 14A and Fig. 15A show most of their activity in the dark phase, activity is not limited to the dark phase. There are also some fragments of activity in the light phase. Furthermore, activity in the dark phase does not span

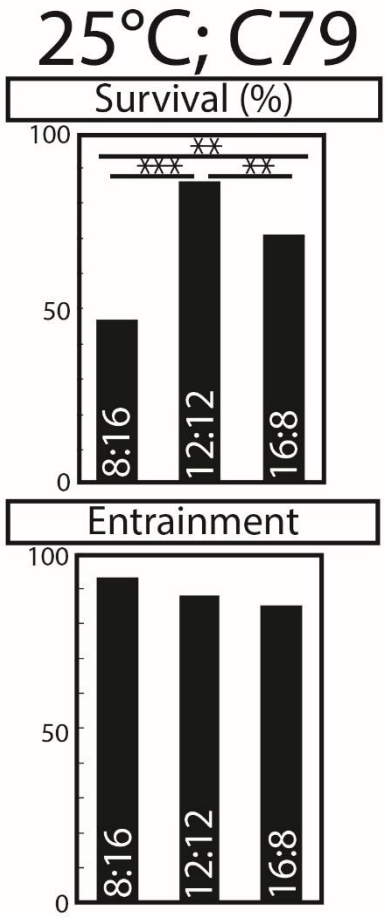

Figure 13: Survival and Entrainment of Individuals kept at LD 8:16, 12:12 and 16:8 at 25°C. Survival: The percentage of ants that were still alive after seven days. Significance levels are indicated by stars, * p≤0.05, **p≤0.01, ***p<0.001. Sample size: LD 8:16 n=128, LD 12:12 n= 126, LD 16:8 n=126. Entrainment: The percentage of entrained ants, no significant differences. Sample size: LD 8:16 n=59; LD 12:12 n=112, LD 16:8 n=91.

through the whole dark phase, but stops after approximately 10 hours. Fig. 14D depicts another example of an ant at LD 8:16, which has a longer duration of activity during the dark phase.

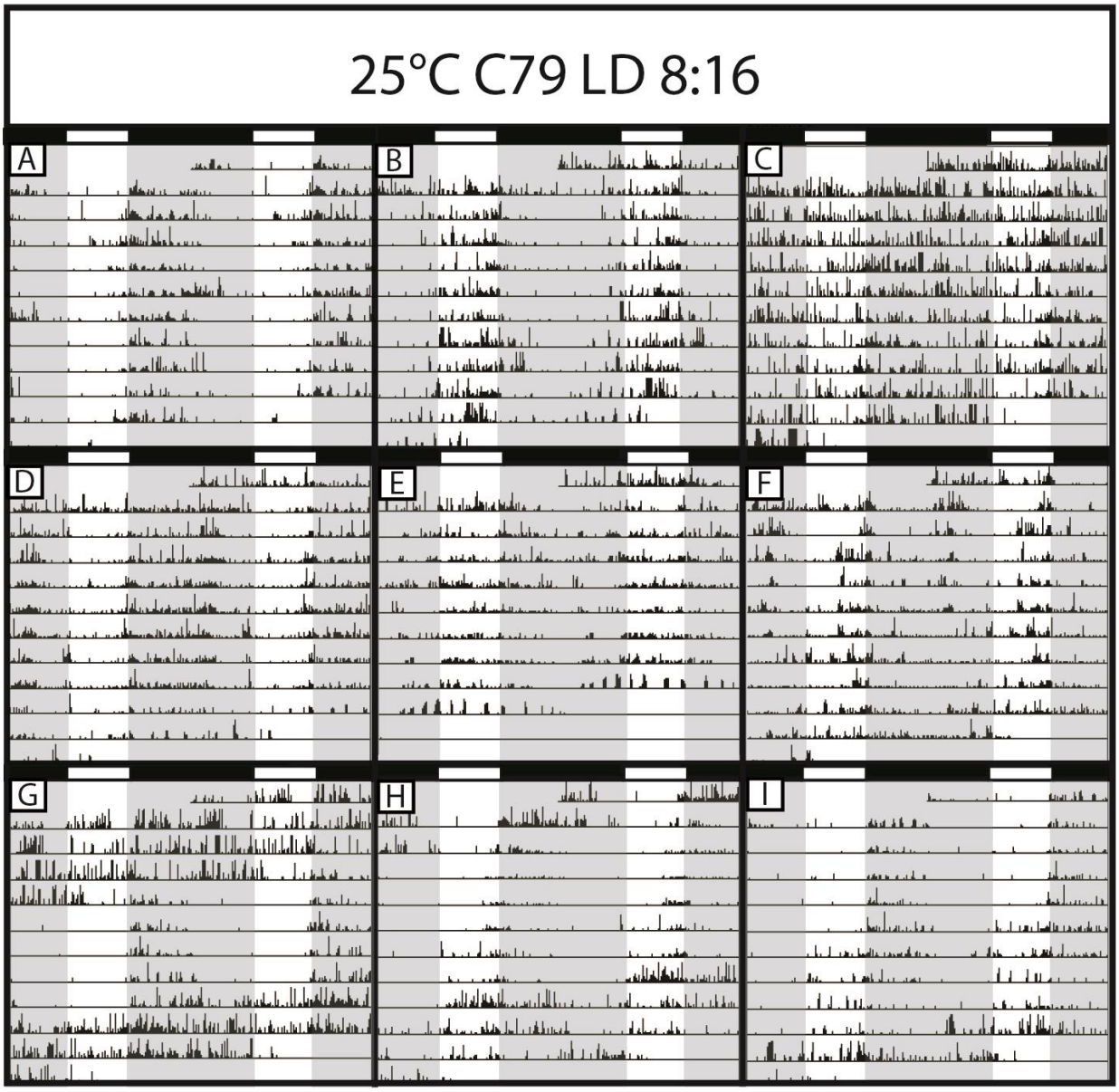

Figure 14: Selected actograms of individuals at LD 8:16, 25°C. A-I) A light bar over each actogram indicates the LD cycle in black (dark) and white (light). The light gray rectangles in the actograms also indicate the dark phase. Each actogram is double-plotted, representing two consecutive days per line. Each line starts at ZT16 and ends at ZT 16 of the consecutive day, showing 48 hours of recording. The black ticks on the line represent activity in beam crosses/minute, upper level =7. A,D) individuals with main entrained activity during the dark phase B,E) individuals with main entrained activity during the light phase C) not entrained/arrhythmic individual F) individual with simultaneous activity peaks in dark and light g) animal switching from arrhythmic to dark phase to arrhythmic activity H) individual with activity in the light phase (pseudo-switch) I) individual switching activity from the dark to the light phase.

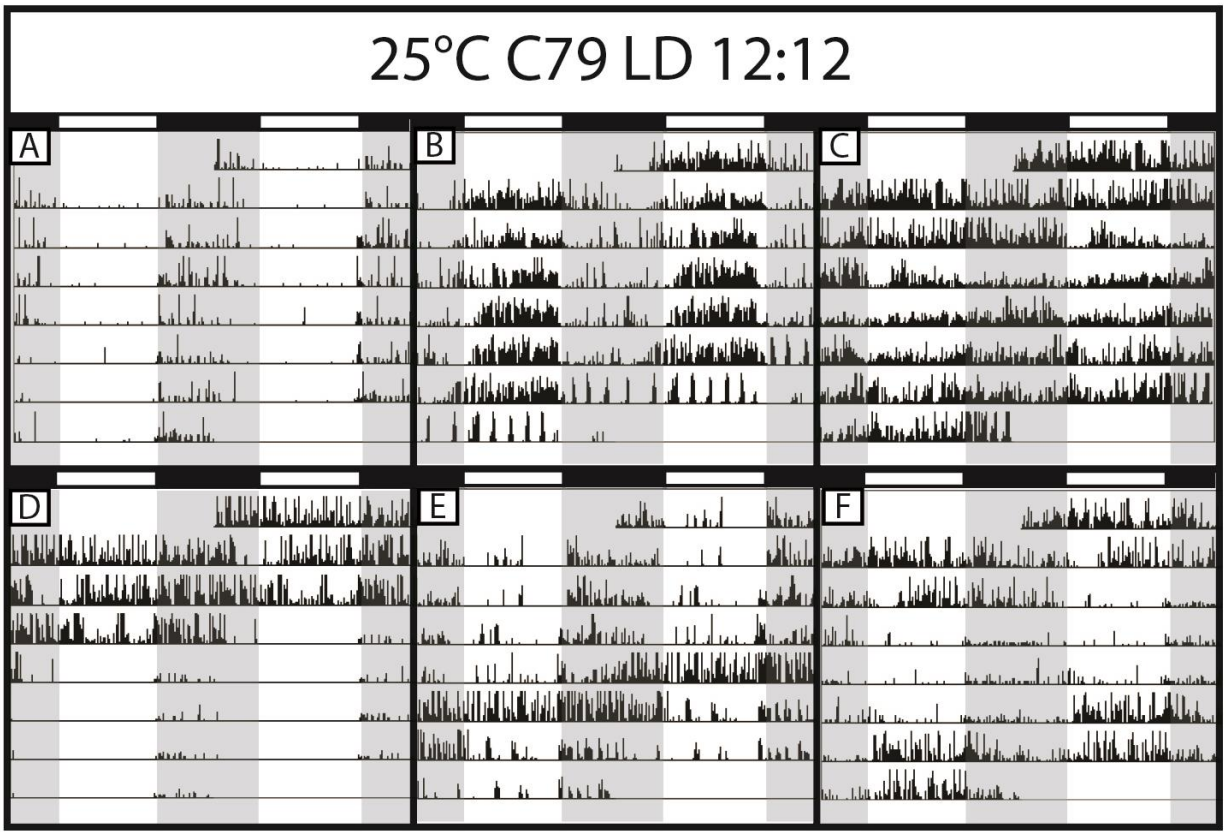

Figure 15: Selected actograms of individuals at LD 12:12, 25°C. A-F) A light bar over each actogram indicates the LD cycle in black (dark) and white (light). The light gray rectangles in the actograms also indicate the dark phase. Each actogram is double-plotted, representing two consecutive days per line. Each line starts at ZT18 and ends at ZT 18 of the consecutive day, showing 48 hours of recording. The black ticks on the line represent activity in beam crosses/minute, upper level =7. A) individual with main entrained activity during the dark phase B) individual with main entrained activity during the light phase C) not entrained/arrhythmic individual D) animal switching from arrhythmic to dark phase activity E) individual with simultaneous activity peaks in dark and light F) individual switching from dark to light phase activity

Overall, the amount of time during the dark phase at which dark-preferring ants were active seems to be individual at LD 8:16 and LD 12:12. While there were no ants active during the complete 16 hours of darkness at LD 8:16, ants kept at LD 12:12 sometimes were active during the whole 12 hours of darkness (not depicted). At LD 16:8, all dark-preferring ants were active for the complete 8 hours of darkness. The light-phase active ants in Fig. 14B,E; 15B and 16B, have their main activity phase during the light, but also extend some activity into the dark phase. The ant in Fig. 15E does the same thing to such an amount that it is even debatable whether the animal prefers the light or dark phase, though it could be argued that it prefers the light phase, which represents the center of this ants` activity phase. All ants that preferred the light phase were active throughout the whole light phase. The arrhythmic ants in Fig. 14C, 15C and

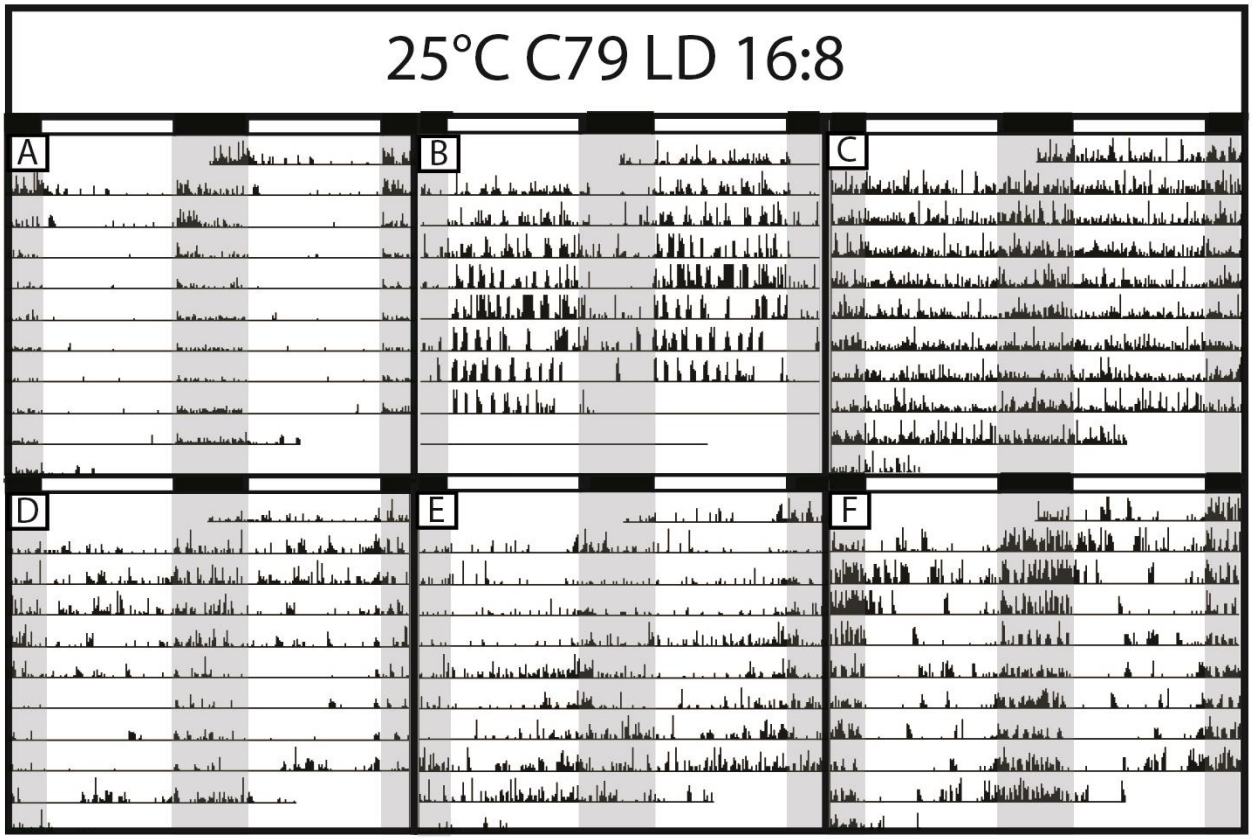

Figure 16: Selected actograms of individuals at LD 16:8, 25°C. A-F) A light bar over each actogram indicates the LD cycle in black (dark) and white (light). The light gray rectangles in the actograms also indicate the dark phase. Each actogram is double-plotted, representing two consecutive days per line. Each line starts at ZT20 and ends at ZT 20 of the consecutive day, showing 48 hours of recording. The black ticks on the line represent activity in beam crosses/minute, upper level =7. A) individual with main entrained activity during the dark phase B) individual with main entrained activity during the light phase C) not entrained/arrhythmic individual D) animal switching from arrhythmic to dark phase to arrhythmic activity E) individual switching from dark to light phase activity F) individual with simultaneous activity peaks in dark and light

16C are active all day and show no distinct peaks at any distinct time. In Fig. 14G, 15D and 16D, individuals starting with random activity, switch to a clear preference for the dark phase after some days, and completely restrain their activity to that phase. The individuals at LD 8:16 (Fig. 14G) and LD 16:8 (Fig. 16D) switch back to arrhythmic activity shortly before the end of recording. Though most animals have either a clear preference for one phase or are completely arrhythmic, the individuals in Fig. 14F,I; 15E-F and 16E-F show defined activity in both phases. This preference for both phases can be either simultaneous (Fig. 14F, 15E, 16F) or switching from one phase to the other (Fig. 14I, 15F, 16E). Fig. 14F shows an ant that has distributed its activity peaks between the light and dark phase and is clearly entrained to both on days 2 to 6 of the recording. The first peak is visible at the end of the light phase, the second approximately 12 hours later shortly after the middle of the dark phase. After five days the activity peak in the

dark is lost and the ant seems to progress towards arrhythmic activity. While the individuals in Fig.15E and 16F exhibit the highest levels of activity during the dark phase, a small yet defined peak can be seen in the light phase too. Disturbances in the pattern as on day 5 (Fig. 15E), where the ant becomes uniformly active for 24 hours, then switches back to its former behavior, can be found at all LD regimes. Fig. 14I, 15F and 16E on the other hand most probably show a switch of preferred phase of activity. After 5 days of clear activity in the dark phase (Fig. 14I), activity starts from the beginning of the light phase but still extends into the dark phase on day six. After two days, activity is limited to the light phase and seems to dissolve into arrhythmicity after two further days of activity in the light phase. The individual in Fig. 15F also displays dark preference after two days of arrhythmicity, and then switches to locomotor activity in the light phase for the last two days of recording. The individual in Figure 16F switches from a slight preference for the dark phase to a slight preference for the light phase after approximately four days. To verify whether these ants truly prefer the light phase from there on, more days of recording would have been necessary. Though the individual in Fig. 14H could be thought to be switching from dark to light phase activity, a closer look reveals that main activity started shortly before the end of the light phase from the beginning of the recording, and simple extended into the dark phase. After six days activity is shifted to start at the beginning of the light phase and thus completely lies within the light phase, before it dissolves in arrhythmicity on day eight. In summary, all different types of individual activity could be found under all LD conditions, none were limited to a certain type of LD. The evaluation of the preferred LD phase of individuals recorded at each LD can be found in Figure 17 and reveals that the majority of minor workers preferred the dark phase (LD 8:16 = 67%, LD 12:12 = 73%, LD 16:8 = 73%) and that there was no significant difference in the composition of preferences between the different conditions (Chi^2=13.0, p=0.11). When looking at differences between the single preference types at the three LD conditions in detail, the individuals showing a preference for a distinct phase of the LD were compared in reference to all other individuals that did not prefer this phase. The preference for the light phase proved to be significantly different between the LD conditions (Chi^2=9.1, p=0.01).

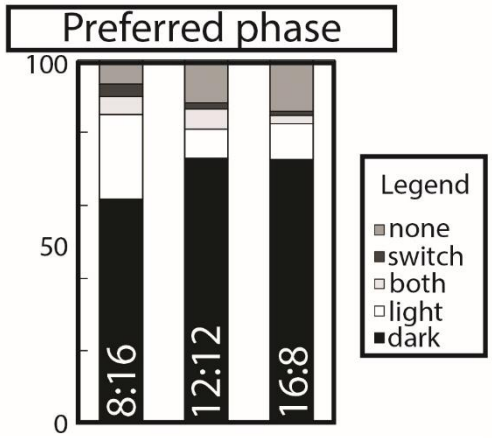

Figure 17: The distribution of preference for the different LD phases in each LD condition. Main entrained activity in dark phase (black), light phase (white), both (light gray), switching between light and dark (dark gray), none/arrhythmic (medium gray). Sample size: LD 8:16 n=59; LD 12:12 n=112, LD 16:8 n=91.

Whereas 23% of all ants were mostly active in the light phase at LD 8:16, only 8% and 10% chose this phase at LD 12:12 or LD 16:8. This results in significant differences in preference for the light phase between conditions LD 8:16 and LD 12:12 (Chi^2=7.8, p=0.005) and LD 8:16 and LD 16:8 (Chi^2=5.1, p=0.025), but not LD 12:12 and LD 16:8 (Chi^2=15.5, p<0.001). The numbers of animals that were arrhythmic were not significantly different between the different conditions (LD 8:16 = 13%, LD 12:12 = 14%, LD 16:8 = 9%, Chi^2=2.1, p=0.35). The number of individuals that showed preference for both phases is very low, only 5% of ants show rhythmic activity in both light and dark phase simultaneously at LD 8:16 and LD 12:12, at LD 18:6 the percentage shrinks to 2% and there is no significant difference between conditions (Chi^2=1.8, p=0.41). The ants displaying switching preferences are even lower in abundance, only 3% at LD 8:16, 2% at LD 12:12 and 1% at LD 16:8 display this type of behavior and there is no significant difference between conditions (Chi^2=0.9, p=0.63).

Looking at the average activity profiles of all ants in Figure 18, behavior under all three LD regimes shows similar trends. All average activity profiles show distinct peaks at lights off and smaller peaks at lights on. Under LD 8:16, activity is the lowest from the middle of the dark phase to the middle of the light phase, then starts to slowly rise and peaks at lights off, from where activity declines again until the middle of the dark phase. At LD 12:12 and 16:8 activity is uniformly lowest during the light phase and rises

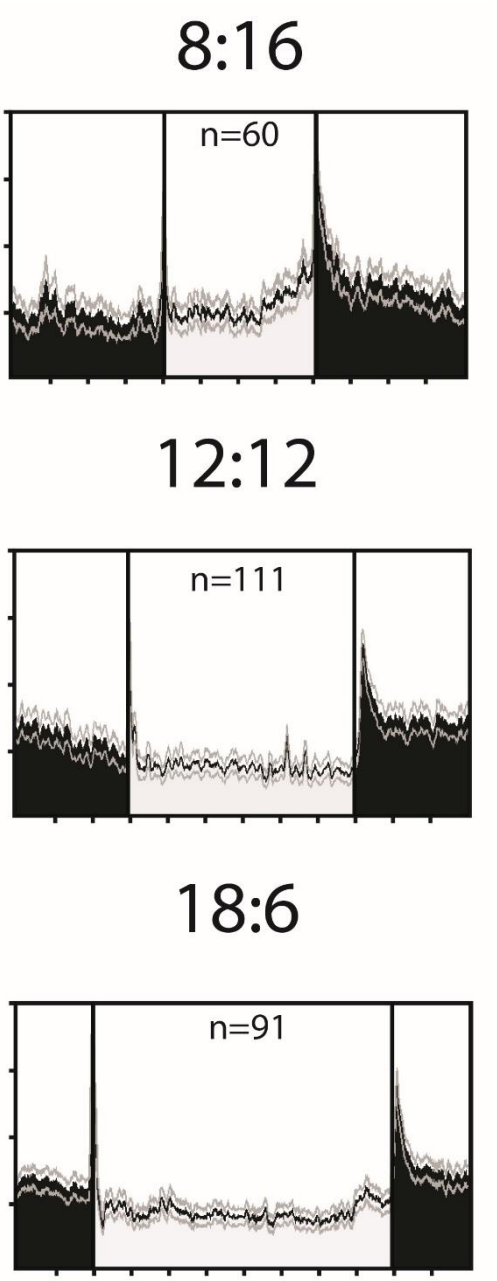

Figure 18: Average daily activity profiles of all individuals at LD 8:16, LD 12:12 and LD 16:8; n= number of averaged individuals; x-axis: time/hours starting in the middle of the dark phase, two-hour intervals; y-axis: moving average (beam crosses/minute); vertical black lines =lights on and off; black areas = dark phase , light gray areas = light phase; horizontal black line = average of beam crosses; horizontal gray lines = standard deviation.

into a sharp peak at the onset of the dark phase, without an anticipatory rise at the end of the light phase. Activity levels then decline but stay higher during the dark phase than during the light phase. Comparing average activity during the whole day, dark and light phases (Figure 19), only the average activity during the dark phase shows significant differences between the different conditions (Kruskal-Wallis: H(2)= 22.7, p =0.000012). While average activity during the whole day did not differ significantly between 0.9 ± 0.1 (LD 8:16), 1.0 ± 0.1 (LD 12:12) and 1.1 ± 0.1 (LD 16:8) beam crosses per minute (Kruskal-Wallis: H(2)= 2.5, p =0.29), there were significant differences between the average activity during the dark phase at LD 8:16 (0.9 ± 0.1 beam crosses per minute) and LD 12:12 (1.3 ± 0.1 beam crosses per minute) (Post-hoc pairwise Wilcoxon p=0.002) and between LD 8:16 and LD 16:8 (1.5 ± 0.1 beam crosses per minute) (Post-hoc pairwise Wilcoxon p<0.0001). Average activity during the dark phase was not significantly different between LD 12:12 and LD 16:8 (Post-hoc pairwise Wilcoxon p=0.15). During the light phase, no significant differences of average activity were recorded (Kruskal-Wallis: H(2)= 4.2, p =0.12) at 0.9 ± 0.1 (LD 8:16), 0.8 ± 0.1 (LD 12:12) and 0.9 ± 0.1 (LD 16:8) beam crosses per minute.

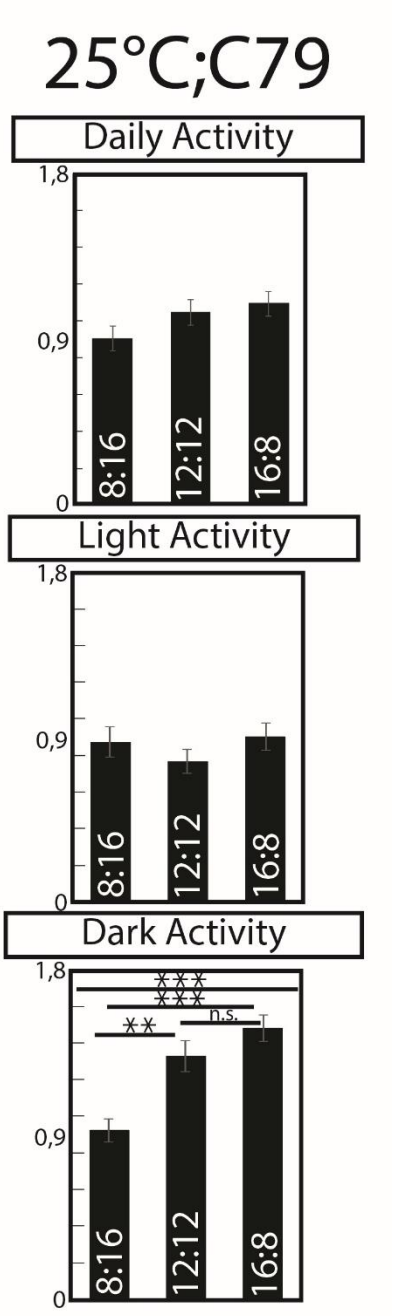

Figure 19: Average activity during the whole day, the light and the dark phases in beam crosses per minute. Only the activity during the dark phase differed significantly. Significance levels are indicated by stars, * p≤0.05, **p≤0.01, ***p<0.001. Sample size LD 8:16 n=59; LD 12:12 n=112, LD 16:8 n=91.

3.1.2 *C. floridanus* has an endogenous period that is temperature compensated

Additional to testing the influence of different LD-cycles, the influence of different temperatures on locomotor behavior has been tested on two different colonies. Since free-running behavior, with an endogenous period length close to 24 hours under constant conditions, is also a defining property of the circadian clock, ants were also monitored under constant darkness after they had been entrained by a LD-cycle. Since the effect of changing temperature was tested, the LD was kept constant at 12:12 hours of light and darkness for both experiments. In both colonies, temperature had a significant effect on survival, but there was no significant effect of colony when comparing within one temperature (25°C: Chi^2=0.15, p=0.69; 30°C: Chi^2=0.8, p=0.37). In colony C79, survival was higher at 30°C with 56%, than at 25°C with 36% (Chi^2=4.3, p=0.03). In contrast, survival was higher at the lower temperature of 25°C with 64% and only 25% at 30°C in colony C152 (Chi^2=7.0, p=0.008). Entrainment to the LD cycle was equally high in all conditions (83-93%) and there were no significant differences between temperatures within colonies or

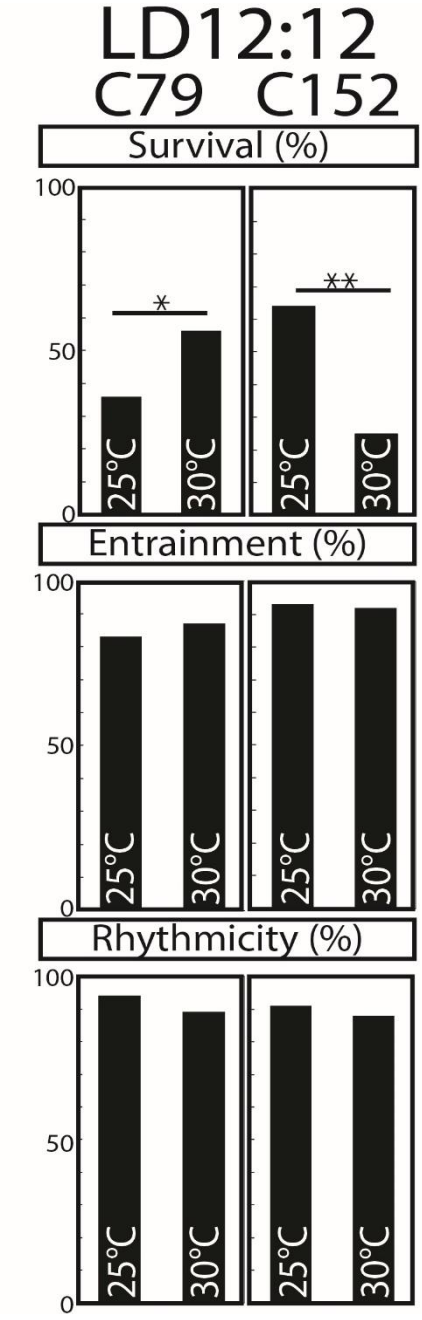

Figure 20: Survival, Entrainment and Rhythmicity of Individuals kept at LD 8:16, 12:12 and 16:8 at 25°C. Survival: The percentage of ants that were still alive after 18 days. Sample size: C79: 25°C n=128; 30°C n=64; C90: 25°C n=64, 30°C n=64. Entrainment: The percentage of ants showing patterns of activity in the LD. Sample size: C79: 25°C n=47; 30°C n=36; C90: 25°C n=46, 30°C n=32. Rhythmicity: The percentage of ants with a significant period length in DD. Significance levels are indicated by stars, * p≤0.05, **p≤0.01, ***p<0.001. Sample size: C79: 25°C n=128; 30°C n=64; C90: 25°C n=64, 30°C n=64.

colonies within temperatures (C79: Chi^2=0.21, p=0.64; C152: Chi^2=0.01, p=0.92; 25°C: Chi^2=2.12, p=0.15; 30°C: Chi^2=0.48, p=0.49). The rhythmicity of the same ants under DD was equally high, at 94% (C79) and 91% (C152) at 25°C and 89% (C79) and 88% (C152) at 30°C. Again, no statistically significant differences were detected between temperature conditions or colony (C79: Chi^2=0.59, p=0.44; C152: Chi^2=0.29, p=0.59; 25°C: Chi^2=0.18, p=0.67; 30°C: Chi^2=0.03, p=0.85). In summary, almost all living individuals were able to entrain and showed rhythmic free-running behavior under both temperatures and in both colonies. There are several types of behavior that can be found in actograms of all conditions (Fig. 21-24). The most common type preferred the dark phase in LD, then started rhythmic activity from the subjective dark phase in constant conditions (Fig. 21A, 22A, 23A,D, 24A). Whether activity in

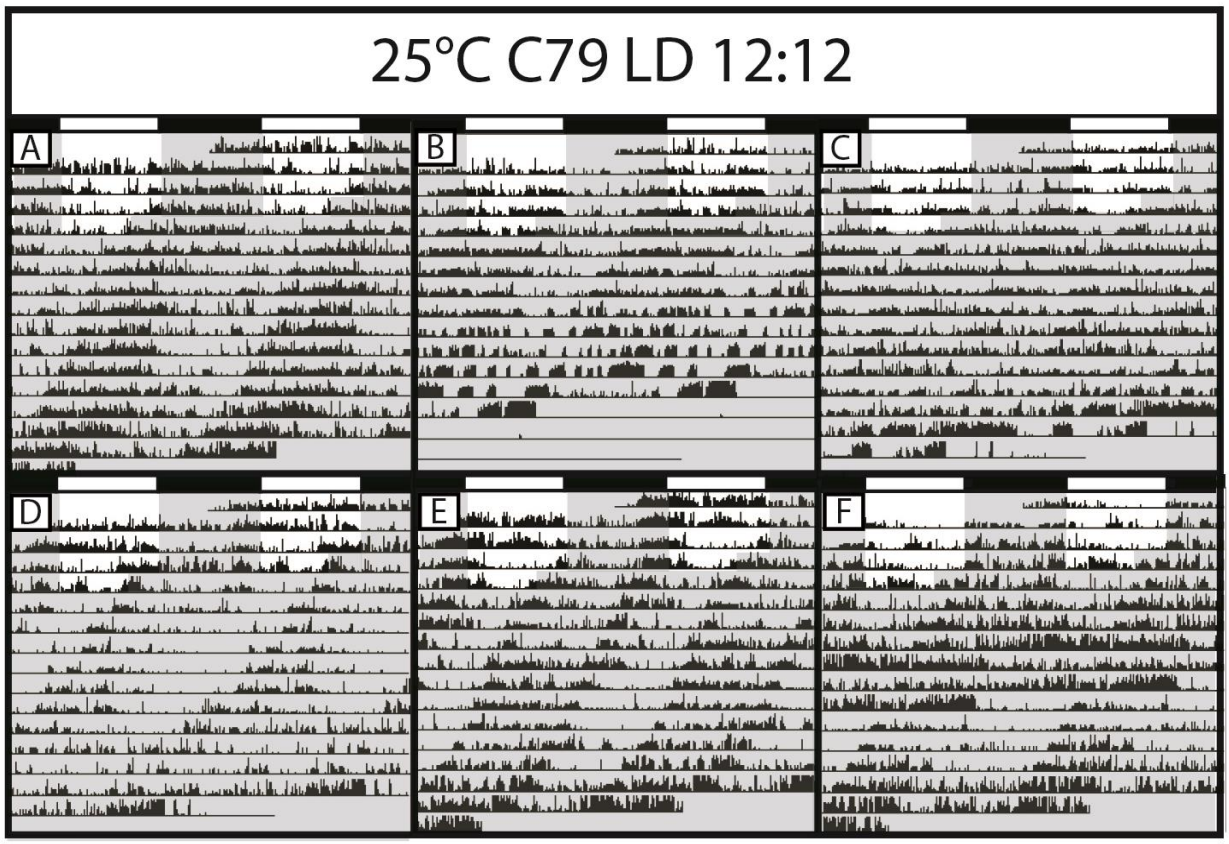

Figure 21: Selected actograms of individuals of colony C79 at LD 12:12, 25°C. A-F) A light bar over each actogram indicates the LD cycle in black (dark) and white (light). The light gray rectangles in the actograms also indicate the dark phase. Each actogram is double-plotted, representing two consecutive days per line. Each line starts at ZT18 and ends at ZT 18 of the consecutive day, showing 48 hours of recording. The black ticks on the line represent activity in beam crosses/minute, upper level =7. A) individual with main activity during the dark phase, free-run starting from the dark phase B) individual with main activity during the light phase, free-run starting from the light phase C) not entrained/arrhythmic individual D) animal switching from arrhythmic to free- run from the dark phase, then becoming arrhythmic again E) individual with simultaneous activity peaks in dark and light, free run starting from the dark phase F) individual active during dark phase, arrhythmic at beginning of constant darkness, then switching to rhythmic activity with start from the dark phase.

the LD spanned the whole dark phase (Fig. 21A, 23D, 24A) or only a part of it (Fig. 22A, 23A), did not depend on colony or temperature, both could be observed under all conditions. Two other typical types of activity are preference for the light phase, with activity starting from the subjective light phase (Fig. 21B, 22B, 23B, 24B) and complete arrhythmicity in both, the LD and DD (Fig. 21C, 22C, 23C, 24C). Again, whether the ant was active throughout the whole light phase (Fig. 23B,E, 24B) only during parts (Fig.22B) or even spilling some activity into the dark phase (Fig. 21B) was not dependent on the temperature or colony.

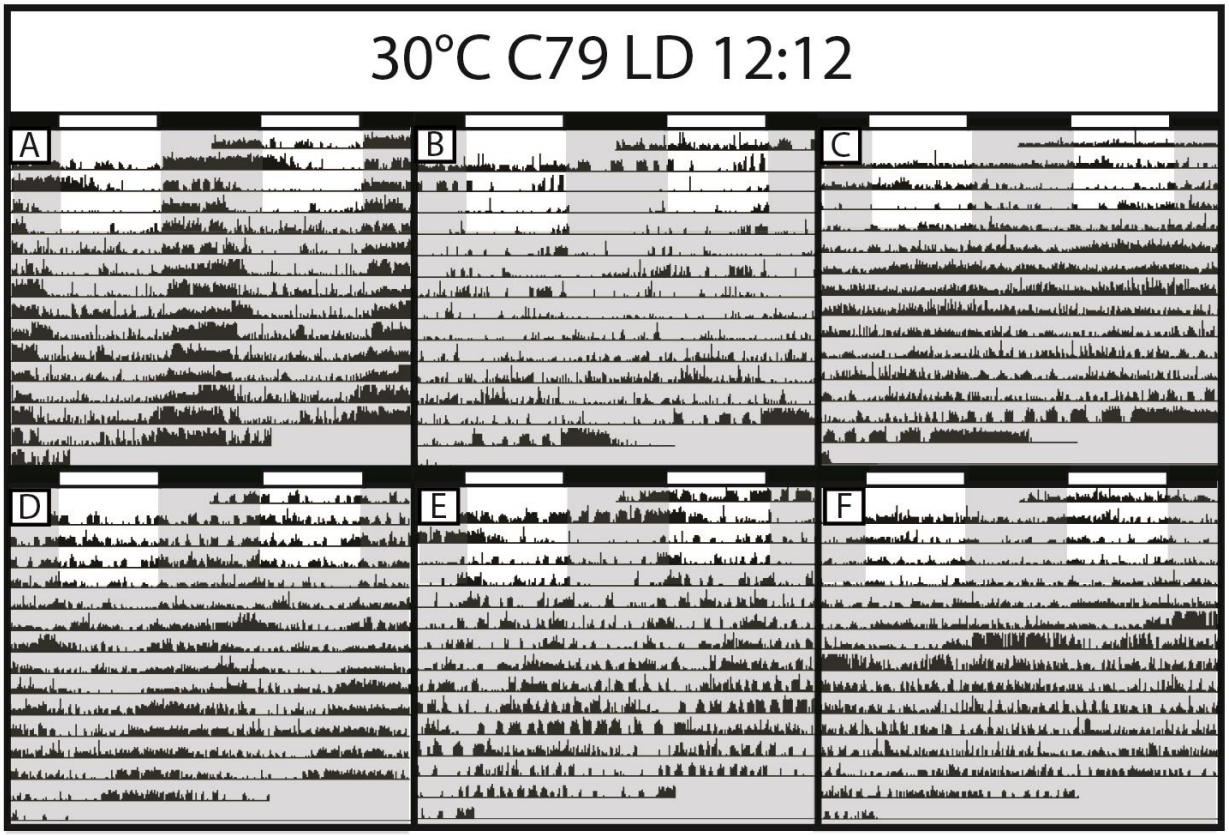

Figure 22: Selected actograms of individuals of colony C79 at LD 12:12, 30°C. A-F) A light bar over each actogram indicates the LD cycle in black (dark) and white (light). The light gray rectangles in the actograms also indicate the dark phase. Each actogram is double-plotted, representing two consecutive days per line. Each line starts at ZT18 and ends at ZT 18 of the consecutive day, showing 48 hours of recording. The black ticks on the line represent activity in beam crosses/minute, upper level =7. A) individual with main activity during the dark phase, free-run starting from the dark phase B) individual with main activity during the light phase, free-run starting from the light phase C) not entrained/arrhythmic individual D) animal switching from arrhythmic to free- run from the dark phase E) individual with simultaneous activity peaks in dark and light, free run starting from the dark phase F) individual active during light phase, arrhythmic in constant darkness.

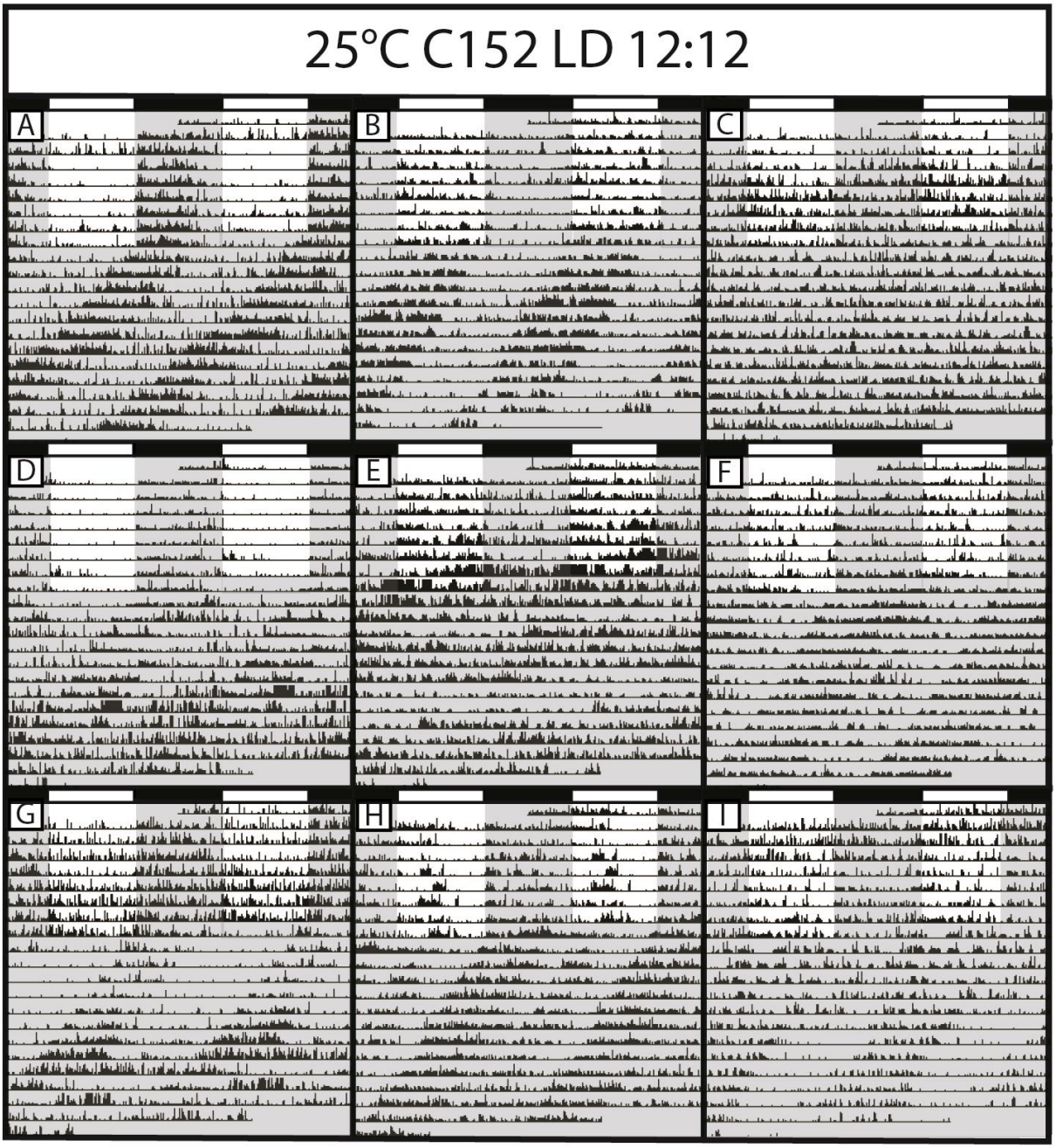

Figure 23: Selected actograms of individuals of colony C152 at LD 12:12, 25°C. A-I) A light bar over each actogram indicates the LD cycle in black (dark) and white (light). The light gray rectangles in the actograms also indicate the dark phase. Each actogram is double-plotted, representing two consecutive days per line. Each line starts at ZT18 and ends at ZT 18 of the consecutive day, showing 48 hours of recording. The black ticks on the line represent activity in beam crosses/minute, upper level =7. A) individual with main activity during the dark phase, free-run starting from the dark phase B) individual with main activity during the light phase, free-run starting from the light phase C) not entrained/arrhythmic individual D) animal switching from dark entrained to free- run from the dark phase, then becoming arrhythmic E) individual with main activity in light phase becoming arrhythmic in DD F) arrhythmic individual in LD with rhythmic DD behavior starting from dark phase G) arrhythmic individual in LD, with rhythmic activity in DD starting from dark phase H)individual with simultaneous activity peaks in dark and light, free run starting from the dark phase with a second peak coming from the light phase I) arrhythmic individual in LD, arrhythmic at beginning of constant darkness, then switching to rhythmic activity with start from the light phase.

Some ants showed preference for both phases of the LD, either at the transition points between dark and light (Fig. 21E, 22E), or with primary (strongest) activity during the dark phase and a second, smaller but distinct, peak in the middle of the light phase (Fig. 23H, 24E). If these ants were rhythmic in constant darkness, activity always started from the dark phase, sometimes the second peak persisted (Fig. 24H), sometimes it disappeared after a few days in DD changing to complete subjective nocturnality (Fig. 21E, 22E, 24E) Though these types of consistent activity were the most common (see above, 79-89% of individuals showed

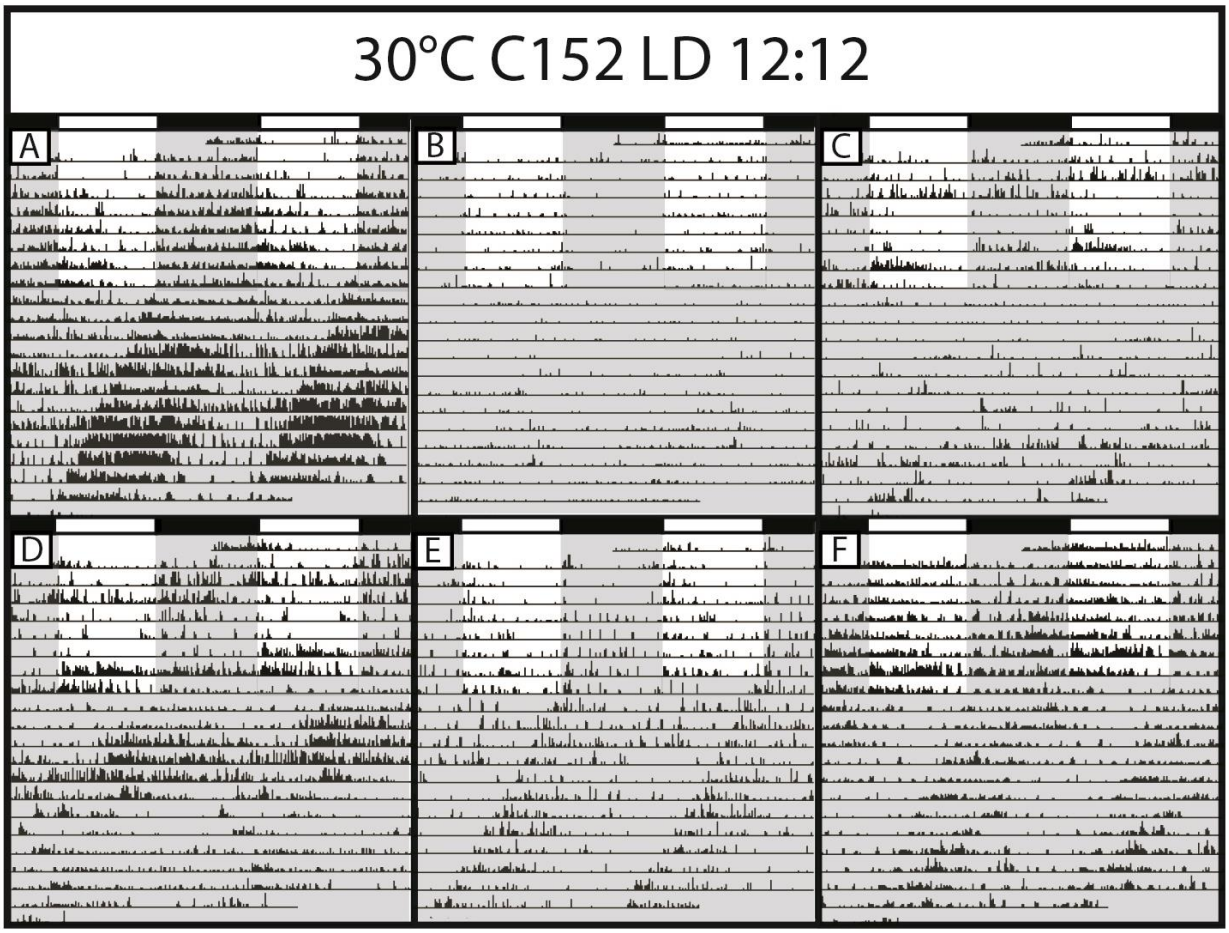

Figure 24: Selected actograms of individuals of colony C152 at LD 12:12, 30°C. A-F) A light bar over each actogram indicates the LD cycle in black (dark) and white (light). The light gray rectangles in the actograms also indicate the dark phase. Each actogram is double-plotted, representing two consecutive days per line. Each line starts at ZT18 and ends at ZT 18 of the consecutive day, showing 48 hours of recording. The black ticks on the line represent activity in beam crosses/minute, upper level =7. A) individual with main activity during the dark phase, free-run starting from the dark phase B) individual with main activity during the light phase, free-run starting from the light phase C) not entrained/arrhythmic individual D) animal switching from arrhythmic to free- run from the dark phase, then changing period from shorter than 24h to longer than 24h E) individual with simultaneous activity peaks in dark and light, free run starting from the dark phase F) individual arrhythmic in LD, rhythmic activity in DD with start from the dark phase.

consistency between behavior in LD and DD) there were also some individuals that changed between arrhythmic, entrained and rhythmic behavior. Figures 21D, 22D, 23F,G,I, and 24F all show examples of animals that are arrhythmic in the LD, but display rhythmic behavior under constant conditions. The rhythmic activity can be both, nocturnal (Fig. 21D, 22D, 23F,G, 24F) or diurnal (Fig. 23I), Figure 24F even shows nocturnal activity with a second activity where the subjective day is. Just as some individuals change from arrhythmic to rhythmic, others are entrained to the LD and become arrhythmic in constant darkness (Fig. 21F, 22F, 23E). Again, the prefered phase can be either light (Fig. 22F, 23E) or dark (Fig. 21F). Some ants lose their rhythmicity after a few days of rhythmic behavior in DD (Fig. 23E), others from the onset of constant conditions (Fig. 21F, 22F). Whether the individual stays arrhythmic from then on (Fig. 22F) or reverts back to rhythmic activity (Fig. 21F, in this case with start of activity from the preferred phase) is up to the individual ant. In Figure 25, the composition of preferences for a certain phase of the LD, the activity type (nocturnal, diurnal, arrhythmic) under DD and the consistency between those two properties is plotted. Again, the majority of workers preferred the dark phase, with 60% and 63% at 25°C and 30°C in colony C79 and 57% and 50% in colony C152. Overall, there was no significant difference in preference for the dark phase between the temperatures in colony C79 (Chi^2=0.40, p=0.94) or C152 (Chi^2=1.28, p=0.73), and also no differences between the

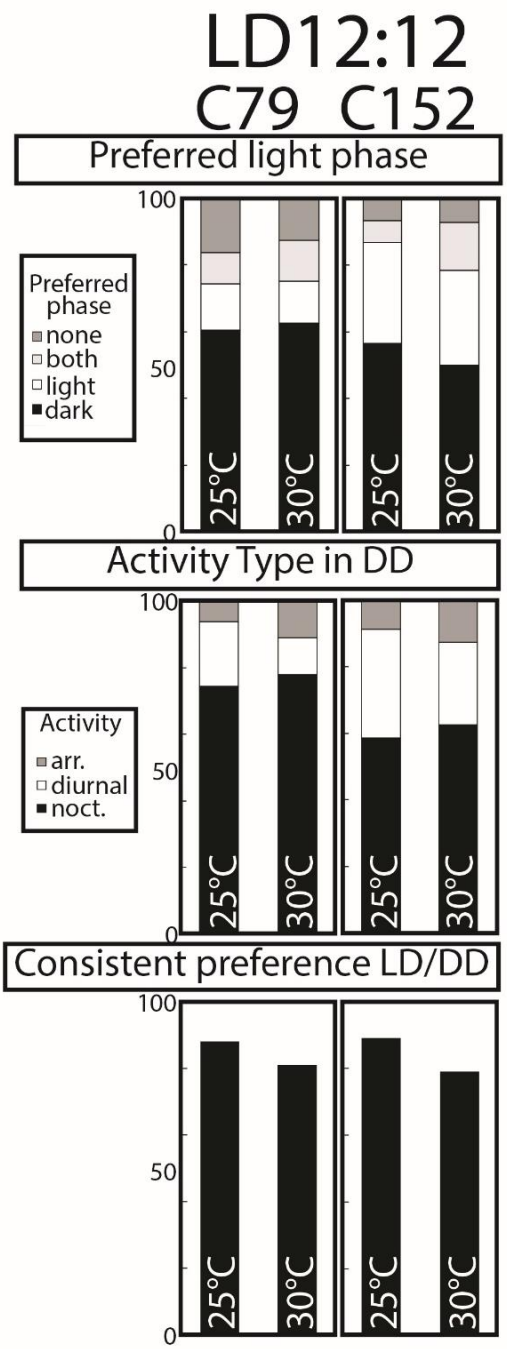

Figure 25: The distribution of preference for the different LD phases, activity type and the consistency of both at 25°C and 30°C in Colonies C79 and C152. Legend Preferred Phase: Main entrained activity in dark phase (black), light phase (white), both (light gray), none/arrhythmic (medium gray). Legend Activity Type: Nocturnal (black), Diurnal (white), Arrhythmic (medium gray). Consistent preference: The percentage of ants that started their free-run from their entrained phase of the LD. Sample size: C79: 25°C n=128; 30°C n=64; C90: 25°C n=64, 30°C n=64

two colonies (25°C: Chi^2=0.7.5, p=0.10; 30°C: Chi^2=2.8, p=0.42). A closer look at the percentage of preference for the light phase (C79: 25°C=14%, 30°C=13%; C152: 25°C=30%, 30°=29%) revealed no differences between the two temperatures in each colony (C79: Chi^2=0.03, p=0.85; C152: Chi^2=0.02, p=0.36), but between the two colonies at 25°C. Here, a significantly higher percentage of ants of colony C152 preferred the light phase (Chi^2=3.47, p=0.06). At 30°C, the difference between the two colonies was not significant (Chi^2=2.41, p=0.12). Looking at the activity in DD, nocturnality is, in reference to preference for the dark phase, also the most common type of behavior. At 25°C, 75% of individuals from colony C79 and 59% of all individuals from colony C152 were nocturnal. At 30°C, 78% of individuals from colony C79 and 63% of all individuals from colony C152 were nocturnal. Even though there seems to be a trend of a slight increase in nocturnal animals at higher temperatures, this is not significant (C79: Chi^2=0.12, p=0.73; C152: Chi^2=0.11, p=0.74), and there is also no significant difference between the colonies (25°C: Chi^2=2.60, p=0.11; 30°C: Chi^2=1.90, p=0.17). The same is true for diurnal ants. The consistency between entrainment to a phase of the LD and start of free-running activity from this phase was high under all conditions, ranging from 79% at 30°C (C152), over 81% at 30°C (C79) and 88% at 25°C (C79) to 89% at 25°C (C152). No significant differences in consistency were found between any of the conditions (C79: Chi^2=0.31, p=0.58; C152: Chi^2=2.56, p=0.11; 25°C: Chi^2=0.19, p=0.66; 30°C: Chi^2=0.34, p=0.65). Comparing the average days calculated for all individuals of each condition in Figure 26, it becomes apparent that both colonies have prominent peaks of activity at lights-on and lights-off at both temperatures. Activity declines after both peaks and stays constant throughout the dark phase, before it rises again slightly before lights off. The rise before lights-on is more prominent in colony C79 at 25°C, than in the other conditions. There are also some slight differences between the two colonies in the average behavior during the light phase. The average of individuals in colony C79 first decline in activity until the middle of the light phase, then show a rise before the peak at lights off. Ants of colony C152 on the other hand show a steady decline of activity with no rise before the peak at lights off. The average of activity during the whole day, the light and the dark phase (Fig. 27) was tested in a two-way ANOVA for influences of temperature and colony. The only significant effects where those of colony on the average activity during the whole day and dark phase. For activity during the whole day, the main effect of temperature yielded an F ratio of $F_{(1,224)}$=0.24, p=0.61, indicating no significant difference between 25°C (mean=1.31, SD=0.73) and 30°C (mean=1.22, SD=0.59). The main effect of

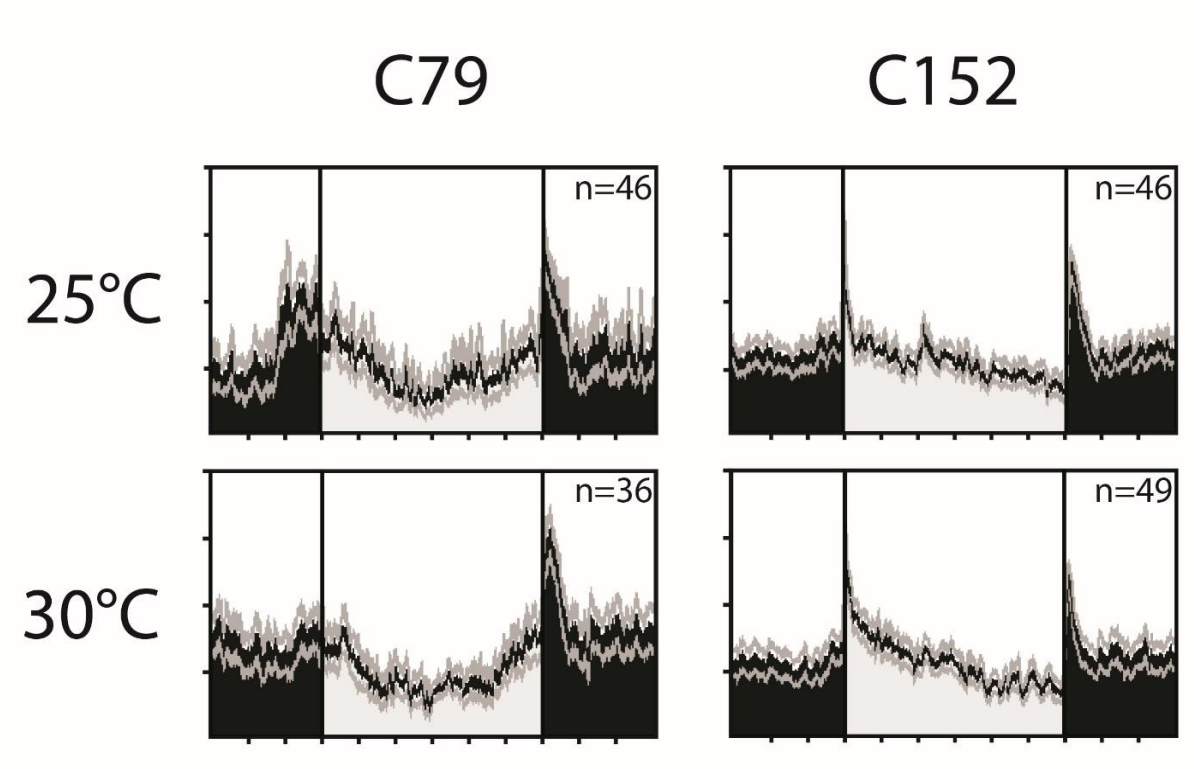

Figure 26: Average daily activity profiles of all individuals at 25°C and 30°C for each colony; n= number of averaged individuals; x-axis: time/hours starting in the middle of the dark phase, two-hour intervals; y-axis: moving average (beam crosses/minute); vertical black lines =lights on and off; black areas = dark phase , light gray areas = light phase; horizontal black line = average of beam crosses; horizontal gray lines = standard deviation.

colony yielded an F ratio of $F_{(1,224)}$=5.22, p=0.02, indicating significant difference between colonies C79 (mean=1.37, SD=0.75) and C90 (mean=1.15, SD=0.35). The interaction effect was not significant $F_{(1,224)}$=0.50, p=0.48. For activity during the light phase, the main effect of temperature yielded an F ratio of $F_{(1,224)}$=1.57, p=0.21, indicating no significant difference between 25°C (mean=1.19, SD=0.85) and 30°C (mean=1.06, SD=0.61). The main effect of colony yielded an F ratio of $F_{(1,224)}$=0.70, p=0.41, indicating no significant difference between colonies C79 (mean=1.19, SD=0.88) and C90 (mean=1.08, SD=0.60). The interaction effect was not significant $F_{(1,224)}$=2.28, p=0.13. For activity during the dark phase, the main effect of temperature yielded an F ratio of $F_{(1,224)}$=0.13, p=0.71, indicating no significant difference between 25°C (mean=1.42, SD=0.73) and 30°C (mean=1.38, SD=0.77). The main effect of colony yielded an F ratio of $F_{(1,224)}$=11.12, p=0.001, indicating significant difference between colonies C79 (mean=1.55, SD=0.76)and C90 (mean=1.22, SD=0.69). The interaction effect was not significant ($F_{(1,224)}$=0.076, p=0.78). This indicates that colony C79 is on average more

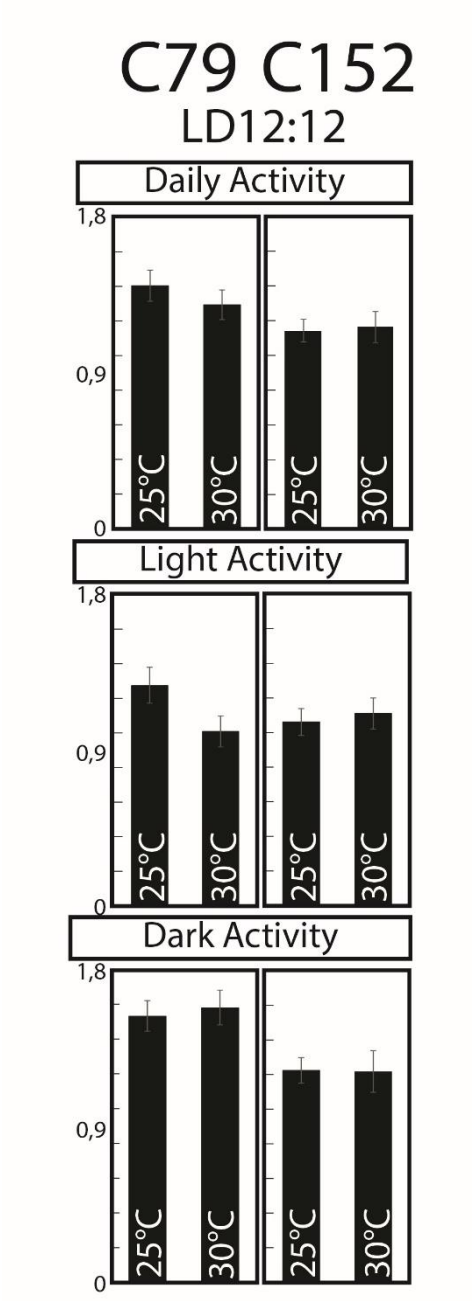

Figure 27:Average activity of colonies C79 and C152 at 25°C and 30°C, during the whole day, the light and the dark phases in beam crosses per minute. Sample size: C79: 25°C n=128; 30°C n=64; C90: 25°C n=64, 30°C n=64

active during the whole day and the dark phase, but not the light phase, than colony C152. Looking at the behavior of rhythmic individuals during the constant dark period of the experiment, several conclusions about the free-running behavior and period length can be drawn (Fig. 21- 24). The onset of activity is shifted to the left every day, indicating a period shorter than 24 hours (e.g. Fig. 21A,B, 22A,B, 23A,B, 24 A,B). Comparing the two nocturnal ants in Fig. 21A and 22A, it becomes apparent that the shift of activity is much more pronounced at 25°C than at 30°C. This bigger shift at 25°C can be found in most individuals of colony C79 and colony C152, though it is less prominent (compare e.g. Fig. 23A and 24A), and indicates a shorter period length at the lower temperature. The average of period lengths calculated from the actograms confirm this (Fig. 27). A two-way ANOVA was conducted to test for influences of temperature and colony on the period length. Significant effects of temperature and temperature:colony interaction on the average period length were found. The main effect of temperature yielded a F ratio of $F_{(1,142)}=80.57$, $p<0.0001$, indicating significant difference between 25°C (mean=1432, SD=29.46) and 30°C (mean=1392, SD=40.77). The main effect of colony yielded a F ratio of $F_{(1,142)}=0.53$, $p=0.47$, indicating no significant difference between colonies C79 (mean=1365 min, SD=49.84) and C90 (mean=1360 min, SD=33.07). The interaction effect was significant $F_{(1,142)}=9.88$, $p=0.002$. A Tukey post-hoc test revealed that the difference between the period length of 22.3h at 25°C and 23.8h at 30°C was significant ($p<0.0001$) for colony C79. The period lengths of 22.5h at 25°C and 23.0h at 30°C were also significantly

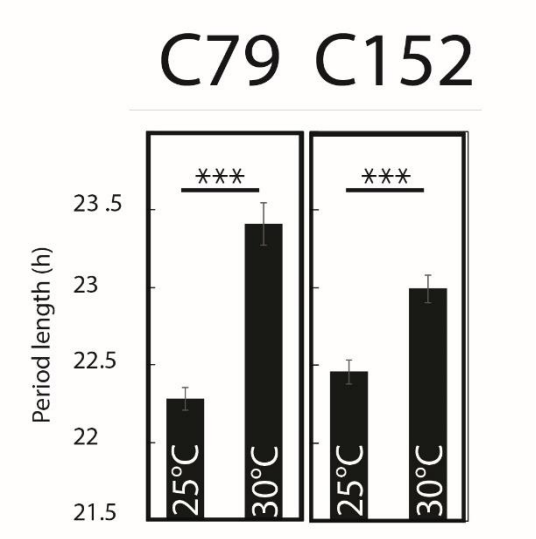

Figure 28: Average period lengths of colonies C79 and C152 at 25°C and 30°C. Significance levels are indicated by stars, * p≤0.05, **p≤0.01, ***p<0.001. Sample size: C79: 25°C n=128; 30°C n=64; C90: 25°C n=64, 30°C n=64

different (p=0.0008) for colony C152, indicating a temperature overcompensation of their clocks.

3.2 Minor and major ants of *C. floridanus* have a similar PDF-network

The PDF-network and neuropils of minor and major workers of *C. floridanus* were very similar in overall organization, but not size. Figures 29 and 30 provide an overview of the PDF fibers and neuropils in minor and major brains of *C. floridanus*. To gain a first impression, composition pictures of the complete brains from anterior and posterior, and the reconstruction of PDF fiber networks and all neuropils from anterior, posterior dorsal and ventral, are depicted here. The brain of *C. floridanus* features neuropils that can be found in many insects, a protocerebrum (PB), that consists of several smaller neuropils, optic lobes (OL), consisting of lamina (LA), medulla (ME) and lobula (LO), mushroom bodies (MB) with very prominent and large medial and lateral calyces (MCX,LCX), peduncles (PED), vertical and medial lobes (VL, ML), antennal lobes (AL) consisting of a large number of glomeruli and a subeosophageal ganglion (SOG) (Fig. 29 A,C and 30A,C) . A further common structure can be found inside the protocerebrum, the central complex (CCX) and protocerebral bridge (Pb). All these neuropils are present in both, the major and minor brains (see Figures 29A,C and 30A,C), though their shapes and sizes vary slightly. The biggest differences can be found in the optic lobes. Major workers have elongated optic stalks with a large, spherical lobula and medulla, and a bean-shaped lamina. The optic lobes of minor workers on the other hand are very compact and hardly protrude from the central brain, resulting in seemingly smaller and more hemispherically shaped laminae and an overall smaller distance between the single neuropils of the optic lobes.

Fibers of the PDF network can be found in almost all neuropils of the minor and major brain, with the most prominent and widespread arborizations in the optic lobes and the protocerebrum (Fig. 29A,B and 30A,B). The somata of the network rest slightly anterior to level with the medulla, and can be found between the medullas dorso-proximal edge, the distal face of the ventrolateral protocerebrum and the distal edge of the lateral calyx, superior of the lobula (Fig. 29A,B and 30A,B). Since there is less space overall in the minor brain, the somata are often pushed a little more to the dorsal area anterior of the medulla (Fig. 29A left pictures). In the major brains, somata are usually not this far dorsal in relation to the medulla, but rest at its proximal elongation (Fig. 30A). The number of PDF cell bodies varied in both sizes of ants. In minor ants, a cluster consists of minimally 5 up to maximally 9 cell bodies, with an average of 7 ± 1 cells (see Fig. 29B for examples of clusters of different cell number). The numbers of PDF stained somata at 8 different time-points (data taken from Experiment 6) were evaluated. There is no significant effect of the time point of staining on the number of cell bodies (Kruskal-Wallis: $H(7)=10.12$, $p=0.18$).

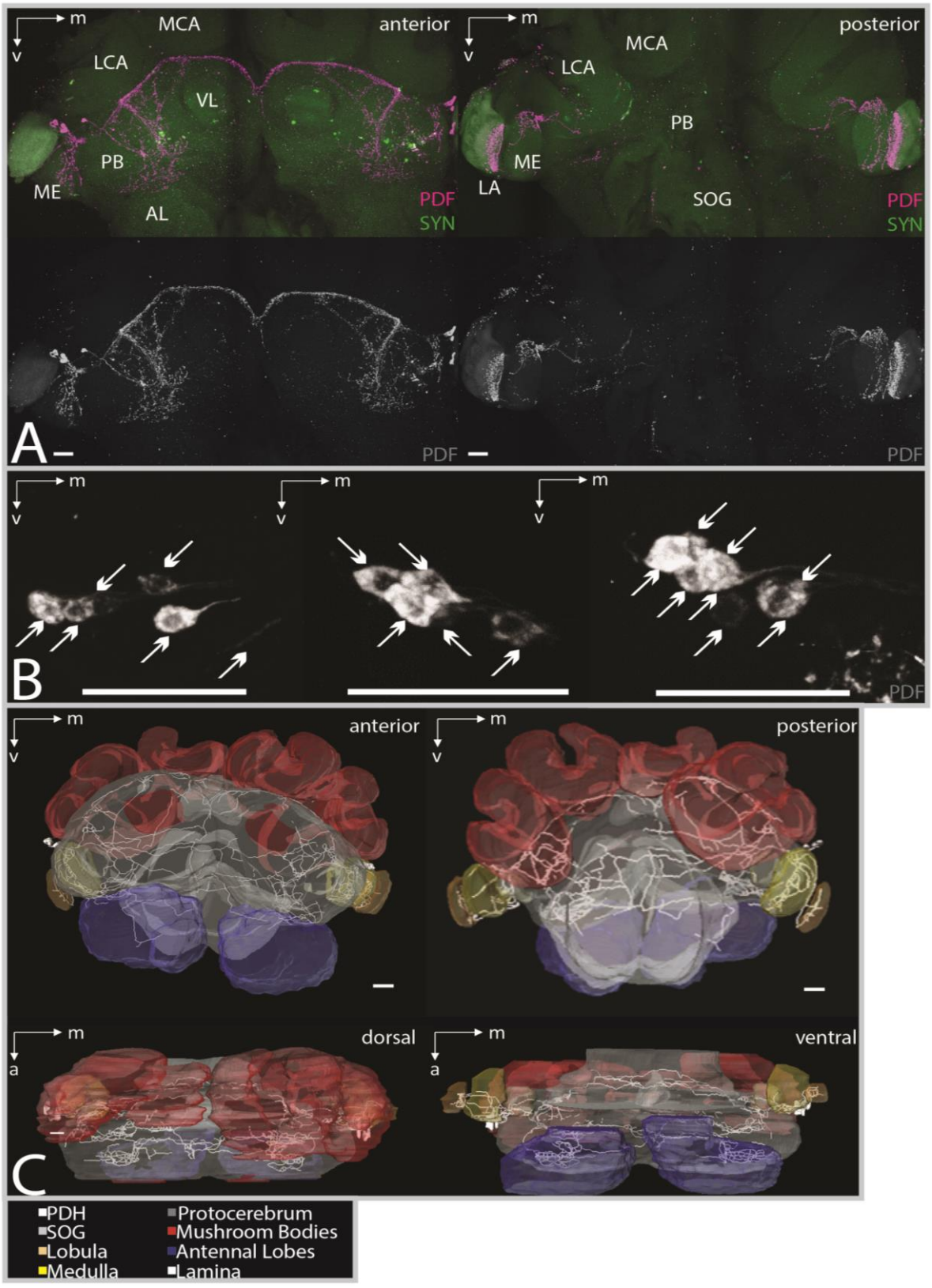

Figure 29: description see next page

Figure 29: An overview of the PDF-network and the neuropils of the minor brain. All scale bars are set to 50µm. Abbreviations: AL = antennal lobes, MCA/LCA = medial/lateral calyx, ME = medulla, PB = protocerebrum, VL = vertical lobe. A) Staining of the PDF-fibers (magenta, grey) and SYNAPSIN (green) in a whole minor brain, the left picture depicts the anterior part of the brain, the right the posterior. The upper pictures show a merging of the PDF and SYN channels, the lower the PDF channel alone. PDF staining can be found in the optic lobes, protocerebrum, in the antennal lobes, the SOG, with the densest arborizations of fibers in the anterior distal regions of the protocerebrum and the superior protocerebrum. The somata of the network can be found between the proximal side of the medulla and the distal edges of the lateral calyx and protocerebrum. B) The PDF cell bodies (gray) of three individuals, each cell body is marked with an arrow. From left to right: 6, 5 and 8 somata. In the picture on the left some somata are a little bit separated from the rest of the cluster, in the middle and left picture all somata form a dense cluster. C) The reconstruction of the PDF network (white) and neuropils (see legend) from anterior (upper left), posterior (upper right), dorsal (lower left) and ventral (lower right). As in the staining, PDF fibers can be found throughout the protocerebrum, optic lobes, antennal lobes and SOG. The rotated reconstruction seen from the dorsal or ventral side reveals that fibers can be found in different layers (from anterior to posterior) of the brain, with the most fibers in the anterior part of the protocerebrum and on the anterior surface. The medulla is also innervated in two layers, one on the anterior surface, the other in the middle. Number of images (2µm thickness) of the confocal stack overlayed per picture: A) 47(left), 56(right) B) 10 (left), 9 (middle), 11 (right).

Since there was additional staining of PDF-fibers in individuals from another colony, C90, the four timepoints available for this (Experiment 7) were also evaluated and again no significant effect of timepoint stained on the average number of cell bodies ($H(3)=1.91$, $p=0.59$) was found. Table 13 lists average cell body numbers (±SD) of all timepoints in both colonies.

Table 13: Average number of PDF somata of individuals from two different colonies at different time-points. nA= Data not available at this timepoint

Timepoint	ZT0	ZT3	ZT6	ZT9	ZT12	ZT15	ZT18	ZT21
Colony C79	7.1 ± 0.82	7.0 ± 0.82	7.25 ± 0.96	7.33 ± 0.71	5 ± 0.96	6.25 ± 0.96	7.5 ± 1.05	6.56 ± 1.67
Colony C90	7.0 ± 0.82	nA	6.0 ± 1.67	nA	6.67 ± 0.52	nA	6.88 ± 1.36	nA

There is also no significant difference between the mean numbers of 6.62 ±1.21 PDF somata for C90 and 6.86 ±1.28 for colony C79 ($H(1)=1.35$, $p=0.25$), indicating a conserved range of PDF somata number in minor workers. The number of major cell bodies of on average 8 ± 2 cell bodies on the other hand differs significantly from that of minor cell bodies (both counted in 20 wholemount brains collected at ZT 4), with on average 7 ± 1 cell bodies ($H(1)=9.08$, $p=0.002$). The lower boundary of cell numbers was again at 5 cell bodies, but the upper boundary now exceeded to 11 cell bodies. Figure 30B shows cell body clusters of major brain hemispheres, ranging from 6 (middle), over 8 (left) to 9 cell bodies (right).

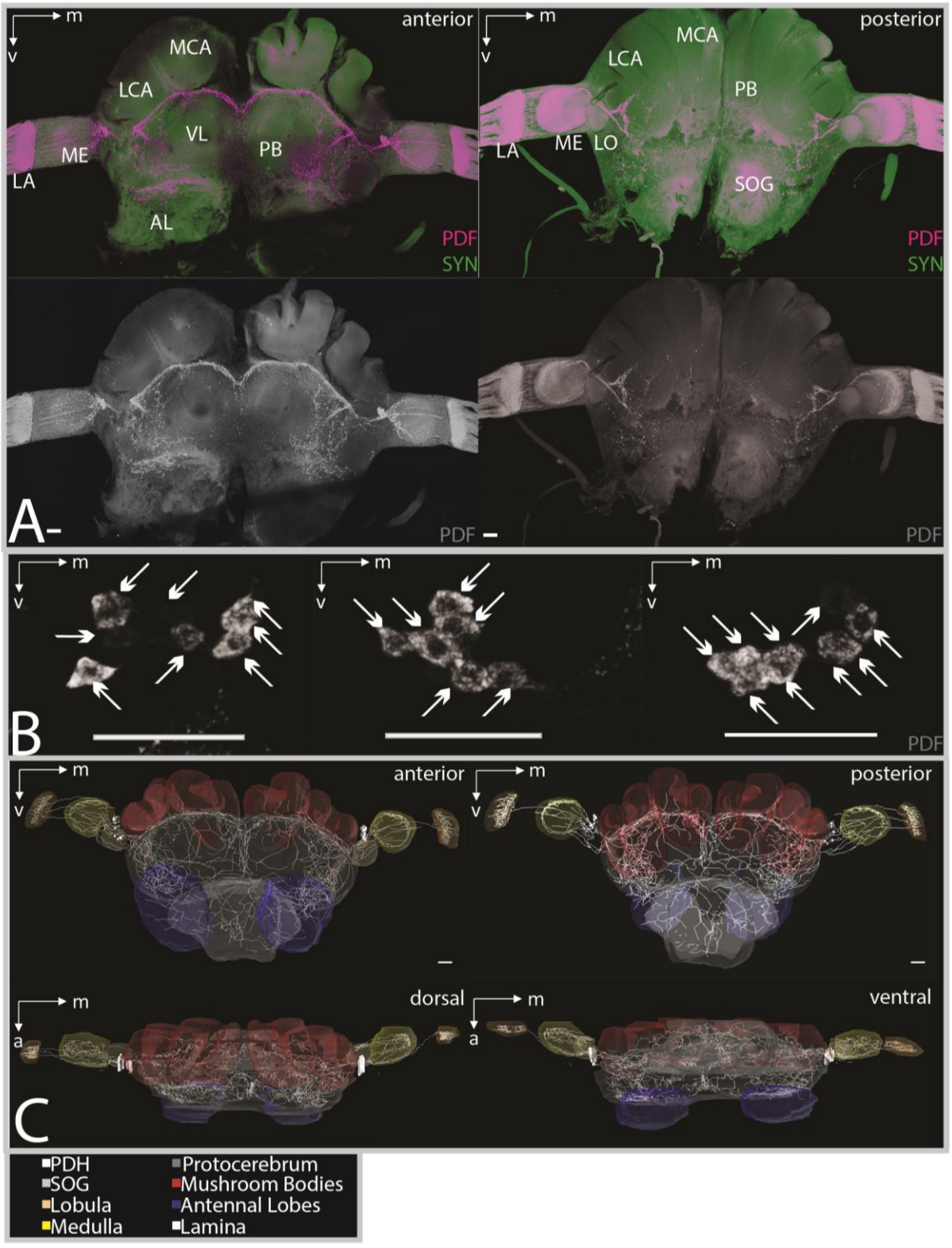

Figure 30: description see next page

Figure 30: An overview of the PDF-network and the neuropils of the major brain. All scale bars are set to 50µm. Abbreviations: AL = antennal lobes, MCA/LCA = medial/lateral calyx, ME = medulla, PB = protocerebrum, VL = vertical lobe. A) Staining of the PDF-fibers (magenta, grey) and SYNAPSIN (green) in a whole minor brain, the left picture depicts the anterior part of the brain, the right the posterior. The upper pictures show a merging of the PDF and SYN channels, the lower the PDF channel alone. PDF staining can be found in the optic lobes, protocerebrum, in the antennal lobes, the SOG, with the densest arborizations of fibers in the anterior distal regions of the protocerebrum and the superior protocerebrum. The somata of the network can be found between the proximal side of the medulla and the distal edges of the lateral calyx and protocerebrum. B) The PDF cell bodies (gray) of three individuals, each cell body is marked with an arrow. From left to right: 6, 5 and 8 somata. In the picture on the left some somata are a little bit separated from the rest of the cluster, in the middle and left picture all somata form a dense cluster. C) The reconstruction of the PDF network (white) and neuropils (see legend) from anterior (upper left), posterior (upper right), dorsal (lower left) and ventral (lower right). As in the staining, PDF fibers can be found throughout the protocerebrum, optic lobes, antennal lobes and SOG. The rotated reconstruction seen from the dorsal or ventral side reveals that fibers can be found in different layers (from anterior to posterior) of the brain, with the most fibers in the anterior part of the protocerebrum and on the anterior surface. The medulla is also innervated in two layers, one on the anterior surface, the other in the middle. Number of images (2µm thickness) of the confocal stack overlayed per picture: A) 39 (left), 33 (right) B) 12 (left), 15 (middle), 18 (right).

Most clusters were as dense as the rightmost cluster, with somata overlaying each other and thus complicating the counting of the exact number. All cell body numbers were evaluated by scrolling through the confocal image stacks, to avoid missing single cells that were obscured by others in the overlay images. From the somata, fibers protrude into the optic lobes, innervating the medulla and lamina but not the lobula in both minor (Fig. 29A,C, Fig. 31) and major (Fig.30A,C, Fig. 32) brains. A dense bundle of fibers also runs medially into the protocerebrum, giving rise to several branch-offs innervating the anterior and posterior protocerebrum, as well as the antennal lobes and subesophageal ganglion (Fig.29A,C, 30A,C, 32-37). All overviews of complete brain staining, showing the anterior and posterior parts of the PDF-network, are in relation to the fiber-bundle running from the cell bodies towards the protocerebrum. Anterior views contain overlays of all images from the anterior face of the brain until this bundle is fully visible, posterior views overlays of all images from this point to the posterior face of the brain. Since it is not possible to determine whether fibers originate from or run into a structure in these staining, it is always to be assumed that fibers might be running the other way.

3.2.1 The fiber projections in the optic lobes

The fibers in the optic lobes form dense arborizations directly next to the proximal edge of the medulla in minor (Fig. 31A,B,C,E,G) as well as major brains (Fig. 32A,B,D).

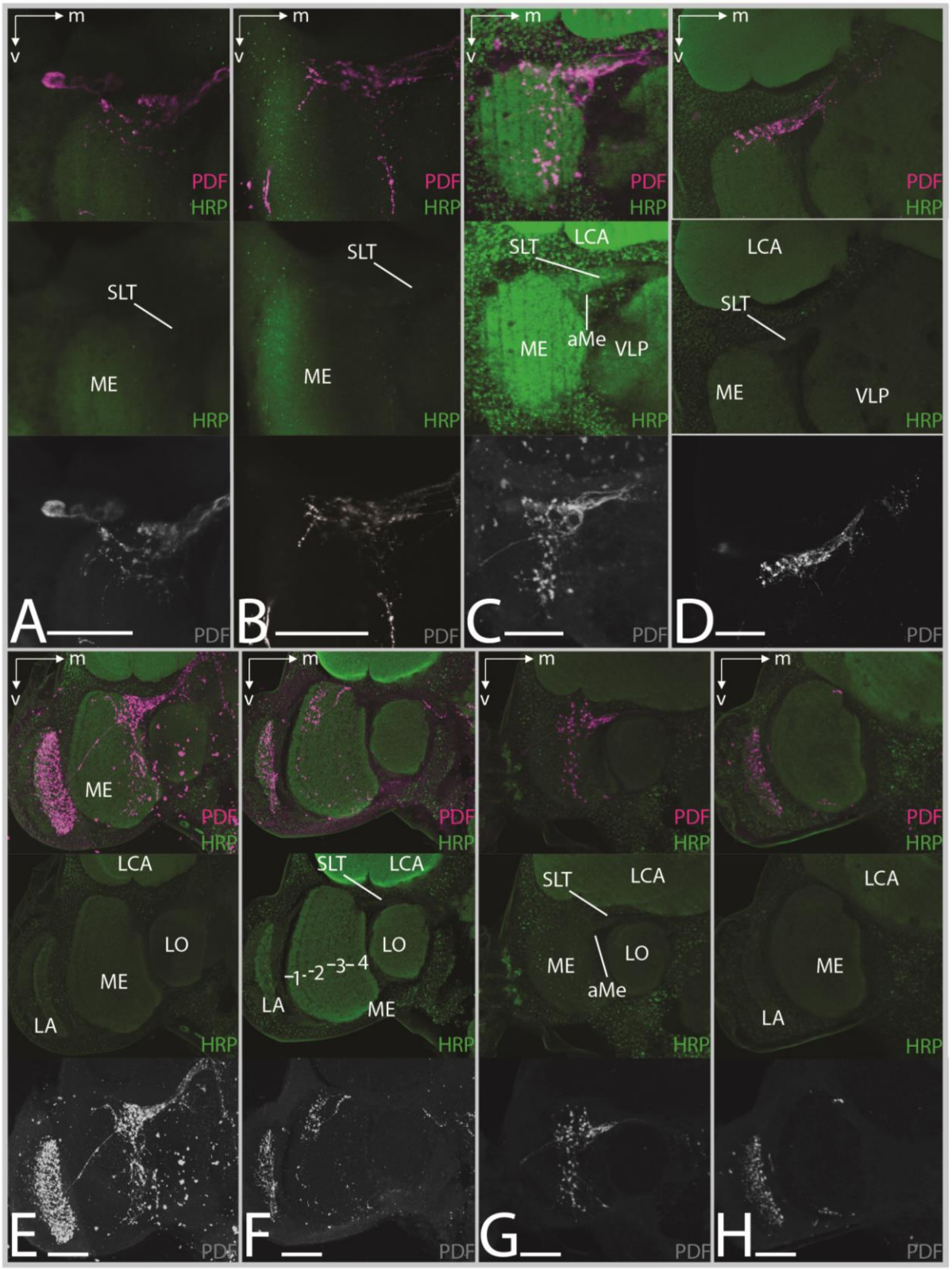

Figure 31: description see next page

Figure 31: The PDF network in optic lobes of minor brains. Confocal image stacks of PDF staining co-stained with HRP. Overlays of the PDF (magenta) and HRP (green) channel, and single channel images of the HRP channel (green) and the PDF channel (grey). All scale bars are set to 50µm. Abbreviations: aMe= accessory medulla, LA = lamina, LCA = lateral calyx, LO = lobula, ME = medulla, SLT = superior lobula tract, VLP = ventrolateral protocerebrum. A-C) Detailed images of the triangular shape formed by the arborizations at the proximal edge of the lamina in different brains. D) The SLT tract. E-G) The PDF-fibers in anterior (E,G) and posterior (F,H) parts of the medulla and lamina. E+F are consecutive images of the same optic lobe (anterior to posterior), the same applies to G+H. The anterior fiber fan, and a single fiber crossing the optic chiasma can be seen in E and G, as well as innervations in the lamina in E. More medial innervations of the serpentine layer of the medulla and more fibers in the lamina in F and H. The layers of the medulla are indicated in F). Number of images (2µm thickness) of the confocal stack overlayed per picture: A) 6 B) 6 C) 4 D) 6 E) 35 F) 30 G) 10 H) 9.

This arborization area is triangular in shape and seems to innervate a tiny, triangle-shaped part of the medulla (Fig. 31B,C,G and Fig, 32B,E), most likely the accessory medulla, that later leads into an commissure travelling towards the central brain (Fig. 31 A-E,G and Fig. 32 A-C,E; discussed below). The fibers in this triangle are very dense but show tiny holes, as if growing around an as of yet unstained structure (Fig. 31 B,C and 32A,B). From this triangle, fibers extend into the proximal medulla where they arborize and send projections anterior and distal, forming the anterior fiber fan on the anterior face of the medulla (Fig. 31E,G 32D,E). At least one of the fibers forming the fiber fan crosses the first optic chiasma and extends into the lamina (Fig. 31E,G 32D,E). The anterior fiber fan however is not the only layer of fibers in the medulla. Some fibers extend towards the distal part of the medulla in a more medial layer, innervate the medulla in the first layer (Fig. 31 F,H and 32 F,G) and arborize there. Some fibers from this layer also cross the first optic chiasma (Fig. 32C) adding to the innervations in the lamina. Inside the lamina, both, fibers crossing the optic chiasma anterior and medial, split up and grow dorsal and ventral along the proximal side of the lamina, where numerous smaller fibers branch off perpendicular to innervate the proximal and distal parts of the lamina (Fig. 31E,F,H and Fig. 32 D-F) These sheets of fibers are very dense, innervating the complete lamina. An especially dense region can be found at the ventral edge of each lamina (Fig. 31E, 32D,F). Fibers from the triangle at the base of the medulla do not only travel distal towards the lamina, but also medial, towards the lobula and protocerebrum (Fig. 31A-G and 32A-C,E). These fibers grow inside a tract that is visible in the Synapsin-channel of the confocal images (Fig. 31 A-C,F,G and 32 A,B,E) and travels dorsal of the lobula into the ventrolateral protocerebrum. Thus, this structure will be referred to as the superior lobula tract (SLT). The fibers in this tract form a very dense bundle, making it effectively impossible to follow a single fiber. No innervations of the lobula could be found, all fibers run over its surface.

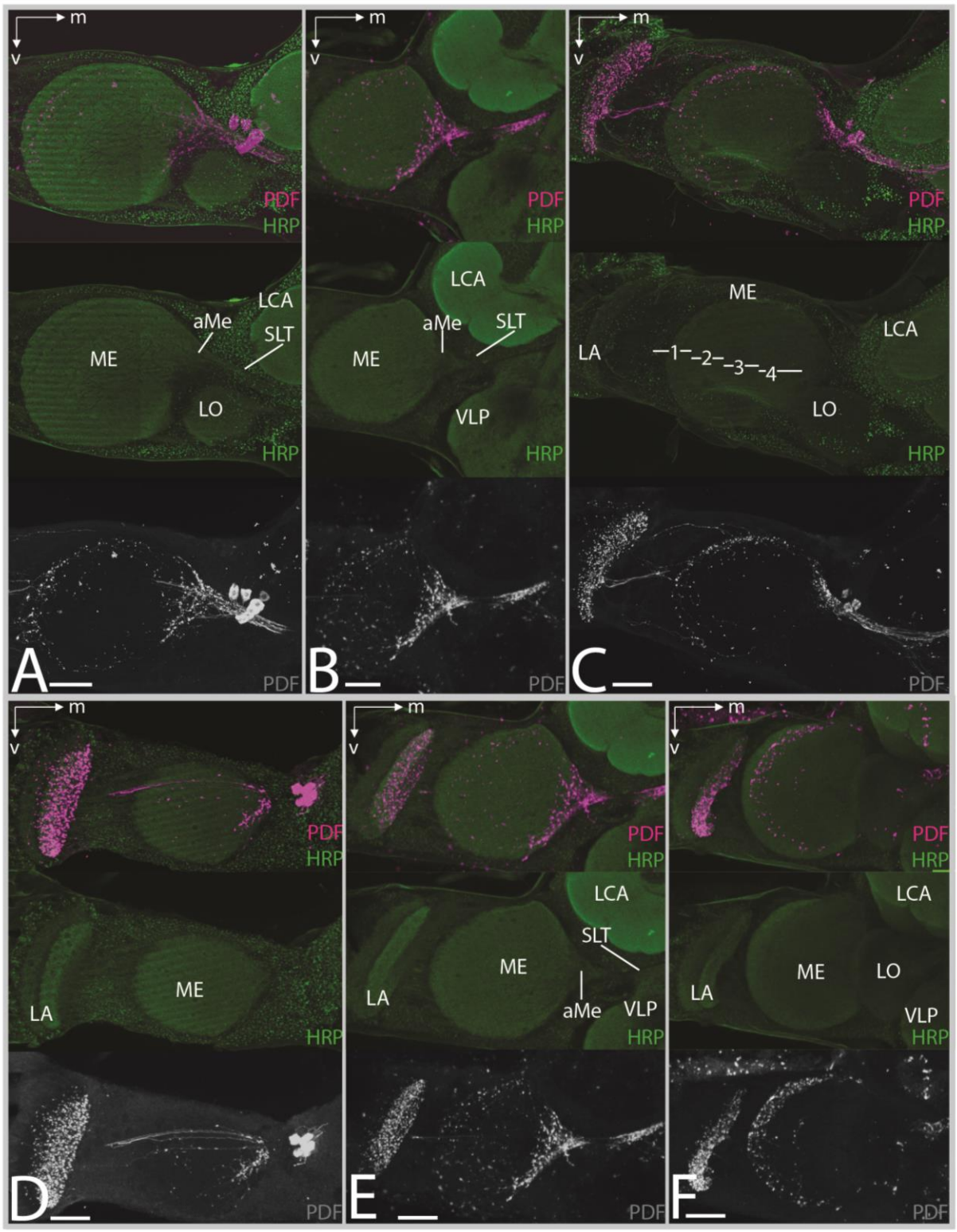

Figure 32: description see next page

Figure 32: The PDF network in optic lobes of major brains. Confocal image stacks of PDF staining co-stained with HRP. Overlays of the PDF (magenta) and HRP (green) channel, and single channel images of the HRP channel (green) and the PDF channel (grey). All scale bars are set to 50µm. Abbreviations: aMe = accessory medulla, LA = lamina, LCA = lateral calyx, LO = lobula, ME = medulla, SLT = superior lobula tract, VLP = ventrolateral protocerebrum. A-B) Detailed images of the triangular shape formed by the arborizations at the proximal edge of the lamina in different brains. C-E) E-G) The PDF-fibers in anterior (D,E) and posterior (C,F) parts of the medulla and lamina. C+D are consecutive images of the same optic lobe (posterior to anterior), the same applies to E+F but from anterior to posterior. The anterior fiber fan, and a single fiber crossing the optic chiasma can be seen in D and E, as well as innervations in the lamina. More medial innervations of the serpentine layer of the Medulla and more fibers in the lamina in C and F, as well as a further fiber crossing the optic chiasma in C. The layers of the medulla are indicated in C. A, B, C and E also provide pictures of the SLT. Number of images (2µm thickness) of the confocal stack overlayed per picture: A) 19 B) 7 C) 34 D) 22 E) 14 F) 18

3.2.2 Fibers in the anterior part of the protocerebrum

Fibers running into the protocerebrum through the SLT split up at the distal edge of the ventrolateral protocerebrum to proceed either into the anterior or posterior part of the protocerebrum, as can be seen in the overviews in Figures 29A,C and 30A,C. The projections running into the anterior part of the protocerebrum can be seen in detail in Figures 33 (minor) and 34 (major). The majority of fibers entering the ventrolateral protocerebrum continue running dorsal and anterior along the superior edge of ventrolateral protocerebrum, superior lateral protocerebrum and superior medial protocerebrum, directly underneath the mushroom body calyces, in the anterior optic commissure (AOC) (Fig. 33A,B and 34A,B). The AOC from both hemispheres meet at the midline in the superior medial protocerebrum, directly underneath the pars intercerebralis (Fig. 33E,G and 34E). Here they either join or merge with the fibers from the other hemisphere, and arborize, creating a small plexus, the midline plexus (p_m). Some fibers from this plexus run down the midline towards the inferior protocerebrum, just anterior of the medial lobes of the mushroom bodies (Fig. 33E and 34D,E). Several fibers and plexi branch off the AOC, forming an intricate network in the anterior ventrolateral protocerebrum, inferior protocerebrum, superior lateral protocerebrum and superior medial protocerebrum. Directly at the border between the ventrolateral protocerebrum and the optic lobes a first, small plexus, the plexus 1 (p_1) is located (Fig. 33A and Fig. 34A,B). Some fibers leave this plexus (arrow next to p_1 in Fig. 33A and 34B), travelling ventrally towards the inferior protocerebrum and antennal lobe (see Fig. 33A,B 34 B,D), joining a huge plexus of fibers, the anterior fiber plexus (AFP) which ramifies extensively in the inferior protocerebrum dorsal of the antennal lobes (more information on the AFP follows below).

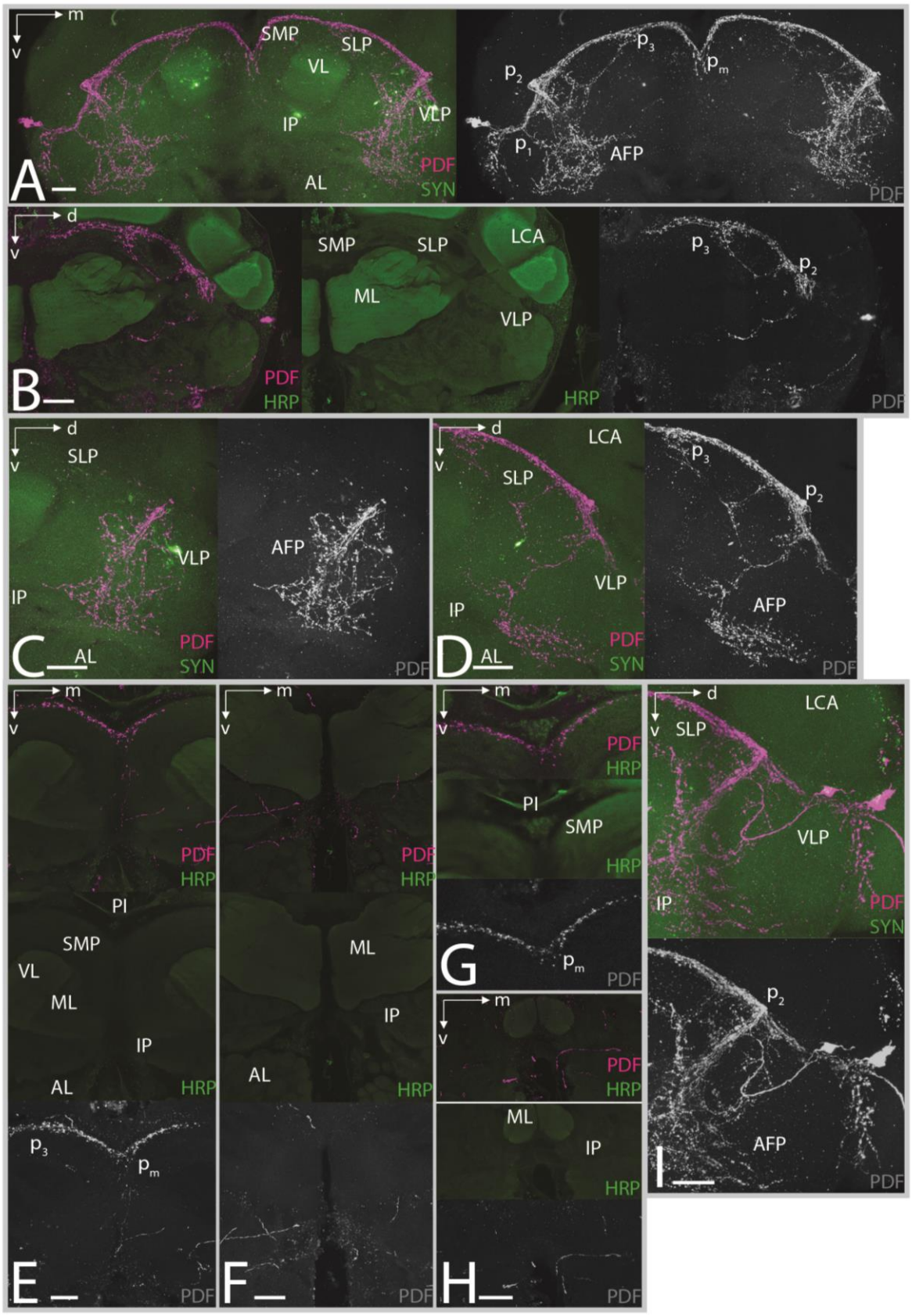

Figure 33: description see next page

Figure 33: The PDF network in the anterior protocerebrum of minor brains. Confocal image stacks of PDF staining co-stained with HRP or SYN (stated in image). Overlays of the PDF (magenta) and HRP/SYN (green) channel, and single channel images of the HRP/SYN channel (green) and the PDF channel (grey). If single image channels did not provide new information, they were omitted. All scale bars are set to 50µm. Abbreviations: AFP = anterior fiber plexus, AL = antennal lobe, AOC = anterior optic commissure, IP = inferior protocerebrum, MCA/LCA = medial/lateral calyx, ML = medial lobe, p_1 = Plexus 1, p_2 = Plexus 2, p_3 = Plexus 3, p_m = medial Plexus, PI = pars intercerebralis, SMP = superior medial protocerebrum, SLP = superior lateral protocerebrum, SLT = superior lobula tract, VL = vertical lobe, VLP = ventrolateral protocerebrum. A) An overview of all anterior structures in the Protocerebrum. B) A more medial layer of the AOC and its plexi. C-D) Consecutive layers (anterior to posterior) of the AFP and its connections to the plexi of the AOC. E-G) The medial plexus and its connected fibers. H) Fibers travelling towards the ventral midline. I) Isolated soma and fiber reaching into the AFP. Number of images (2µm thickness) of the confocal stack overlayed per picture: A) 73 B) 25 C) 11 D) 39 E) 10 F) 15 G) 10 H) 10 I) 35.

Sometimes, these fibers travelling ventrally towards the AFP in a medial layer of the brain, did not originate from a plexus, but from a single PDF-soma that was a little distant from the other PDF somata (Fig. 33I). This was observed only in minor brains, and only in 5 out of 30 brains. A second plexus of fibers branching off the AOC is directly adjacent to p_1 at the border between the ventrolateral protocerebrum and superior lateral protocerebrum (Fig. 33A and Fig. 34A,B), the plexus 2 (p_2). This plexus is very large and several distinct fibers leave it in different layers of the brain. The most distinct bundle of fibers leaving p_2 first travels perpendicularly to p_2 towards the anterior face of the medulla, then dorsally, branching out into the biggest plexus of fibers in the whole brain, the AFP (Fig. 33A,C and 34A,C). On the anterior-posterior axis, the AFP stretches out from the anterior surface of the ventrolateral protocerebrum and inferior protocerebrum, to the middle of the brain (level with the SLT and medial lobes of the mushroom bodies, see Fig. 33A,C,D and 34A-D). On the dorsal-ventral axis the main AFP reaches from the antennal lobes (posterior), almost until p_2 in the superior lateral protocerebrum (anterior, see Fig. 33A,C,D and 34A-D). Lastly, on the medial-distal axis, it is located between the ventral lobe of the mushroom bodies and the distal edge of the protocerebrum (anterior, see Fig. 33A,C,D and 34A-D), thus spanning over a large portion of the anterior and ventral surface of the protocerebrum. In the more posterior part of the AFP, single fibers enter or leave the plexus in dorsal direction, joining p_2 again directly posterior of the large bundle of fibers that first branched off there anteriorly, thus creating a loop that runs from p2 along the anterior surface of the protocerebrum and back (Fig. 33d and 34 D). This fiber branches out before it joins p_2 again, connecting to other parts of the PDF-network. One of these fibers branches off approximately level with the dorsal edge of the medial lobes, travelling towards the middle of the protocerebrum (Fig. 33A,B,D and 34A,B). This fiber is very weakly stained and it is unclear whether it stops underneath the medial lobes of the mushroom bodies or connects to its counterpart from the other hemisphere, and/or the fibers travelling dorsal from p_m.

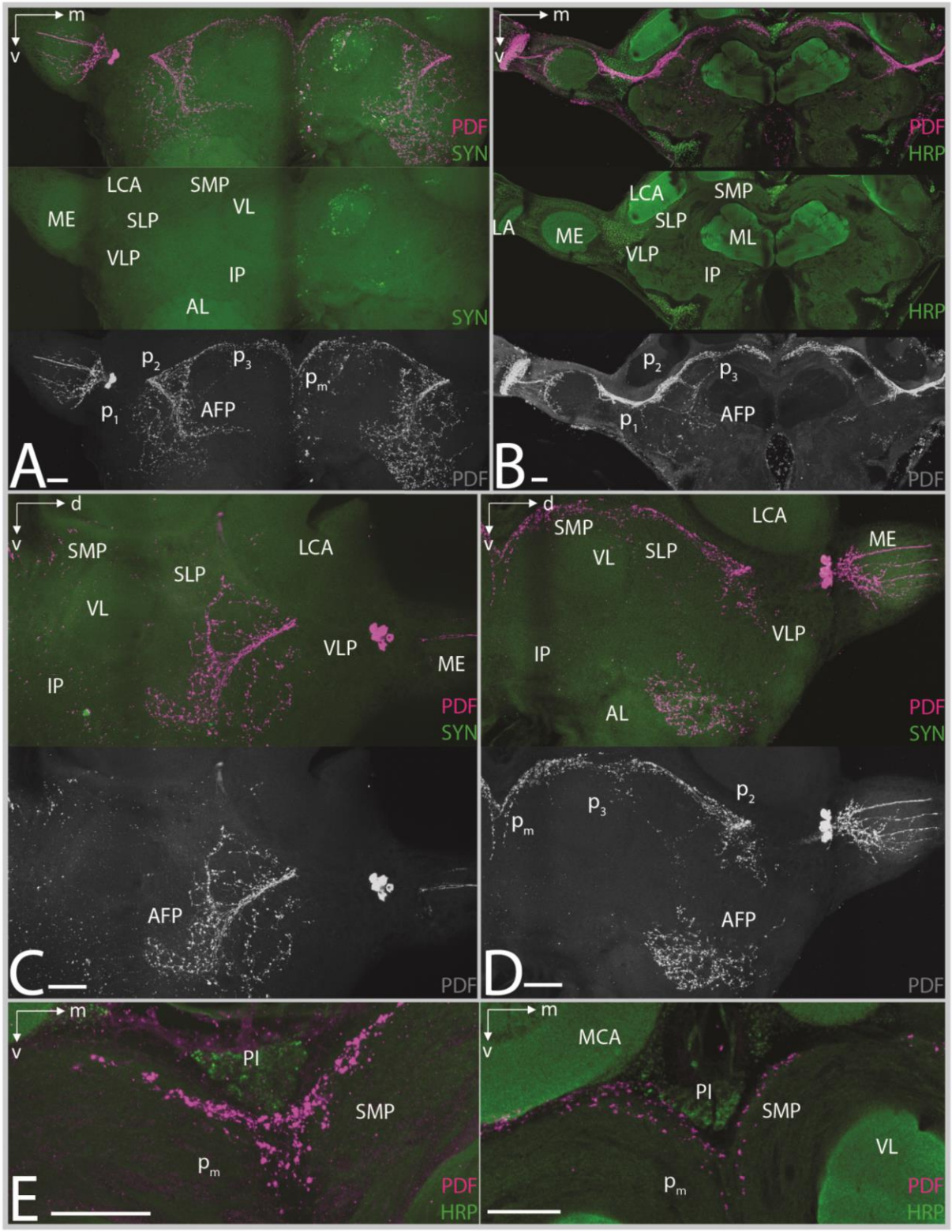

Figure 34: description see next page

Figure 34: The PDF network in the anterior protocerebrum of major brains. Confocal image stacks of PDF staining co-stained with HRP or SYN (stated in image). Overlays of the PDF (magenta) and HRP/SYN (green) channel, and single channel images of the HRP/SYN channel (green) and the PDF channel (grey). If single image channels did not provide new information, they were omitted. All scale bars are set to 50µm. Abbreviations: AFP = anterior fiber plexus, AL = antennal lobe, AOC = anterior optic commissure, IP = inferior protocerebrum, MCA/LCA = medial/lateral calyx, ML = medial lobe, p_1 = Plexus 1, p_2 = Plexus 2, p_3 = Plexus 3, p_m = medial Plexus, PI = pars intercerebralis, SMP = superior medial protocerebrum, SLP = superior lateral protocerebrum, SLT = superior lobula tract, VL = vertical lobe, VLP = Ventrolateral Protocerebrum. A) An overview of all anterior structures in the Protocerebrum. B) A more medial layer of the AOC and its plexi. C-D) Consecutive layers (anterior to posterior) of the AFP and its connections to the plexi of the AOC. E) The medial plexus and its connected fibers. Number of images (2µm thickness) of the confocal stack overlayed per picture: A) 53 B) 26 C) 10 D) 38 E) 7 (left), 10 (right).

Fig. 33F provides the only picture of a fiber that was stained brightly enough to follow to the middle of the brain, on the whole indications of this fiber were observed in 7 of 30 minor and 8 of 30 major brains. Dorsally from the point where this fiber branches off from the posterior fiber between the AFP and p_2, there is a second split with a number of fibers branching off towards dorsal, joining a third plexus on the AOC, located beneath the medial calyx of the mushroom body, plexus 3 (p_3) (Fig. 33B,D and 34 B,D). This connection between the AFP and p_3 runs parallel to the AOC, between the AOC and the medial lobe. It is also directly connected to another fiber leaving p_2 on the same level of the anterior-posterior axis as the posterior fiber connecting p_2 with the AFP, but is located again slightly more dorsally, at the dorsal edge of p_2, thus creating a sort of ring-shape, that is bisected into two parts, between p_2 and p_3 (Fig. 33 A,B,D and 34 A,B,D). Fig. 33D indicates that there might also be a second connection linking the AFP and p_3 directly, without any connections to other plexi, but this was only detected in two of 30 minor brains. Though the central complex was detected posteriorly of the medial lobes of the mushroom bodies, no PDF-fibers ever entered it.

3.2.3 PDF fibers in the antennal lobes

In the reconstruction of the PDF-network in minor and major ants (Fig. 29C and 30C), a number of PDF fibers was found in the antennal lobes that seemed to enter from the AFP, dorsal of the antennal lobes. This close proximity and possible entering of the antennal lobes by the AFP could also be observed in confocal image stacks, but it is usually hard to tell whether fibers indeed enter the antennal lobe or simply arborize anterior or posterior to it (Fig.29A, 30A, 33A,B,D, 34A,D). Fig. 35 and 36 shed some further light on the PDF fibers in the antennal lobe. Fig. 35A shows a number of fibers skirting the glomeruli of the antennal lobe directly ventral of the AFP.

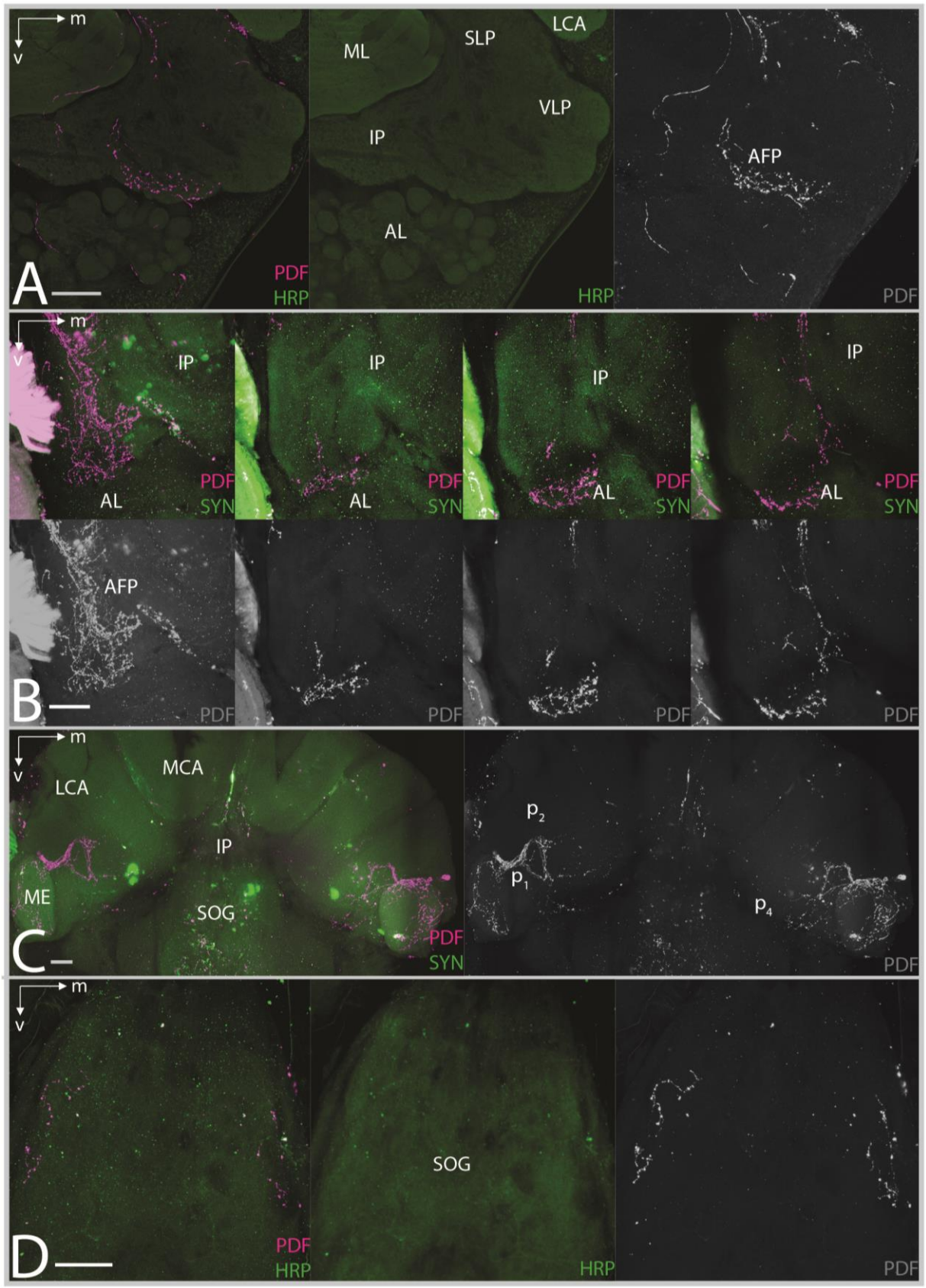

Figure 35: description see next page

Figure 35: The PDF network in the antennal lobes and posterior protocerebrum of minor brains. Confocal image stacks of PDF staining co-stained with HRP or SYN (stated in image). Overlays of the PDF (magenta) and HRP/SYN (green) channel, and single channel images of the HRP/SYN channel (green) and the PDF channel (grey). If single image channels did not provide new information, they were omitted. All scale bars are set to 50µm. Abbreviations: AFP = anterior fiber plexus, AL = antennal lobe, IP = inferior protocerebrum, MCA/LCA = medial/lateral calyx, ML = medial lobe, p_1 = Plexus 1, p_2 = Plexus 2, p_3 = Plexus 3, p_4 = Plexus 4, SLP = superior lateral protocerebrum, SOG = suboesophageal ganglion, VLP = ventrolateral protocerebrum. A) Stained fibers skirting the glomeruli of the antennal lobe and a connection to p_3. B) Consecutive images (anterior to posterior) of the AFP extending into the AL C) The projections originating from the SLT into the posterior brain. D) PDF fibers in the SOG. Number of images (2µm thickness) of the confocal stack overlayed per picture: A) 14 B) 14 (left), 8 each for the rest C) 59 D) 8

A second fiber in the inferior protocerebrum, medial of the AFP, seems to be connected to one of the fibers in the antennal lobe, travelling dorsally from there, towards p_3. This connection was only seen in this single staining. More commonly, fibers seemed to enter the antennal lobe from the AFP, Figure 35B shows consecutive stacks of few images of a confocal image stack of the complete AFP extending from anterior dorsal edge to posterior dorsal edge of the antennal lobe. In the second and third image from the left, fibers can be seen overlaying the glomeruli of the antennal lobe. Since further glomeruli can be seen in the pictures anterior (left) and posterior (right) of this, on the same level as the PDF staining is observed in the middle two pictures, fibers must indeed protrude into the antennal lobe. In Figure 36A, a very faint trail of dots originating from the AFP can be seen running down into the antennal lobe. Though this is only weak, it might be a hint at the entrance point of the PDF fibers into the antennal lobe. In Fig. 36B, PDF-fibers seem to encircle the most dorsal of the antennal lobe glomeruli. One slightly tilted section of a major brain, cut not exactly frontal but at a slight angle, reveals numerous fine fibers running between the glomeruli, seemingly entering the antennal lobe from posterior (Fig. 36C). Due to the unclear angle of cutting it is not quite clear which neuropil is adjacent to the glomeruli, but the inferior protocerebrum and subesophageal ganglion present good candidates.

3.2.4 PDF fibers in the posterior part of the protocerebrum

Though the majority of PDF fibers extends anteriorly from the SLT, a number of sparse innervations of the posterior protocerebrum of minor and major workers can be found in Figures 35C and 36D. These fibers are branching off of p_1 (see posterior overview in Fig. 29A,C and 30A,C right side).

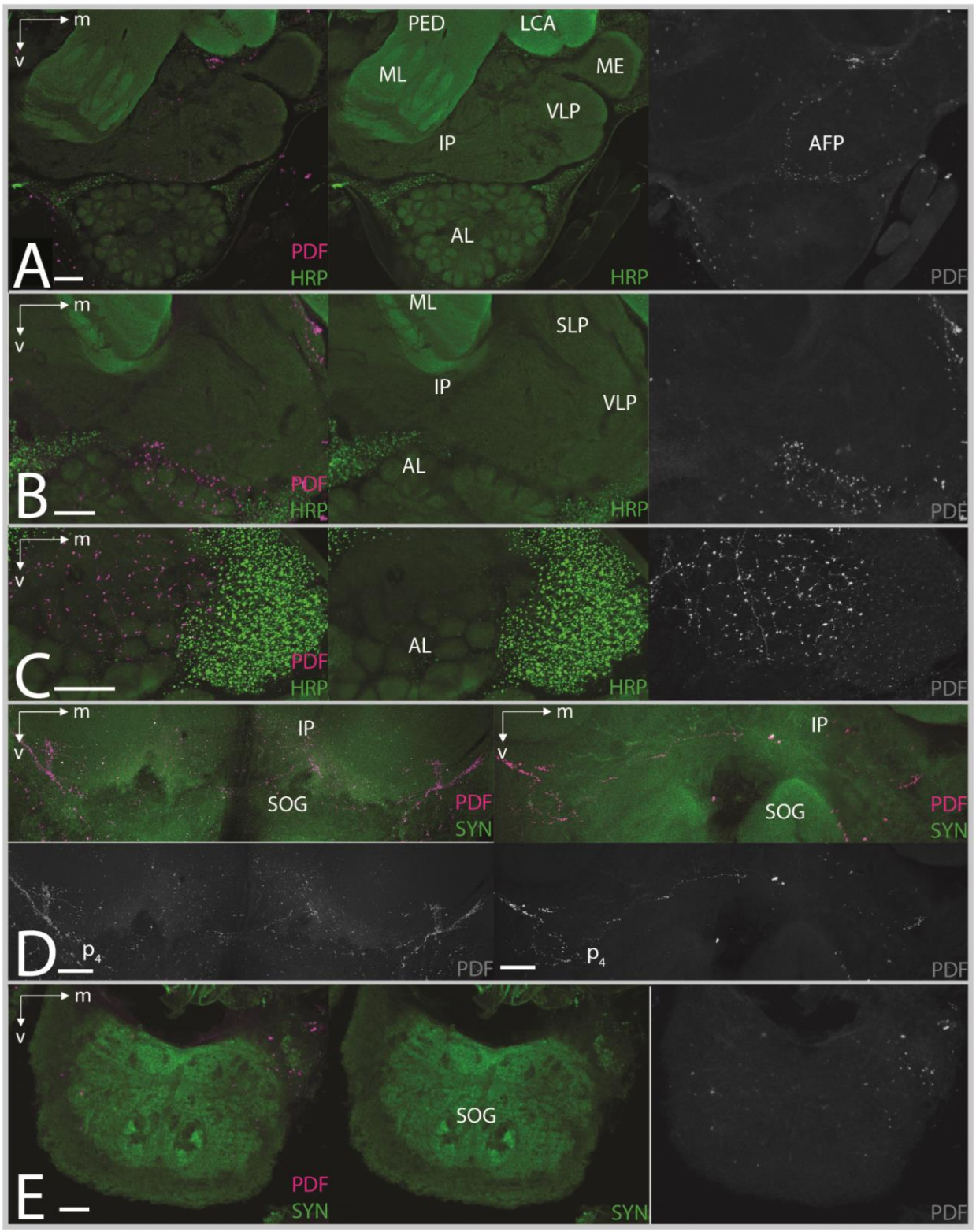

Figure 36: description see next page

Figure 36: The PDF network in the antennal lobes and posterior protocerebrum of minor brains. Confocal image stacks of PDF staining co-stained with HRP or SYN (stated in image). Overlays of the PDF (magenta) and HRP/SYN (green) channel, and single channel images of the HRP/SYN channel (green) and the PDF channel (grey). If single image channels did not provide new information, they were omitted. All scale bars are set to 50µm. Abbreviations: AFP = anterior fiber plexus, AL = antennal lobe, IP = inferior protocerebrum, MCA/LCA = medial/lateral calyx, ML = medial lobe, p_1 = Plexus 1, p_2 = Plexus 2, p_3 = Plexus 3, p_4 = Plexus 4, SLP = superior lateral protocerebrum, SOG = suboesophageal ganglion, VLP = ventrolateral protocerebrum. A) Stained fibers skirting the glomeruli of the antennal lobe. B) The AFP extending into the AL C) A slightly tilted cut of the antennal lobe with numerous fibers extending into the AL and skirting the glomeruli. D) The projections originating from the SLT into the posterior brain, single fiber crossing the midline. E) PDF fibers in the SOG. Number of images (2µm thickness) of the confocal stack overlayed per picture: A) 22 B) 7 C) 10 E) 10 each E) 10.

The same sparse fibers can also be seen in the reconstruction of the network from dorsal, running along the posterior edge of the protocerebrum (Fig. 29C and 30C). After extending posteriorly from plexus 1, the fibers travel ventral and medial, branching into two strands of fibers close to p_1 (Fig.29A, 30A, 35C).The majority of fibers travels dorsally in a straight line, joining p_2 again and forming a triangular connection between p_1, the branching point in the posterior IP and p_2. Ventrally of the branching point, a few fibers arborize and form another plexus, Plexus 4 (p_4) (Fig.29A, 30A, 35C, 36D).Very few fibers, one or two at most, also leave the branching point dorsal of p_4 and run towards the middle of the protocerebrum (Fig. 35C and 36D). In minor brains, these weakly stained fibers seem to end shortly before the subesophageal ganglion begins (35C) and were never seen to cross the midline or join the fiber from the other hemisphere. In major brains however, though very weakly stained, single fibers joining the two hemispheres or crossing the midline (see Fig. 36D for two examples) were observed in 10 out of 30 brains.

3.2.5 Fibers in the subesophageal ganglion

In almost all individuals, single PDF-positive fibers can be found in the subesophageal ganglion (Fig. 35 D and 36E). These fibers are not very abundant, usually limited to the distal edges of the subesophageal ganglion and of unclear origin, though it is possible that they arise from p_4. In Figure 35C, single fibers from p_4 travel very close to the subesophageal ganglion and possibly enter it.

3.3 The localization and cycling of the Period protein in *C. floridanus*

The PERIOD (PER) protein and PDF were successfully double-labelled in minor individuals of *C. floridanus* from colonies C79 and C90. Four clusters of neurons were identified at ZT0, which were located in the dorsal and lateral regions of the brain (Figure 37). Those clusters are conserved throughout all individuals and were named according to their respective position in the brain. Moving through the brain from anterior to posterior, the first cluster is located dorsally on the very anterior surface of the SLP and consists of approximately 11 neurons of similar shape and staining intensity. The cluster is labelled “Dorsal Neurons” (DN), due to its location between the medial and lateral calyces and the vertical lobes of the mushroom bodies. The cluster can be further subdivided into two groups, the ~5 “anterior Dorsal Neurons” (DN_a) (Fig. 37A) and the ~6 more posteriorly located “posterior Dorsal Neurons” (DN_p) (Fig. 37B). More laterally, but still in the dorsal rim between the medial calyx and the superior lateral protocerebrum, lies a larger cluster of on average 30 cells, which is thus named “Dorso-Lateral Neurons” (DLN) (Fig. 37B,C). These cells are densely packed in the space between the calyces and the protocerebrum, leading to a rather elongated cluster, and are very brightly labelled. Sparse PDF-staining can be observed close to this cluster. More lateral and approximately on the same level as the most posterior part of the DLN is the largest cluster of PER-positive cells (Fig. 37C,D,E), the “Lateral Neurons 1” (LN1). This cluster consists of ~ 40 neurons spreading out widely in the vicinity of the medulla, from anterior, next to the distal edge of the lateral calyx (Fig. 37C), to posterior and more medial between the proximal edge of the medulla and the ventrolateral protocerebrum (Fig. 37E). A small cluster, consisting of exactly six cells that are clearly isolated from the rest, is located directly at the proximal edge of the medulla (Fig. 37E). Even though they are separate, their staining intensity and size indicates that they might belong to the LN_1. Since they are still consistently removed by approximately 6µm from the rest of the LN_1 (white arrow in Fig. 37E), they were treated as a separate cluster by the name of $LN_{1'}$. A further subset of ~3 cells co-expresses PDF in the cytoplasm and is larger and stained more weakly than the LN_1. This cluster is named “Lateral Neurons 2” (LN_2) since it is located in the same area as the LN_1 and only differs in shape and staining intensity. Even though PER staining was mostly nuclear, a few neurons with weak cytoplasmic staining were detected. The exact number of cells per cluster is given in Table 14.

Table 14: The average number of PER neurons per cluster (evaluated from 14 Hemispheres)

DN_a	DN_p	DLN	LN_1	$LN_{1'}$	LN_2
4.93 ± 0.25	5.71 ± 0.32	31.29 ± 0.84	43.21 ± 1.29	6.00 ± 0.10	3.29 ± 0.30

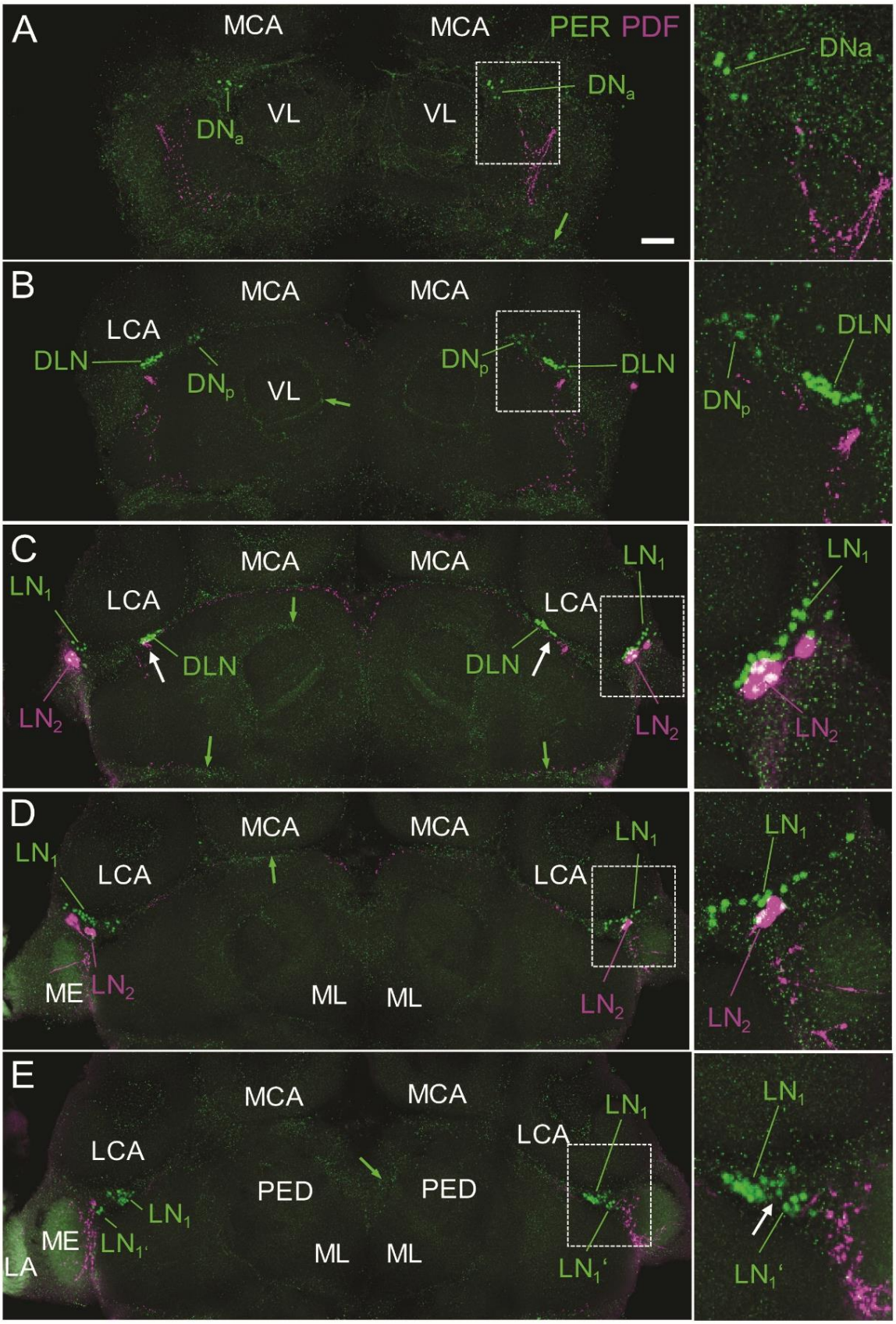

Figure 37: description see next page

Figure 37: PER (green) and PDF (magenta) double-labelled consecutive projections of confocal scans of one minor brain at ZT 0, from anterior (A) to posterior (E). White rectangles indicate the location of the inset magnified areas, the white arrow the distance between the LN_1 and $LN_{1'}$. The scale bar is set to 100µm. Abbreviations: DLN =Dorsal Lateral Neurons, DN_a= Dorsal Neurons anterior, DN_p= Dorsal Neurons posterior, LN_1/$LN_{1'}$= Lateral Neurons 1, LN_2= Lateral Neurons 2, LCA= lateral calyxes, MCA= medial calyces, VL= vertical lobes, ML =medial lobes, LA= lamina, ME= medulla. Number of images (2µm thickness) of the confocal stack overlayed per picture: 10 each

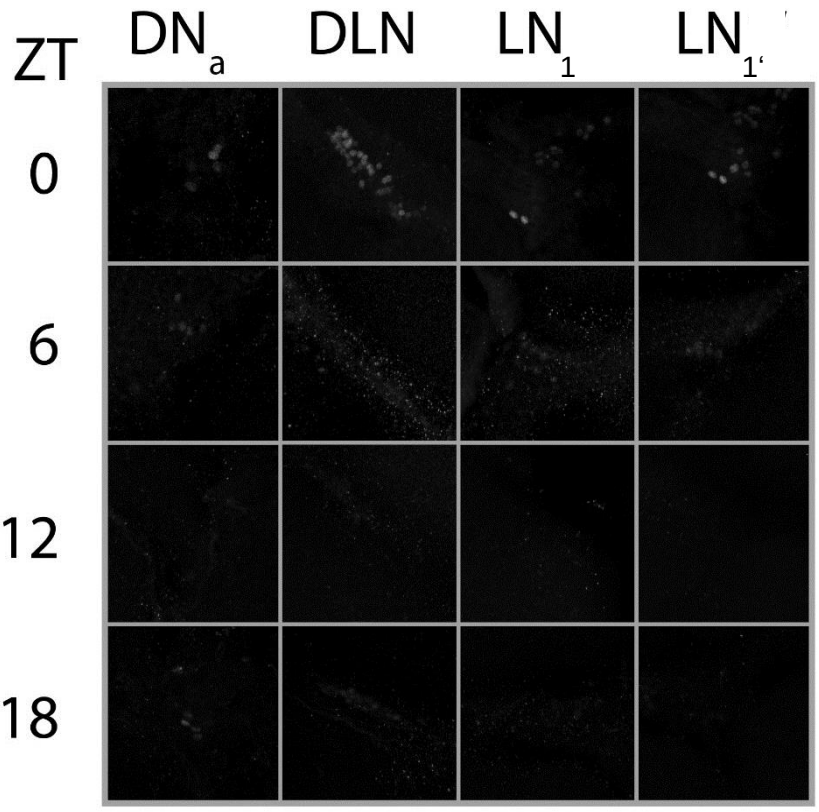

Figure 38: Overlays of confocal scans of PER staining in the clusters DN_a, DLN, LN1 and LN1', in brains of minor individuals of colony C90 at ZT0, 6, 12 and 18. The staining intensity visibly declines from ZT 0 to ZT12, then brightens again. ZT 0 is the brightest stained timepoint. Number of images (2µm thickness) of the confocal stack overlayed per picture: DN_a and LN_1' = 5, DLN and LN_1 = 10

To test whether PER staining intensity changed throughout the day, brains of ants were collected either every 3 hours (C79) or every 6 hours throughout the 24 hour day. The change in PER intensity can be seen qualitatively in Figures 38 (C90) and 39 (C79), which show overlays of the measured clusters at all Timepoints normalized for background staining. The LN_2 are not depicted, since their staining is very weak. In Figure 38, it is clearly visible that all neuron clusters are stained the most brightly at ZT0. This is in accordance with the measured staining intensities in Figure 40. Also, it is clearly visible that staining intensity declines from ZT0 to ZT12, where it is at its lowest, then rises again at ZT18. The measured staining intensity of all clusters (Fig. 40) differed significantly over time, as revealed by a Kruskal-Wallis test (DN_a: $H(3)=8.98$, $p=0.03$; DLN: $H(3)=166.07$, $p<0.00001$; LN_1: $H(3)=225.61$, $p<0.00001$; $LN_{1'}$: $H(3)=44.66$, $p<0.00001$; LN_2: $H(3)=10.18$, $p=0.02$). Figure 39 shows the same as Figure 38, but for individuals from colony C79 and 4 more timepoints, ZTs 3, 9, 15, and 21.

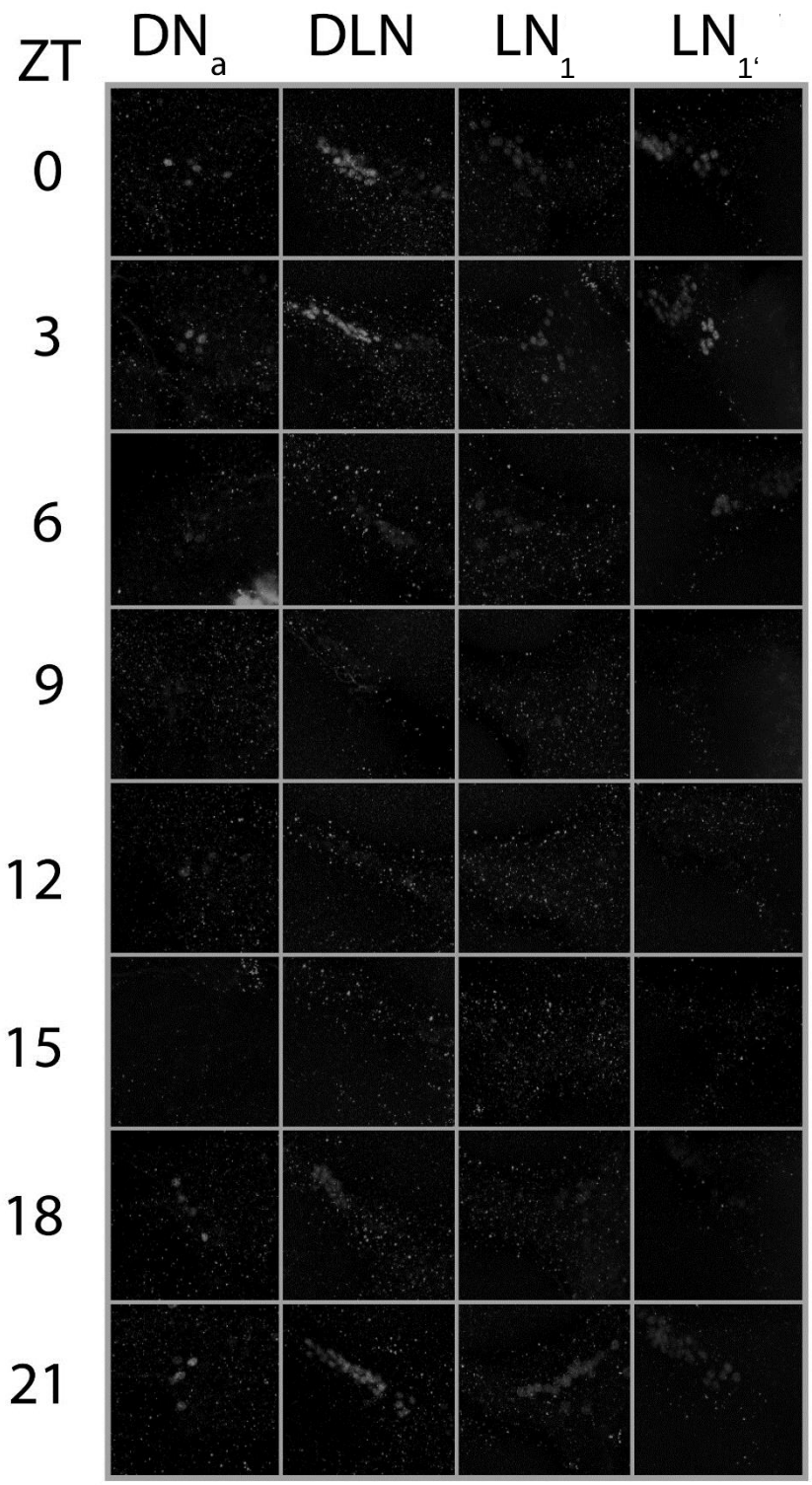

Figure 39: Overlays of confocal scans of PER staining in the clusters DN_a, DLN, LN_1 and $LN_{1'}$, in brains of minor individuals of colony C79 at ZT0, 3, 6, 9, 12, 15, 18 and 21. The staining intensity visibly declines from ZT 0 to ZT15, then brightens again. ZT 0 is the brightest stained timepoint, with ZT21 and ZT3 in close range. Number of images (2µm thickness) of the confocal stack overlayed per picture: DN_a and LN_1' = 5, DLN and LN_1 = 10.

Here, it becomes apparent that the least brightly stained time-point is ZT15, not ZT12, and that ZT 21, 0 and 3 are equally bright to the eye. Indeed, when measuring the intensity levels with FiJi, the curve that depicts the cycling intensity levels reveals a peak at ZT0, with almost equally high levels at ZTs 3 and 21, a very steep decline from ZT3 to ZT6 and then a milder decline until the lowest levels at ZT15 in all clusters, except the DN_a. This cycling of intensity is significant in all measured clusters (DN_a: $H(7)=94.44$, $p<0.00001$; DLN: $H(7)=622.47$, $p<0.00001$; LN_1: $H(7)=644.88$, $p<0.00001$; $LN_{1'}$: $H(7)=165.87$, $p<0.00001$; LN_2: $H(7)=14.93$, $p=0.037$). Though the overall pattern of the DN_a is similar (red line), there is a tiny trough at ZT0, leaving ZT21 and ZT3 the timepoints with the highest staining intensity levels. A pairwise Wilcoxon post-hoc test revealed that these staining levels at ZT 21,0 and 3 were not significantly different from one another ($p=1.0$ in all pairings).

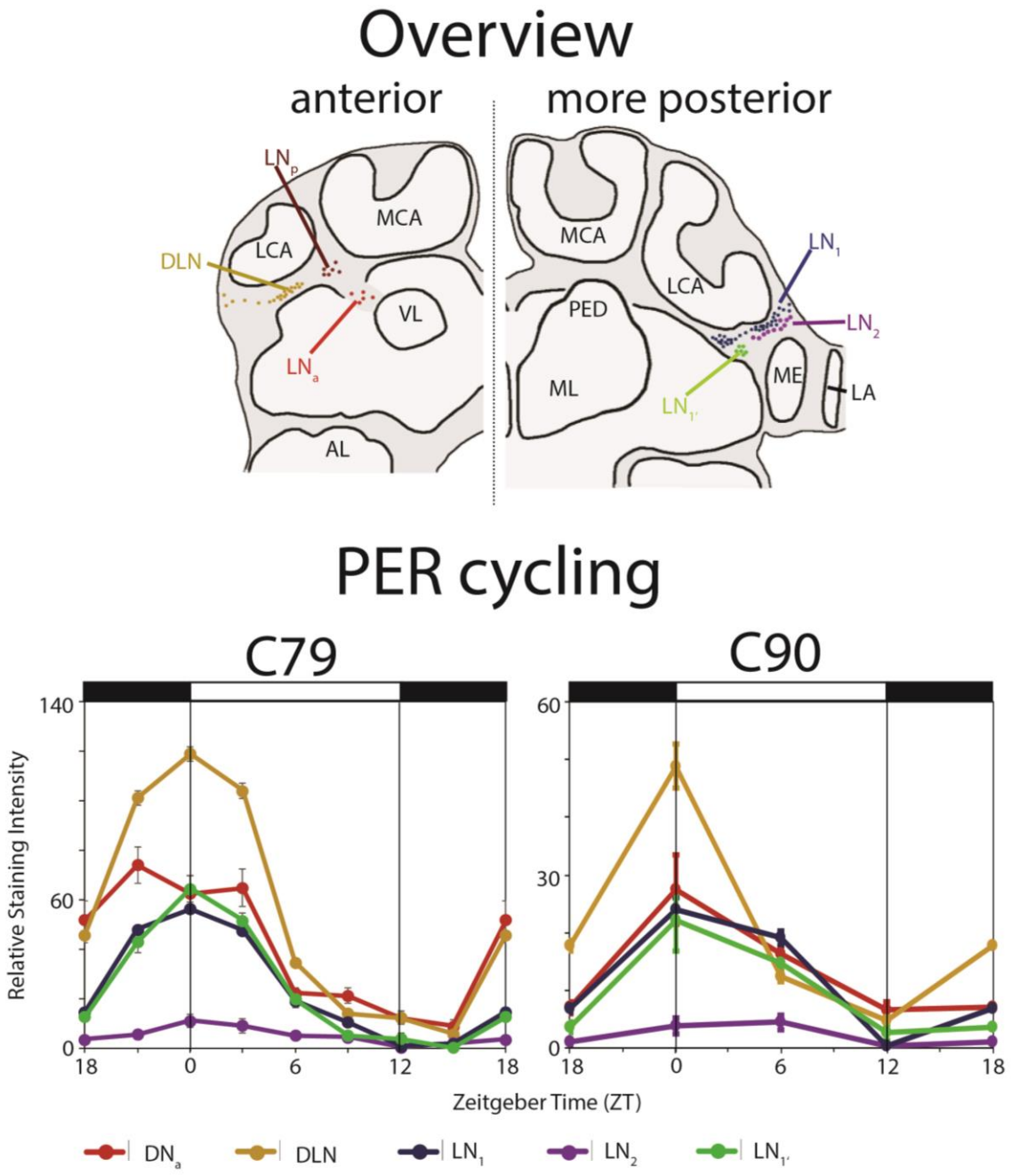

Figure 40: A schematic overview of the PER and PDF neurons and their location in the brain, and the staining intensities of PER neuron clusters in the course of 24 hours measured in brains of colony C79 or C90. The schematic depicts the most anterior clusters, DN_a, DN_p and DLN on the left hand side; the a little more posterior clusters of LN_1, $LN_{1'}$ and LN_2 on the right hand side. Neurons are marked in the same color their staining intensity is plotted in below. The relative staining intensity is plotted against the ZT, error bars represent the standard error. A black and white scale bar over the graph indicates the LD-cycle. All clusters except for the DN_a in colony C79 show cycling intensities with maxima at ZT0 and minima at ZT 15 (C79) and ZT12 (C90).

4. DISCUSSION

4.1 The endogenous behavior of *C. floridanus* in response to light and temperature

The locomotor behavior of minor workers of *C. floridanus* in response to light cycles fulfills the three main criteria for the presence of an endogenous clock: [1] it free-runs with a distinct period length. [2] It is entrainable to different zeitgebers, in this case different day lengths. [3] It´s period length is temperature compensated.

4.1.1 *C. floridanus* entrains to different light cycles

Experiments 1-3 proved that *C. floridanus* ants can entrain to different LD cycles, from “short” days of 8 hours of light and 16 hours of darkness, over “normal” days with 12 hours of light and dark each, to “long” days with 16 hours of light and 8 hours of darkness. Since no period of constant lighting conditions was added after the LD-cycle, one might argue that the observed behavioral patterns, with raised levels of activity during the night and conspicuous peaks of behavior at the transitions from light to dark and vice versa, are a masking effect caused by the light-dark cycle. Still, the presence of completely arrhythmic animals indicates that this is not the case, since those individuals should also react to the LD if it were only masking. Furthermore, some animals are active during the light phase or show distinct and simultaneous bouts of raised activity during both phases of the LD or switch their activity from the light to the dark phase or vice versa. If the ants merely reacted to the light with avoidance, this would not be possible.

4.1.2 Survival is dependent on light phase and temperature

Survival of *C. floridanus* differed significantly between light conditions, as well as between temperatures. Interestingly, ants survived better at normal and long days, than at short days. It might have been assumed that short days, with a long dark phase, might be optimal for the primarily nocturnal ants. Still, when correlating the natural temperature at which this photoperiod would occur in the wild, 25 °C is much too warm (winter temperature in *C. floridanus* habitat rest between -3°C and 15°C). This correlation of the photoperiod with a very wrong temperature might somehow upset the organism and lead to a premature death. The normal and long day conditions did lie in the range of temperatures in their natural habitat during summer, which might explain the lower death rates. Both colonies reacted differently to lower and higher temperatures. While C79 survived better at higher temperatures, C152 survived better at lower temperatures. Even though this might be a preference that is colony-

specific, this is unlikely since queens of both colonies were collected at the same place and reared in the same lab, thus having been exposed to the same environmental conditions. It is more likely that the arbitrarily chosen ants for the experiments were simply very old and thus likely to die in one of the experiments, therefore masking the true effect of temperature on survival. This could be easily verfified by testing age-cohorts from the colonies to see if the effect disappears. Of course, old age could also be an explanation in the case of the LD cycles.

4.1.3 *C. floridanus* is primarily nocturnal and might be able to switch to diurnality

In all conditions, most ants preferred to be active during the dark phase of the LD and were nocturnal in constant conditions. This indicates that *Camponotus floridanus* has an endogenous preference for nocturnal activity. Since starting the free-running activity from the preferred phase was the most common case, it is quite safe to assume that animals that are entrained to the light phase are diurnal and animals that entrain to the dark phase nocturnal. When looking at the distribution of nocturnal and diurnal animals under different conditions, it is quite striking that temperature does not have an effect on the average activity during any phase of the day or the number of animals belonging to any activity type. However,the LD-cycle and colony identity do. Individuals of colony C79 tend be more active on average than individuals of colony C152, during the whole day, but especially in the dark phase. More interestingly, individuals kept at a short day LD, which correlates with day length in winter conditions, are on average more active during the light phase. There are indeed more diurnal individuals than at normal or long day conditions, which correlates to summer conditions of day length. Thus, the LD seems to have more influence on the preference for a certain light-period than the temperature. Perhaps this is not surprising, since switching from nocturnal foraging behavior in summer, to diurnal foraging behavior in winter has been reported before for the closely related *C. rufipes (*Del-Claro and Oliveira, 1999). Ants are not the only organisms who have been reported to be able to switch their activity from day to night or vice versa. Small rodents also do so depending on their energy balance (Hut et al., 2011; Hut et al., 2012; van der Vinne et al., 2014b). Coldness and hunger can induce diurnal behavior in nocturnal mice (van der Vinne et al., 2014a). Even though in this case a putative switch in behavior was not triggered by the temperature, which might have a big effect on the metabolism and thus energy expenditure, but the length of the day (photoperiod), this might still follow the same underlying principles. Photoperiod in natural conditions is after all a strong indicator for winter or summer, and a much more stable one than temperature. Several organisms, such as plants and gold-hamsters, are known to induce seasonal shifts in accordance with changes in photoperiod

(Garrett and Campbell, 1980; Searle and Coupland, 2004). Non-tropical birds, that depend on seasonal environmental conditions for breeding, molt and other behaviors, have been shown to depend mostly on photoperiod to induce these behaviors (reviewed in (Dawson et al., 2001)). This strategy allows them to avoid unwarranted changes in behavior due to outliers in temperature. Sympatric species of Myrmecia ants were shown to rely on different cues for timing their foraging behavior (Jayatilaka et al., 2011). Whereas the diurnal *M. croslandi´*s foraging activity strongly depends on ground temperature at light onset, the nocturnal *M. pyriformi* solely relies on the sunset time. It would be interesting to see if temperature cycles in combination with LD might trigger a stronger response in *C. floridanus*, since colder temperatures in the night and warmer temperatures in the day might be an additional incentive to switch to the physiologically ideal phase. As a subtropical species, *C. floridanus* would naturally be exposed to temperatures ranging from -3°C to 36°C and a light phase of 10 to 15 hours. It is therefore possible that our chosen temperatures were unsuited to induce a significant change in behavior. Jayatilaka et al. (2011) also found that temperature ranges tolerated in the laboratory were wider than those observed in the wild. Thus, experiments with a fixed LD and a much increased range of temperatures, might also shed new light on the importance of temperature and photoperiod for the induction of behavioral switching. In summary, many more experiments are needed to truly understand the mechanisms behind this behavior.

4.1.4 Differences in activity type might be linked to behavioral caste

Even though most ants were nocturnal, other types of activity were observed too. This indicates that activity during the dark phase may not be suitable for all ants. Due to the organization in behavioral castes, differential timing might be needed in each individual, corresponding to the task at hand. A link between social organization and behavioral rhythmicity has been reported for other social hymenoptera, like the honeybee (Shemesh et al., 2010). Arrhythmicity was observed in young bees, typically grooming and feeding the brood around the clock, older bees, going out to forage, showed strong rhythms on the other hand. Unlike ants, nurse bees try to keep temperature as constant as possible (Bloch et al., 2001) , whereas ant nurses have been shown to relocate brood to different temperatures in the course of the day (Roces and Nunez, 1989a). Indeed, it has been shown that changing temperatures might be beneficial for brain development of ants (Falibene et al., 2016), indicating that arrhythmicity is not a suitable type of activity for ant nurses. Mildner and Roces (2017) even showed that nurses of *C. rufipes* were nocturnal in social isolation, but showed arrhythmic behavior in the colony context and

presence of brood. An interesting type of behavior that emerged in the experiments was rhythmic activity in both phases of the day. All ants that showed this type of behavior either displayed two prominent peaks of behavior at the transitions between light and dark or main activity during the dark and a second smaller peak in the middle of the light phase. The first type of simultaneous activity can be observed in other animals too, for example bears, and is usually referred to as crepuscularity, activity during dusk and dawn (Garshelis and Pelton, 1980). It is unclear in which context dusk and dawn might play a role for tasks performed by *C. floridanus*. A potentially interesting experiment might be the release of marked crepuscular ants (monitored in social isolation) back into social context, to identify the sorts of tasks they take on and whether crepuscularity truly is necessary and displayed in social context. The number of individuals displaying this behavior was very low, indicating that it is of little importance within the colony. Still, since there were no gradual transitions between light and dark, but only the stark contrast of on and off, it might be worthwhile to test if this changes in LD conditions with gradual transitions. The second group, with primarily nocturnal activity and a second peak of activity in the middle of the light phase is reminiscent of the temperature preference in *C. mus* nurses (Roces and Nunez, 1989a). These nurses exhibit preference for relocating brood to two different temperatures at different times of the LD cycle, the first relocation happening in the middle of the light phase, the second exactly 8 hours later. Though this interval of 8 hours usually means the second relocation takes place in the dark phase, it is solely dependend on the first relocation, not on the onset of dark phase. The first relocation however does depend on the light phase. In the case of *C. floridanus*, the locomotor activity observed in social isolation also had a peak in the middle of the light phase, but the second activity interval was coupled to the onset of dark phase, not a fixed interval, since this behavior was consistent between the different LD-cycles which varied from 4 hours to 8 hours in time interval between the middle of the light phase and the onset of dark phase. Still, the similarity is striking and it would be very interesting to test circadian rhythms in brood relocation of *C. floridanus*, to see if these rhythms match with those observed here. Since only few ants displayed this type of rhythm, it might still be linked to other behaviors, that are less common than nursing, or alternatively only few nurses might be responsible for brood relocation. Nocturnality or diurnality might also play a role in foraging behavior, since Simola et al. (2016) showed strong nocturnal foraging rhythms in *C. floridanus* minors. Indeed, strong rhythmic behavior is important for foraging, since most food sources are only available at fixed periods of time and need to be visited accordingly. Additionally, as discussed above, it might be beneficial to time foraging to the most energy conserving time of day. Few individuals were also seen to switch between different activity types. This might be due to different reasons. First of all, these ants might have been in the

transition between two social castes, displaying different rhythms. Since it is not known how caste is determined and the monitored ants were not of uniform age, it is entirely possible that they simply reached an age at which they transitioned to another task. Second, if switching to or/and from arrhythmic behavior, the ants are likely to be rhythmic and influenced by some unknown factor to mask their rhythmicity. Third, ants that were dying usually switched to arrhythmic behavior some days before.

Since the ants in my experiments were collected randomly from the colonies, and social caste identity was not established, no true link between locomotor behavior and social caste can be established. Ants in social isolation behave differently than in the context of the colony as shown by (Mildner and Roces, 2017), where nurses of *C. rufipes* were nocturnal in social isolation but arrhythmic in the colony context. Further experiments in *C. floridanus*, like those described in (Mildner and Roces, 2017) would be necessary to draw conclusions on circadian organization of the single castes and to establish whether the behavior recorded in isolation truly reflects the circadian character of *C. floridanus*.

4.1.5 *C. floridanus* clock is circadian and temperature compensated

Last but not least, *C. floridanus* did not only display rhythmic behavior in constant conditions, its period length was close to 24 hours in both colonies and at both temperature conditions, making it a truly circadian rhythmicity. The slightly shorter than 24 hours period even became significantly longer at higher temperatures (still close to 24 hours), meaning the clock slowed down at higher temperatures. This phenomenon is called temperature over-compensation. Of course, a difference of 10°C, as postulated to raise reaction rate two- to four-fold (van´t Hoffsch regulation) would be a more suitable indicator of temperature compensation than the tested difference of 5°C. Unfortunately, survival rates at 20°C high could not be kept high enough to test ants at this temperature. Still, reaction rate according to the van´t Hoffsch regulation does not rise stepwise, but steadily, and the period length should get shorter if reaction rates increased. The fact that the period length declined at 5°C higher temperature indicates that reaction rates did not rise and so they also should not do so if the temperature difference was raised to 10°C.

4.2 The PDF-network in minor and major workers of *Camponotus floridanus*

The PDF network is an important component of the clock network of many insects and has been reported in various insects, such as cockroaches (Stengl and Homberg, 1994), crickets (Homberg et al., 1991), flies (Nässel et al., 1991; Helfrich-Förster and Homberg, 1993; Nässel et al., 1993; Shiga et al., 1993), bees (Bloch et al., 2003; Závodská et al., 2003; Weiss et al., 2009; Sumiyoshi et al., 2011) and other insects (Závodská et al., 2003). Though it was named after its role in integumental color change and eye pigment movements (Rao, 2001), PDF seems to serve other functions as well. Its widespread arborization patterns and presence in the vicinity of (or co-expression with) clock neurons and higher brain centers, like the mushroom bodies or antennal lobes, make it an ideal candidate for relaying information between them. A reconstruction of the PDF network in whole-mount brains was performed with FiJi, in the hope of gaining information on the 3-dimensional information on the organization of the network. This reconstruction however, proved to be useful only to gain a rough overview of the projection patterns. Though tracing the fibers through the brain by hand provided information on the organization of the network, the visualization of the traced structures by the program was very poor. Since the program did not allow for true manual selection of the course of fibers, but instead searched for the brightest spot of staining next to the selected area, it was near impossible to follow faintly stained fibers in the vicinity of brightly stained fibers, or several brightly stained fibers in a bundle, as only the brightest fiber was continuously marked. Furthermore, the program could not interpolate connections between parts of the network were staining was fractured, instead “jumping” to stained structures in areas surrounding the fiber that was being traced to fill the gap. This lead to shaky and zig-zagging character of the reconstructed fibers that could not be avoided. Though these mechanisms should provide a much stricter measure for truly connected fibers, they actually distorted the real image by taking away the possibility to correct where the program erred. Lastly, fibers reconstructed were not “filled” to their true extend, but all represented in the same volume. This also distorts the true nature of the network by equalizing very thick and very thin fibers. In summary, the information gained by the reconstruction is not satisfying, since the expected information on PDF in other dimensions of the brain (e.g. seen from a dorsal view-point to investigate distribution of the Fibers on an anterior-posterior axis) could not reliably be extracted. Instead, slices, this time cut from dorsal to ventral, might give more reliable information on the branching of fibers in anterior/posterior direction or the relation of the PDF fibers to brain centers and answer the still remaining questions.

4.2.1 The PDF cell bodies in minor and major brains of *C. floridanus* are variable

The number of PDF cell bodies varies within brains, and also between the two size castes of *C. floridanus* and is comparatively low. The variance in *C. floridanus* is quite striking and often also seen between the two hemispheres of one brain. Since there is no information available on the neurotransmitter or clock gene content of these cells, it would be interesting to investigate whether the variable number is somehow linked to differential expression of co-localized proteins in these cells. We know that PER protein was only stained in a subset of PDF-positive cells in minor brains (see below), if this is indeed true and not due to the staining procedure, it would be of interest to test PER staining in major brains and look for differences there. Furthermore, a detailed analysis on the arborization patterns of single somata would be very interesting. This was not possible here, since fibers and somata lay very close together. Since there was on average one cell body more in major brains, and those brains also seem to have a larger abundance of fibers, the additional cell bodies might be needed for a more voluminous network. Considering that major ants were the only ones sometimes showing posterior fibers crossing the midline, it might prove informative to investigate whether this fiber arises from the additional cell body.

4.2.2 The accessory medulla of *C. floridanus* is similar to the cockroach and honeybee

A triangular neuropil, slightly separated but connected to the proximal medulla, was found to be densely innervated by PDF-fibers. It is highly likely that this structure is homologous to the accessory medulla found in cockroaches (Petri et al., 1995; Reischig and Stengl, 1996), fruit flies (Helfrich-Förster et al., 1998) and bees (Beer, accepted). Several factors speak for the hypothesis that this triangular neuropil is the accessory medulla of *C. floridanus*. First, the location at the anterior, proximal side of the medulla is identical to the location of the aMe in fruit flies and cockroaches (Petri et al., 1995; Helfrich-Förster et al., 1998). Second, there are conspicuous spherical “holes” in the PDF network invading the putative accessory medulla. It is known from the cockroach that the accessory medulla is composed of dense noduli and internodular neuropil (Reischig and Stengl, 1996). These holes might be the noduli around which the PDF fibers are growing. Electron-microscopical studies of the accessory medulla might shed further light on this hypothesis. Third, PDF fibers from the accessory medulla are connected to most parts of the brain, and maybe even to the contralateral accessory medulla through the AOC, indicating that it might influence them or vice versa.

4.2.3 PDF in the optic lobes and connections to higher brain centers

4.2.3.1 *C. floridanus* optic lobes are connected to the clock network

C. floridanus is a ”generalized” ant, which means it does not only rely on visual input, but predominantly on tactile and olfactory input. This is also represented by its relatively small optic lobes and large antennal lobes (Gronenberg, 1999; Gronenberg and Holldobler, 1999). This is visible when comparing its optic lobes to the much bigger (in relation to the protocerebrum) optic lobes of the bee or cockroach, which rely much more on vision. The differences in optic lobe size between minor and major ants might reflect a difference in the use of visual cues. Since major workers of *C. rufipes* for example, often belong to the soldier caste and are entrusted with the defense of the nest (Jaffe and Sanchez, 1984), visual detection of enemies might play a bigger role in their lives. Fibers from the accessory medulla innervate the structures of the optic lobes in several layers. The anterior fiber fan, a very prominent structure on the anterior face of the medulla, closely resembles the homologous structures in the cockroach and honeybee brain, as well as the fibers in the first layer of the medulla and the fibers in the lamina. Fibers from the anterior fiber fan and the first layer innervate the lamina, crossing the first optic chiasma and densely innervate it. The varicosity of the fibers in the lamina indicate that is a site of output of the PDF-network. Most photoreceptor axons terminate in the lamina, and visual processing in the lamina underlies adaptation in response to changing light intensities, summation, enhancement of signal-to-noise-ratio, and lateral inhibition (Strausfeld, 1989; Gronenberg, 2008). Thus, output of PDF might play a role in the circadian control of these adaptations. In the first and second layer of the medulla of *C. floridanus*, axons from the lamina terminate (Ribi, 1975). In general, the medulla seems to be involved in processing color information and maybe also extraction of motion information from visual input (Gronenberg, 2008). Visual stimuli entering the medulla in the first and second layer might therefore be related to the clock neurons via the PDF network, or the PDF network might play a role in circadian control of color and motion vision, e.g. making the soldiers more sensitive to motion during times of putative predator attacks. No serpentine layer, or innervations of such a structure could be found.

4.2.3.2 The PDF-network in medullae of *C. floridanus* is not connected through a POC

Though the majority of the PDF-network in *D. melanogaster´*s optic lobes arborizes in the distal medulla, some fibers can be found in the serpentine layer (Helfrich-Förster and Homberg, 1993). The tangential fibers of the serpentine layer contribute to the fibers that project via the posterior optic commissure towards the contralateral medulla (Helfrich-Förster and Homberg, 1993). There was no innervation of the serpentine layer in *C. floridanus* and PDF fibers could not be found in the posterior optic commissure. Only a single fiber crosses the posterior midline of some major brains, but the quality of the staining of Synapsin does not allow conclusions on the presence of this fiber in the POC. In sections stained with HRP, no fibers were detected in the POC or posterior optic tubercles, and minor brains never exhibited a posterior fiber crossing the midline. Though this fiber might just be stained very weakly and could thus not be detected, this result fits with a subordinate role of vision in *C. floridanus*. This presents a major difference to *Apis mellifera* and *Leucophea maderae*. The POC and also posterior optic tubercles are clearly innervated in *Apis mellifera*, joining the PDF-cell bodies of both hemispheres (Beer, accepted). In the cockroach, the POC and tubercles are also clearly innervated, though here, the number of fibers in the POC is also limited to two (Wei et al., 2010). Another insect with a characterized PDF-network is the cricket *Teleogryllus cornmodus* (Homberg et al., 1991). Interestingly, there is also no connection of the hemispheres via a POC in this insect, only one anterior fiber is found to cross the midline. Therefore, *C. floridanus* is not the only insect without connection of the hemispheres though a POC.

4.2.3.3 The AOC might relay information from the clock to higher brain centers

A second connection between the optic lobes of both hemispheres in *C. floridanus* was found in the anterior optic tract, which arises from the superior lobula tract. The superior lobula tract is most probably homologous to the lobula valley tract found in bees and cockroaches (Reischig and Stengl, 2002; Bloch et al., 2003), due to its location morphology. All tested ants displayed a large and dense bundle of fibers, the AOC, running along the dorsal rim area of the protocerebrum underneath the mushroom body calyces. This coincides with a structure that has been described for *Camponotus* ants before, the anterior superior optic tract (asot), which connects the optic lobes to the mushroom bodies (Ehmer and Gronenberg, 2004). The mushroom bodies are centers for higher order sensory integration, learning and memory

formation (Strausfeld, 1989; Heisenberg, 2003; Giurfa, 2007; Devaud et al., 2015; Falibene et al., 2015). Of course, further studies with co-staining of the asot and the PDF network would be absolutely necessary to verify whether the AOC runs through the asot. Nevertheless, the resemblance form and location of the two structures are striking, and the plexi 2 and 3 I describe here are approximately in the position were the asot branches off into the mushroom body calyces. It would be most interesting to study whether these structures indeed co-localize. Even if this were not the case, the proximity of the plexi to the lips of the mushroom body calyces is undeniable. The varicose structures in the plexi indicate that PDF might be released here, which would hint at an involvement of the circadian clock in learning. The proximity of PDF to the mushroom bodies is also found in the bee and cockroach (Beer, accepted; Wei et al., 2010). Bees are able to learn the time-points at which up to nine different flowers yield the maximal pollen and nectar rewards (Kleber, 1935), the relevant time-information for this might be related to the mushroom bodies by the PDF-network (Beer, accepted). Ants of the species *C. mus* are able to estimate nectar flow rates and when to return to a nectary (Roces et al., 1998). To time flow rates and learn how often certain nectaries can be visited, a connection of the mushroom bodies and the clock might be necessary. No fibers could be seen in close vicinity to the central complex, which is in stark contrast to the honeybee, where numerous PDF-fibers encircle the central complex (Beer, accepted). In the cockroach, the PDF fibers do not encircle the central complex as in bees, but the fibers from the two hemispheres connect dorsal of it (Wei et al., 2010). The central complex is associated with sky-compass orientation (reviewed in (Homberg et al., 2011; Homberg, 2015)), which is very important for bees and locusts. Thus the PDF-fibers in close vicinity hint at a relay of time-information to the sky-compass processing center. One of the pathways connecting the optic lobes to the central complex for sky-compass orientation are the posterior optic tubercles, which are connected to the protocerebral bridge. These structures are also densely innervated in bees (Beer, accepted) and cockroaches (Wei et al., 2010), but not in ants. It is not known whether *C. floridanus* uses sky-compass orientation, but the absence of PDF fibers in vicinity to the sky-compass input pathways indicates that it might not play a prominent role in their orientation.

4.2.3.4 A connection between the clock and olfactory memory

Not only is the PDF network arborizing closely to the mushroom bodies, the centers for memory formation, it also reaches out towards the antennal lobes, the center for olfaction, and skirts its glomeruli. The antennal lobes of *C. floridanus* workers are quite large and consist on average of approximately 450 glomeruli, which can be grouped in 7 distinct clusters (Zube et al., 2008).

This again emphasizes the role of olfaction as primary sensory input. It cannot be said definitely which cluster of glomeruli is skirted by the PDF cells. Also, it is not known yet what the functional differences between the clusters are. Zube et al. (2008) could not find specific clusters that were involved in processing of pheromones or other odors. Still, it would be interesting to know if the glomeruli connected to PDF are in some way special, since PDF does not invade the whole antennal lobe. A close vicinity of PDF fibers and the glomeruli might result in circadian differences in olfactory sensitivity. For example, the clock might control sensitivity to different pheromones. Furthermore, the PDF-fibers do not only connect the PDF-cell bodies to the AL, but there are also connections between the antennal lobes and the plexi underneath the mushroom body calyces. The single fiber that was found to connect Plexus 3, directly underneath the medial calyx and the antennal lobe (in only one brain) seemed to grow downward, from the mushroom body lip to the antennal lobe. Taken together, the hypothesis that the clock might play a role in time-based learning of different odors arises. For example, it makes sense for foragers of *C. floridanus* to visit nectaries only during times when the flowers are open. A similar behavior is known in honeybees, which can learn the time of day at which to visit certain flowers (Kleber, 1935). Perhaps the sensitivity to certain odors of flowers is controlled in a circadian fashion after ants have learned when these food sources are available. What can be considered definite, is that the connection between the antennal lobe and the plexi of the anterior optic commissure through the anterior fiber plexus is very prominent, indicating that this indeed a very important connection point for mixing of information from the different brain centers. Since the AFP rolls down anteriorly, touches the antennal lobes and then reverts back to the AOC more posteriorly, the question also arises whether this is some sort of feedback loop. The AOC arises from one of the more distal plexi between the ventrolateral protocerebrum and superior lateral protocerebrum, before fibers reach the medial lobes or midline. It is possible that the presence or absence of certain odors have an influence on the transmission of signals to brain centers lying further downstream, like the mushroom bodies or pars intercerebralis (see below). This might, for example, happen in nurses, which are rhythmic in social isolation, but show arrhythmic behavior in presence of the brood (Mildner and Roces, 2017). The brood of social insects gives off a pheromone (Walsh and Tschinkel, 1974; Le Conte et al., 1990) which would be registered by the antennal lobes, and might disrupt the relay of time-information to locomotor centers. PDF-positive cells have been shown to elicit rhythmic locomotor behavior in Drosophila melanogaster (reviewed in (Helfrich-Förster, 2009)). Thus, pheromonal input through the antennal lobes, disrupting the relay of circadian signals to locomotor activity centers via PDF, might be a good explanation for this phenomenon. Innervations of the antennal lobes can also be found in the honeybee (Beer, accepted) and in

the cockroach (Wei et al., 2010), and the AFP of *C. floridanus* closely resembles the AFP described for *Leucophea maderae* by (Wei et al., 2010).

4.2.3.5 The clock might control rhythmic hormonal secretion in *C. floridanus*

The fibers of PDF travelling in the anterior optic commissure meet in the middle of the brain and form a plexus, the medial Plexus, in direct vicinity to the pars intercerebralis. The varicose nature of the fibers in this plexus indicate that this is an output site of PDF. Since the pars intercerebralis is known as a circadian controlled neurosecretory center in Drosophila melanogaster (Köpf, 1957; Rensing, 1966), it is quite safe to assume that PDF relays time-information from the clock to the pars intercerebralis to trigger time-dependent secretion of hormones. Similar arborizations in close vicinity to the pars intercerebralis can be observed in honeybees (Beer, accepted) and cockroaches (Wei et al., 2010).

4.2.4 The PDF-network of *C. floridanus* partly resembles the cockroach and honeybee

Summarizing the similarities between the carpenter ant, the honeybee and the cockroach, it becomes apparent that all three systems differ only slightly from one another. The most striking dissimilarities rest perhaps in the absence of fibers in the vicinity of the central complex, the POTus and the POT. Both can most probably be explained by the orientation system of *C. floridanus*. Whereas vision and sky-compass orientation plays a big role in the flying honeybee and also the cockroach, it might not be as prominent a factor for orientation in the carpenter ant. Thus, time-information relay to the central complex or the other medulla may simply not be needed. Studies on flying ants, unmated queens and males of *C. floridanus* and their PDF-network might provide useful information in this area. If these ants expressed fibers in vicinity to sun-compass-pathways, it might indeed be a lost trait in non-flying workers. When comparing the PDF-network in ants, cockroaches and bees visually, cockroaches and ants seem to indeed share a more similar network than bees and ants. The very prominent AOC and AFP that can be found in both ants and cockroaches (Wei et al., 2010), seems to be absent bees, instead fibers are arborizing throughout the whole anterior protocerebrum between the borders and the antennal lobes. This might be counterintuitive at first, seeing that ants and bees both belong to the eusocial insects and have similar requirements in their circadian organization. Still, the similarities between the ant and the cockroach might be due to an even more basal common trait, their nocturnality. Both animals need to navigate in the night, and their visual systems should thus be adapted to the special tasks this implies. Since the endogenous clock is closely

coupled to the visual system and nocturnal activity might also enhance the need to activate other sensory receptors (like olfactory reception), the observed structural similarities might be an adaptation to the night life. Though the ant PDF-network differs in the abundance of fibers, it shares properties of the bee and other insects' PDF-networks, indicating conserved structures of PDF-fibers among insects.

4.3 The localization and cycling of the Period protein in *C. floridanus*

4.3.1 The morphology of the PER network of *C. floridanus* resembles that of the honeybee and the fruit fly

The PER-antibody raised against *Apis mellifera* PER by Eva Winnebeck (Fuchikawa et al., 2017) reliably stained four distinct clusters of neurons in the ant brain. Two of these clusters were located in the dorsal, two in the lateral part of the central brain, resembling the overall organization of PER in the honey bee brain, as reported in (Fuchikawa et al., 2017). Though there are slight differences in the number of cells in each cluster, as well as in the presence of subgroups, the similarities are striking when comparing each cluster. The group of DN can be found in the same location in both, *A. mellifera* and *C. floridanus*. The number of cells in this cluster does not differ a lot, with 15 cells in the bee and approximately 12-14 in the ant, if both the anterior and posterior subgroups of the DN are combined. Though anterior and posterior subgroups have not been described in the honeybee (Fuchikawa et al., 2017), personal communication by Katharina Beer revealed that in a more detailed check of the DN cluster, an anterior group of approximately 6 DN can also be found in the bee (not published). The organization into an anterior and posterior cluster of DN is thus consistent in the two hymenopteran species and also reminds of the DN_1 in *Drosophila melanogaster*. *Drosophila´*s DN_1 can also be sub grouped into an anterior and a posterior group that differ from one another in the composition of neurotransmitters and their projection patterns (Shafer et al., 2002). Though there is no data available on the composition of neurotransmitters in PER-positive cells of *C. floridanus* and *A. mellifera*, future studies investigating the connection between the spatial grouping and neurotransmitter content would be very interesting. The most strongly stained cluster of DLN in *C. floridanus* was not as strongly stained in *A. mellifera* and counted approximately double as many cells as in the ant (Fuchikawa et al., 2017). Similarly, the LN_1 of *A. mellifera* (105-120) are more than double the number of *C. floridanus* (40-50), and they cannot be sub grouped visually as in the ant (Fuchikawa et al., 2017). In *C. floridanus*, a subset of 6 LN_1, the LN_1', is clearly separated from the rest of the neurons by a fixed distance. This cannot be observed in the bee. Still, looking at *Drosophila melanogaster*, the group of LN_d also

looks homogenous, but can be subdivided into two, albeit very closely located, subclusters (Helfrich-Förster et al., 2007a; Johard et al., 2009). The last cluster of cells, the PDF-co-expressing LN_2, were the smallest cluster of cells in *C. floridanus*, with only 2-5 cells. Interestingly, not all PDF-expressing cells (~7) were co-labelled with PER. This is quite different in the honeybee, were all 15 PDF-expressing cells were co-labeled with PER (Fuchikawa et al., 2017). This discrepancy might easily be explained by the very low staining intensity of LN_2 cells *in C. floridanus*. It is possible, that the staining in some cells was so faint that it could not be detected. Further staining of PDF and PER on sections of *C. floridanus* brains might be the means to answer this question. A further difference between the staining patterns of PER in honeybee and fruit fly brains to those in the carpenter ant is the absence of glial staining. Again, low staining intensities of glia with the antibody that was originally raised against bees might be the explanation, rather than true differences between the three insects. Looking at the PDF fibers stained in the same brains as PER, it becomes apparent that the PDF network often rests closely to PER-expressing cells, like the DLN, LN_1 and LN_2. Still, more histological studies investigating the connection between PDF and PER in *C. floridanus* are needed to establish the meaning of this feature. In relation to the bee however, this is quite similar, since PDF often arborizes in the vicinity of clock neurons and surrounded by PER-expressing glial cells. In summary, the pattern of PER-staining in *C. floridanus* strongly resembles those found in *Apis mellifera* and *Drosophila melanogaster*.

4.3.2 The levels of PER protein in nocturnal *C. floridanus* cycle like those of diurnal insects

When comparing the rise and fall of PER protein levels in five neuronal groups of two colonies of *C. floridanus*, a common pattern became visible. In both cases, PER levels of all clusters reached their respective maxima around lights on, their minima at or shortly after lights off. This is the same pattern that has been reported for diurnal insects, like flies and bees (Zerr et al., 1990; Shafer et al., 2002; Yoshii et al., 2009; Fuchikawa et al., 2017). Their PER levels also rise to a maximum at the beginning of the light phase, then decline to minimal levels until the beginning of the dark phase. Since the examined individuals of *C. floridanus* were establishedly nocturnal, the PER cycling of nocturnal and diurnal insects seems to be the same, just as in mammals. In mammals, the PER protein of nocturnal and diurnal species also cycles in phase in the cells of the suprachiasmatic nucleus (SCN), the mammalian central pacemaker in the brain (Inouye and Kawamura, 1979; Sato and Kawamura, 1984; Kurumiya and Kawamura, 1988; Challet, 2007; Hut et al., 2012). This cycling and its phase seems to stay conserved, even when mammals of one species switch their activity from one phase of the day to the other

(reviewed in (Riede et al., 2017; van der Veen et al., 2017)). Since *C. floridanus* colonies do not only consist of nocturnal, but also diurnal and arrhythmic animals, the very interesting opportunity of investigating the cycling of PER in ants of the same colony but different activity types arises.

4.3.3 PER accumulates in the nucleus

Just as in bees or mice, PER is a part of the negative limb of the clock of *C. floridanus*, together with CRY (Rubin et al., 2006; Yuan et al., 2007; Ingram et al., 2012), which is a feature of the mammalian-type clock. In fruit flies, on the other hand, PER is also a part of the negative limb but partners with TIM (Sehgal et al., 1994; Gekakis et al., 1995; Sehgal et al., 1995). Here, PER accumulates in the cytoplasm and is translocated into the nucleus in the middle of the night (Curtin et al., 1995; Shafer et al., 2002). In mice and bees on the other hand, PER is not accumulating in the cytoplasm, but instead transferred to the nucleus immediately (Smyllie et al., 2016; Fuchikawa et al., 2017). The absence of PER staining in the cytoplasm of cells, apart from very week cytoplasmic staining of few LN_2 cells, indicates a similar mechanism in the ant.

4.4 *C. floridanus* possesses a circadian clock that is similar to other insects

Summarizing the results on circadian behavior, the neuronal network and the molecular basis of the clock, it is safe to say that *C. floridanus* possesses a circadian clock and that it shares many common properties with other insect and mammalian clocks. First, the entrainment and free-running behavior under different LD cycles and temperatures proved the presence of the basic properties of each circadian clock. Second, the PDF-network resembled that of other eusocial and nocturnal insects in many but not all aspects and connected the putative pacemaker-cells, to the optic lobes and central brain structures which might both provide in-, as well as output of the clock. Third, and lastly, Period, a protein homologous to PER in other insects, proved to cycle in abundance and is a good candidate for the negative limb of the clock. Though there is still an abundance of research that needs to be performed on the clock and circadian behavior of *C. floridanus*, first important insights could be gained from these experiments. Since the timing and behavior of eusocial insects is very intricate, further investigations into the clock of C. floridanus or other eusocial insects may still hold many fascinating revelations on the circadian system.

BIBLIOGRAPHY:

Akten B, Jauch E, Genova GK, Kim EY, Edery I, Raabe T, and Jackson FR (2003) A role for CK2 in the Drosophila circadian oscillator. Nat Neurosci 6:251-257.

Allada R, and Chung BY (2010) Circadian Organization of Behavior and Physiology in Drosophila. Annual Review of Physiology 72:605-624.

Aschoff J (1984) Circadian timing. Ann N Y Acad Sci 423:442-468.

Bae K, Lee C, Sidote D, Chuang KY, and Edery I (1998) Circadian regulation of a Drosophila homolog of the mammalian Clock gene: PER and TIM function as positive regulators. Mol Cell Biol 18:6142-6151.

Beer KK, Esther ; Kahana, Noa; Yayon, Nadav; Weiss, Ron; Menegazzi, Pamela; Bloch, Guy; Helfrich-Förster, Charlotte (accepted) Pigment-Dispersing Factor expressing neurons convey circadian information in the honey bee brain.Open Biology.

Benito J, Zheng H, Ng FS, and Hardin PE (2007) Transcriptional feedback loop regulation, function, and ontogeny in Drosophila. Cold Spring Harb Symp Quant Biol 72:437-444.

Blau J, and Young MW (1999) Cycling vrille expression is required for a functional Drosophila clock. Cell 99:661-671.

Bloch G, Rubinstein C, and Robinson G (2004) Period expression in the honey bee brain is developmentally regulated and not affected by light, flight experience, or colony type. Insect biochemistry and molecular biology 34:879-891.

Bloch G, Solomon SM, Robinson GE, and Fahrbach SE (2003) Patterns of PERIOD and pigment-dispersing hormone immunoreactivity in the brain of the European honeybee (Apis mellifera): Age- and time-related plasticity. The Journal of Comparative Neurology 464:269-284.

Bloch G, Toma DP, and Robinson GE (2001) Behavioral rhythmicity, age, division of labor and period expression in the honey bee brain. J Biol Rhythms 16:444-456.

Bodenstein C, Heiland I, and Schuster S (2012) Temperature compensation and entrainment in circadian rhythms. Phys Biol 9:036011.

Boomsma JJ, and Leusink A (1981) Weather conditions during nuptial flights of four European ant species. Oecologia 50:236-241.

Bünning E (1973) The Physiological Clock: Circadian Rhythms and Biological Chronometry. English Universities Press.

Busza A, Emery-Le M, Rosbash M, and Emery P (2004) Roles of the two Drosophila CRYPTOCHROME structural domains in circadian photoreception. Science 304:1503-1506.

Calabi P (1988) Behavioral flexibility in Hymenoptera: a re-examination of the concept of caste. Advances in myrmecology:237-258.

Challet E (2007) Minireview: Entrainment of the suprachiasmatic clockwork in diurnal and nocturnal mammals. Endocrinology 148:5648-5655.

Currie J, Goda T, and Wijnen H (2009) Selective entrainment of the Drosophila circadian clock to daily gradients in environmental temperature. BMC Biol 7:49.

Curtin KD, Huang ZJ, and Rosbash M (1995) Temporally regulated nuclear entry of the Drosophila period protein contributes to the circadian clock. Neuron 14:365-372.

Cusumano P, Klarsfeld A, Chelot E, Picot M, Richier B, and Rouyer F (2009) PDF-modulated visual inputs and cryptochrome define diurnal behavior in Drosophila. Nat Neurosci 12:1431-1437.

Cyran SA, Buchsbaum AM, Reddy KL, Lin MC, Glossop NR, Hardin PE, Young MW, Storti RV, and Blau J (2003) vrille, Pdp1, and dClock form a second feedback loop in the Drosophila circadian clock. Cell 112:329-341.

Darlington TK, Wager-Smith K, Ceriani MF, Staknis D, Gekakis N, Steeves TD, Weitz CJ, Takahashi JS, and Kay SA (1998) Closing the circadian loop: CLOCK-induced transcription of its own inhibitors per and tim. Science 280:1599-1603.

Dawson A, King VM, Bentley GE, and Ball GF (2001) Photoperiodic Control of Seasonality in Birds. J Biol Rhythm 16:365-380.

Del-Claro K, and Oliveira PS (1999) Ant-Homoptera interactions in a neotropical savanna: The honeydew-producing treehopper, Guayaquila xiphias (Membracidae), and its associated ant fauna on Didymopanax vinosum (Araliaceae). Biotropica 31:135-144.

Devaud JM, Papouin T, Carcaud J, Sandoz JC, Grunewald B, and Giurfa M (2015) Neural substrate for higher-order learning in an insect: Mushroom bodies are necessary for configural discriminations. Proc Natl Acad Sci U S A 112:E5854-5862.

Dircksen H, Zahnow CA, Gaus G, Keller R, Rao KR, and Riehm JP (1987) The Ultrastructure of Nerve-Endings Containing Pigment-Dispersing Hormone (Pdh) in Crustacean Sinus Glands - Identification by an Antiserum against a Synthetic Pdh. Cell and Tissue Research 250:377-387.

Dores RM, and Herman WS (1981) Insect chromatophorotropic factors: the isolation of polypeptides from Periplaneta americana and Apis mellifera with melanophore-dispersing activity in the crustacean, Uca pugilator. Gen Comp Endocrinol 43:76-84.

Ehmer B, and Gronenberg W (2004) Mushroom body volumes and visual interneurons in ants: comparison between sexes and castes. J Comp Neurol 469:198-213.

Emery P, So WV, Kaneko M, Hall JC, and Rosbash M (1998) CRY, a Drosophila clock and light-regulated cryptochrome, is a major contributor to circadian rhythm resetting and photosensitivity. Cell 95:669-679.

Falibene A, Roces F, and Rossler W (2015) Long-term avoidance memory formation is associated with a transient increase in mushroom body synaptic complexes in leaf-cutting ants. Front Behav Neurosci 9:84.

Falibene A, Roces F, Rossler W, and Groh C (2016) Daily Thermal Fluctuations Experienced by Pupae via Rhythmic Nursing Behavior Increase Numbers of Mushroom Body Microglomeruli in the Adult Ant Brain. Front Behav Neurosci 10:73.

Fischbach KF, and Dittrich APM (1989) The Optic Lobe of Drosophila-Melanogaster .1. A Golgi Analysis of Wild-Type Structure. Cell and Tissue Research 258:441-475.

Francois P, Despierre N, and Siggia ED (2012) Adaptive temperature compensation in circadian oscillations. PLoS Comput Biol 8:e1002585.

Fuchikawa T, Beer K, Linke-Winnebeck C, Ben-David R, Kotowoy A, Tsang VWK, Warman GR, Winnebeck EC, Helfrich-Förster C, and Bloch G (2017) Neuronal circadian clock protein oscillations are similar in behaviourally rhythmic forager honeybees and in arrhythmic nurses. Open Biol 7.

Garrett JW, and Campbell CS (1980) Changes in social behavior of the male golden hamster accompanying photoperiodic changes in reproduction. Hormones and Behavior 14:303-318.

Garshelis DL, and Pelton MR (1980) Activity of Black Bears in the Great Smoky Mountains National Park. Journal of Mammalogy 61:8-19.

Gekakis N, Saez L, Delahaye-Brown AM, Myers MP, Sehgal A, Young MW, and Weitz CJ (1995) Isolation of timeless by PER protein interaction: defective interaction between timeless protein and long-period mutant PERL. Science 270:811-815.

Gekakis N, Staknis D, Nguyen HB, Davis FC, Wilsbacher LD, King DP, Takahashi JS, and Weitz CJ (1998) Role of the CLOCK Protein in the Mammalian Circadian Mechanism. Science 280:1564-1569.

Giurfa M (2007) Behavioral and neural analysis of associative learning in the honeybee: a taste from the magic well. J Comp Physiol A Neuroethol Sens Neural Behav Physiol 193:801-824.

Glaser FT, and Stanewsky R (2005) Temperature synchronization of the Drosophila circadian clock. Curr Biol 15:1352-1363.

Glaser W (1978) Varianzanalyse Gustav Fischer Verlag. Stuttgart, New York.
Glossop NR, Houl JH, Zheng H, Ng FS, Dudek SM, and Hardin PE (2003) VRILLE feeds back to control circadian transcription of Clock in the Drosophila circadian oscillator. Neuron 37:249-261.
Gordon DM (1983) Daily rhythms in social activities of the harvester ant. Pogonomyrmex badius. Psyche 90:413-423.
Gordon DM (1989) Dynamics of task switching in harvester ants. Anim Behav 38:194-204.
Gronenberg W (1999) Modality-specific segregation of input to ant mushroom bodies. Brain Behav Evol 54:85-95.
Gronenberg W (2008) Structure and function of ant (Hymenoptera: Formicidae) brains: Strength in numbers.
Gronenberg W, and Holldobler B (1999) Morphologic representation of visual and antennal information in the ant brain. J Comp Neurol 412:229-240.
Halberg F (1959) [Physiologic 24-hour periodicity; general and procedural considerations with reference to the adrenal cycle]. Int Z Vitaminforsch Beih 10:225-296.
Hansen SR (1978) Resource utilization and coexistence of three species of Pogonomyrmex ants in an Upper Sonoran Grassland Community. Oecologia 35:109-117.
Hao H, Allen DL, and Hardin PE (1997) A circadian enhancer mediates PER-dependent mRNA cycling in Drosophila melanogaster. Mol Cell Biol 17:3687-3693.
Hardin PE (2011) Molecular Genetic Analysis of Circadian Timekeeping in Drosophila. Adv Genet 74:141-173.
Hardin PE, Hall JC, and Rosbash M (1990) Feedback of the Drosophila period gene product on circadian cycling of its messenger RNA levels. Nature 343:536-540.
Heisenberg M (2003) Mushroom body memoir: from maps to models. Nat Rev Neurosci 4:266-275.
Helfrich-Förster C (1995) The period clock gene is expressed in central nervous system neurons which also produce a neuropeptide that reveals the projections of circadian pacemaker cells within the brain of Drosophila melanogaster. Proc Natl Acad Sci U S A 92:612-616.
Helfrich-Förster C (1997) Development of pigment-dispersing hormone-immunoreactive neurons in the nervous system of Drosophila melanogaster. J Comp Neurol 380:335-354.
Helfrich-Förster C (2004) The circadian clock in the brain: a structural and functional comparison between mammals and insects. J Comp Physiol A Neuroethol Sens Neural Behav Physiol 190:601-613.
Helfrich-Förster C (2005) Neurobiology of the fruit fly's circadian clock. Genes, Brain and Behavior 4:65-76.
Helfrich-Förster C (2009) Does the morning and evening oscillator model fit better for flies or mice? J Biol Rhythms 24:259-270.
Helfrich-Förster C, and Homberg U (1993) Pigment-dispersing hormone-immunoreactive neurons in the nervous system of wild-type Drosophila melanogaster and of several mutants with altered circadian rhythmicity. J Comp Neurol 337:177-190.
Helfrich-Förster C, Shafer OT, Wülbeck C, Grieshaber E, Rieger D, and Taghert P (2007a) Development and morphology of the clock-gene-expressing lateral neurons of Drosophila melanogaster. J Comp Neurol 500:47-70.
Helfrich-Förster C, Shafer OT, Wülbeck C, Grieshaber E, Rieger D, and Taghert P (2007b) Development and morphology of the clock-gene-expressing lateral neurons of Drosophila melanogaster. The Journal of Comparative Neurology 500:47-70.
Helfrich-Förster C, Stengl M, and Homberg U (1998) Organization of the circadian system in insects. Chronobiol Int 15:567-594.
Helfrich-Förster C, Tauber M, Park JH, Muhlig-Versen M, Schneuwly S, and Hofbauer A (2000) Ectopic expression of the neuropeptide pigment-dispersing factor alters behavioral rhythms in Drosophila melanogaster. J Neurosci 20:3339-3353.

Hofbauer A, Ebel T, Waltenspiel B, Oswald P, Chen YC, Halder P, Biskup S, Lewandrowski U, Winkler C, Sickmann A, Buchner S, and Buchner E (2009) The Wuerzburg hybridoma library against Drosophila brain. J Neurogenet 23:78-91.

Hölldobler B, and Wilson EO (1990) The ants. pp xii, 732 p., 724 p. of plates, Belknap Press of Harvard University Press, Cambridge, Mass.

Homberg U (2015) Sky Compass Orientation in Desert Locusts-Evidence from Field and Laboratory Studies. Frontiers in Behavioral Neuroscience 9.

Homberg U, Heinze S, Pfeiffer K, Kinoshita M, and El Jundi B (2011) Central neural coding of sky polarization in insects. Philos T R Soc B 366:680-687.

Homberg U, Würden S, Dircksen H, and Rao KR (1991) Comparative anatomy of pigment-dispersing hormone-immunoreactive neurons in the brain of orthopteroid insects. Cell and Tissue Research 266:343-357.

Hosokawa N, Hatakeyama TS, Kojima T, Kikuchi Y, Ito H, and Iwasaki H (2011) Circadian transcriptional regulation by the posttranslational oscillator without de novo clock gene expression in Synechococcus. Proc Natl Acad Sci U S A 108:15396-15401.

Hu KG, Reichert H, and Stark WS (1978) Electrophysiological Characterization of Drosophila Ocelli. J Comp Physiol 126:15-24.

Hughes S, Jagannath A, Hankins MW, Foster RG, and Peirson SN (2015) Photic Regulation of Clock Systems. Methods in Enzymology 552:125-143.

Hunt JH (1974) Temporal activity patterns in two competing ant species (Hymenoptera: Formicidae). Psyche 81:237-242.

Hut RA, Kronfeld-Schor N, van der Vinne V, and De la Iglesia H (2012) In search of a temporal niche: environmental factors. Prog Brain Res 199:281-304.

Hut RA, Pilorz V, Boerema AS, Strijkstra AM, and Daan S (2011) Working for food shifts nocturnal mouse activity into the day. PLoS One 6:e17527.

Hyun S, Lee Y, Hong ST, Bang S, Paik D, Kang J, Shin J, Lee J, Jeon K, Hwang S, Bae E, and Kim J (2005) Drosophila GPCR Han is a receptor for the circadian clock neuropeptide PDF. Neuron 48:267-278.

Ikeda M, and Nomura M (1997) cDNA Cloning and Tissue-Specific Expression of a Novel Basic Helix–Loop–Helix/PAS Protein (BMAL1) and Identification of Alternatively Spliced Variants with Alternative Translation Initiation Site Usage. Biochemical and Biophysical Research Communications 233:258-264.

Im SH, Li W, and Taghert PH (2011) PDFR and CRY signaling converge in a subset of clock neurons to modulate the amplitude and phase of circadian behavior in Drosophila. PLoS One 6:e18974.

Im SH, and Taghert PH (2010) PDF receptor expression reveals direct interactions between circadian oscillators in Drosophila. J Comp Neurol 518:1925-1945.

Ingram KK, Kutowoi A, Wurm Y, Shoemaker D, Meier R, and Bloch G (2012) The molecular clockwork of the fire ant Solenopsis invicta. PLoS One 7:e45715.

Inouye ST, and Kawamura H (1979) Persistence of circadian rhythmicity in a mammalian hypothalamic "island" containing the suprachiasmatic nucleus. Proc Natl Acad Sci U S A 76:5962-5966.

Jaffe K, and Sanchez C (1984) On the Nestmate-Recognition System and Territorial Marking Behavior in the Ant Camponotus-Rufipes. Insect Soc 31:302-315.

Jayatilaka P, Narendra A, Reid SF, Cooper P, and Zeil J (2011) Different effects of temperature on foraging activity schedules in sympatric Myrmecia ants. The Journal of Experimental Biology 214:2730-2738.

Johard HA, Yoishii T, Dircksen H, Cusumano P, Rouyer F, Helfrich-Förster C, and Nässel DR (2009) Peptidergic clock neurons in Drosophila: ion transport peptide and short neuropeptide F in subsets of dorsal and ventral lateral neurons. J Comp Neurol 516:59-73.

Kadener S, Stoleru D, McDonald M, Nawathean P, and Rosbash M (2007) Clockwork Orange is a transcriptional repressor and a new Drosophila circadian pacemaker component. Genes Dev 21:1675-1686.

Kaneko M, and Hall JC (2000) Neuroanatomy of cells expressing clock genes in Drosophila: transgenic manipulation of the period and timeless genes to mark the perikarya of circadian pacemaker neurons and their projections. J Comp Neurol 422:66-94.

Kaneko M, Helfrich-Förster C, and Hall JC (1997) Spatial and temporal expression of the period and timeless genes in the developing nervous system of Drosophila: newly identified pacemaker candidates and novel features of clock gene product cycling. J Neurosci 17:6745-6760.

Kannowski P (1959) The flight activities and colony founding behaviour of bog ants in South Eastern Michigan. pp 115-162.

Kannowski PB (1962) The flight activities of formicine ants. Symposia Genetica et Biologica Italica 12:74-102.

King DP, Zhao Y, Sangoram AM, Wilsbacher LD, Tanaka M, Antoch MP, Steeves TDL, Vitaterna MH, Kornhauser JM, Lowrey PL, Turek FW, and Takahashi JS (1997) Positional Cloning of the Mouse Circadian Clock Gene. Cell 89:641-653.

Kleber E (1935) Hat das Zeitgedächtnis der Bienen biologische Bedeutung? Zeitschrift für vergleichende Physiologie 22:221-262.

Kloss B, Price JL, Saez L, Blau J, Rothenfluh A, Wesley CS, and Young MW (1998) The Drosophila clock gene double-time encodes a protein closely related to human casein kinase Iepsilon. Cell 94:97-107.

Kloss B, Rothenfluh A, Young MW, and Saez L (2001) Phosphorylation of period is influenced by cycling physical associations of double-time, period, and timeless in the Drosophila clock. Neuron 30:699-706.

Knowles A, Koh K, Wu JT, Chien CT, Chamovitz DA, and Blau J (2009) The COP9 signalosome is required for light-dependent timeless degradation and Drosophila clock resetting. J Neurosci 29:1152-1162.

Ko CH, and Takahashi JS (2006) Molecular components of the mammalian circadian clock. Hum Mol Genet 15 Spec No 2:R271-277.

Koh K, Zheng X, and Sehgal A (2006) JETLAG resets the Drosophila circadian clock by promoting light-induced degradation of TIMELESS. Science 312:1809-1812.

Kolbe E (2014) Charakterisierung von Neuronen im Bienengehirn, die das Neuropeptid „Pigment-Dispersing Factor "(PDF) exprimieren sowie deren mögliche Rolle in der Inneren Uhr der Honigbiene Apis mellifera. In.

Konopka RJ, and Benzer S (1971) Clock mutants of Drosophila melanogaster. Proc Natl Acad Sci U S A 68:2112-2116.

Köpf H (1957) Zur Topographie und Morphologie neurosekretorischer Zentren bei Drosophila. Naturwissenschaften 44:121-122.

Kurumiya S, and Kawamura H (1988) Circadian oscillation of the multiple unit activity in the guinea pig suprachiasmatic nucleus. J Comp Physiol A 162:301-308.

Le Conte Y, Arnold G, Trouiller J, Masson C, and Chappe B (1990) Identification of a brood pheromone in honeybees. Naturwissenschaften 77:334-336.

Lear BC, Merrill CE, Lin JM, Schroeder A, Zhang L, and Allada R (2005) A G protein-coupled receptor, groom-of-PDF, is required for PDF neuron action in circadian behavior. Neuron 48:221-227.

Lee C, Bae K, and Edery I (1998) The Drosophila CLOCK protein undergoes daily rhythms in abundance, phosphorylation, and interactions with the PER-TIM complex. Neuron 21:857-867.

Levieux J, and Diomande T (1978) Nutrition of Granivorous Ants .1. Cycle of Activity and Diet or Messor-Galla and Messor (= Cratomyrmex) Regalis (Hymenoplera, Formicidae). Insect Soc 25:127-139.
Li Y, Guo F, Shen J, and Rosbash M (2014) PDF and cAMP enhance PER stability in Drosophila clock neurons. Proc Natl Acad Sci U S A 111:E1284-1290.
Lim C, Chung BY, Pitman JL, McGill JJ, Pradhan S, Lee J, Keegan KP, Choe J, and Allada R (2007) Clockwork orange encodes a transcriptional repressor important for circadian-clock amplitude in Drosophila. Curr Biol 17:1082-1089.
Lim C, Lee J, Choi C, Kilman VL, Kim J, Park SM, Jang SK, Allada R, and Choe J (2011) The novel gene twenty-four defines a critical translational step in the Drosophila clock. Nature 470:399-403.
Lin JM, Kilman VL, Keegan K, Paddock B, Emery-Le M, Rosbash M, and Allada R (2002) A role for casein kinase 2alpha in the Drosophila circadian clock. Nature 420:816-820.
Linkert M, Rueden CT, Allan C, Burel J-M, Moore W, Patterson A, Loranger B, Moore J, Neves C, MacDonald D, Tarkowska A, Sticco C, Hill E, Rossner M, Eliceiri KW, and Swedlow JR (2010) Metadata matters: access to image data in the real world. The Journal of Cell Biology 189:777-782.
Longair MH, Baker DA, and Armstrong JD (2011) Simple Neurite Tracer: open source software for reconstruction, visualization and analysis of neuronal processes. Bioinformatics 27:2453-2454.
López-Olmeda JF (2017) Nonphotic entrainment in fish. Comparative Biochemistry and Physiology Part A: Molecular & Integrative Physiology 203:133-143.
Mairan D (1729) J. J. Observation Botanique. Histoir de l'Académie royale des sciences avec les mémoires de mathématique et de physique tirés des registres de cette Académie:35-36.
Matsumoto A, Ukai-Tadenuma M, Yamada RG, Houl J, Uno KD, Kasukawa T, Dauwalder B, Itoh TQ, Takahashi K, Ueda R, Hardin PE, Tanimura T, and Ueda HR (2007) A functional genomics strategy reveals clockwork orange as a transcriptional regulator in the Drosophila circadian clock. Genes Dev 21:1687-1700.
Maywood ES, Reddy AB, Wong GK, O'Neill JS, O'Brien JA, McMahon DG, Harmar AJ, Okamura H, and Hastings MH (2006) Synchronization and maintenance of timekeeping in suprachiasmatic circadian clock cells by neuropeptidergic signaling. Curr Biol 16:599-605.
McCluskey ES (1958) Daily Rhythms in Male Harvester and Argentine Ants. Science 128:536-537.
McCluskey ES (1965) Circadian-RIhythms in Male-Ants of Five Diverse Species. Science 150:1037-1039.
McCluskey ES (1967) Circadian rhythms in female ants, and loss after mating flight. Comp Biochem Physiol 23:665-677.
Mccluskey ES (1974) Generic Diversity in Phase of Rhythm in Myrmicine Ants. J New York Entomol S 82:93-102.
McCluskey ES, and Carter CE (1969) Loss of rhythmic activity in female ants caused by mating. Comp Biochem Physiol 31:217-226.
Medeiros J, Azevedo DL, Santana MA, Lopes TR, and Araujo A (2014) Foraging activity rhythms of Dinoponera quadriceps (Hymenoptera: Formicidae) in its natural environment. J Insect Sci 14.
Meissner RA, Kilman VL, Lin JM, and Allada R (2008) TIMELESS is an important mediator of CK2 effects on circadian clock function in vivo. J Neurosci 28:9732-9740.
Mertens I, Vandingenen A, Johnson EC, Shafer OT, Li W, Trigg JS, De Loof A, Schoofs L, and Taghert PH (2005) PDF receptor signaling in Drosophila contributes to both circadian and geotactic behaviors. Neuron 48:213-219.
Mildner S, and Roces F (2017) Plasticity of Daily Behavioral Rhythms in Foragers and Nurses of the Ant Camponotus rufipes: Influence of Social Context and Feeding Times. PLoS One 12:e0169244.

Miskiewicz K, Pyza E, and Schurmann FW (2004) Ultrastructural characteristics of circadian pacemaker neurones, immunoreactive to an antibody against a pigment-dispersing hormone in the fly's brain. Neurosci Lett 363:73-77.

Miskiewicz K, Schurmann FW, and Pyza E (2008) Circadian release of pigment-dispersing factor in the visual system of the housefly, Musca domestica. J Comp Neurol 509:422-435.

Nässel DR (2002) Neuropeptides in the nervous system of Drosophila and other insects: multiple roles as neuromodulators and neurohormones. Prog Neurobiol 68:1-84.

Nässel DR, and Homberg U (2006) Neuropeptides in interneurons of the insect brain. Cell Tissue Res 326:1-24.

Nässel DR, Persson MG, and Muren JE (2000) Baratin, a nonamidated neurostimulating neuropeptide, isolated from cockroach brain: distribution and actions in the cockroach and locust nervous systems. J Comp Neurol 422:267-286.

Nässel DR, Shiga S, Mohrherr CJ, and Rao KR (1993) Pigment-dispersing hormone-like peptide in the nervous system of the flies Phormia and Drosophila: immunocytochemistry and partial characterization. J Comp Neurol 331:183-198.

Nässel DR, Shiga S, Wikstrand EM, and Rao KR (1991) Pigment-dispersing hormone-immunoreactive neurons and their relation to serotonergic neurons in the blowfly and cockroach visual system. Cell Tissue Res 266:511-523.

Nitabach MN, and Taghert PH (2008) Organization of the Drosophila circadian control circuit. Curr Biol 18:R84-93.

Ohata K, Nishiyama H, and Tsukahara Y (1998) Action spectrum of the circadian clock photoreceptor in Drosophila melanogaster. Biological clocks: Mechanisms and applications:167-170.

Özkaya Ö, and Rosato E (2012) Chapter 4 - The Circadian Clock of the Fly: A Neurogenetics Journey Through Time. In Advances in Genetics, MB Sokolowski, and SF Goodwin, eds, pp 79-123, Academic Press.

Park JH, and Hall JC (1998) Isolation and chronobiological analysis of a neuropeptide pigment-dispersing factor gene in Drosophila melanogaster. J Biol Rhythms 13:219-228.

Pearn MT, Randall LL, Shortridge RD, Burg MG, and Pak WL (1996) Molecular, biochemical, and electrophysiological characterization of Drosophila norpA mutants. J Biol Chem 271:4937-4945.

Peschel N, Chen KF, Szabo G, and Stanewsky R (2009) Light-dependent interactions between the Drosophila circadian clock factors cryptochrome, jetlag, and timeless. Curr Biol 19:241-247.

Peschel N, and Helfrich-Förster C (2011) Setting the clock - by nature: Circadian rhythm in the fruitfly Drosophila melanogaster. Febs Letters 585:1435-1442.

Petri B, and Stengl M (1997) Pigment-dispersing hormone shifts the phase of the circadian pacemaker of the cockroach Leucophaea maderae. J Neurosci 17:4087-4093.

Petri B, Stengl M, Wurden S, and Homberg U (1995) Immunocytochemical characterization of the accessory medulla in the cockroach Leucophaea maderae. Cell Tissue Res 282:3-19.

Pittendrigh CS (1960) Circadian rhythms and the circadian organization of living systems. Cold Spring Harb Symp Quant Biol 25:159-184.

Pittendrigh CS (1993) Temporal organization: reflections of a Darwinian clock-watcher. Annu Rev Physiol 55:16-54.

Rao KR (2001) Crustacean pigmentary-effector hormones: Chemistry and functions of RPCH, PDH, and related peptides. American Zoologist 41:364-379.

Reischig T, and Stengl M (1996) Morphology and pigment-dispersing hormone immunocytochemistry of the accessory medulla, the presumptive circadian pacemaker of the cockroach Leucophaea maderae: a light- and electron-microscopic study. Cell and Tissue Research 285:305-319.

Reischig T, and Stengl M (2002) Optic lobe commissures in a three-dimensional brain model of the cockroach Leucophaea maderae: a search for the circadian coupling pathways. J Comp Neurol 443:388-400.
Reischig T, and Stengl M (2003a) Ectopic transplantation of the accessory medulla restores circadian locomotor rhythms in arrhythmic cockroaches (Leucophaea maderae). J Exp Biol 206:1877-1886.
Reischig T, and Stengl M (2003b) Ultrastructure of pigment-dispersing hormone-immunoreactive neurons in a three-dimensional model of the accessory medulla of the cockroach Leucophaea maderae. Cell Tissue Res 314:421-435.
Reisz-Porszasz S, Probst MR, Fukunaga BN, and Hankinson O (1994) Identification of functional domains of the aryl hydrocarbon receptor nuclear translocator protein (ARNT). Molecular and Cellular Biology 14:6075-6086.
Rensing L (1966) Zur circadianen Rhythmik des Hormonsystems von Drosophila. Zeitschrift für Zellforschung und Mikroskopische Anatomie 74:539-558.
Ribi WA (1975) Golgi studies of the first optic ganglion of the ant, Cataglyphis bicolor. Cell Tissue Res 160:207-217.
Richier B, Michard-Vanhee C, Lamouroux A, Papin C, and Rouyer F (2008) The clockwork orange Drosophila protein functions as both an activator and a repressor of clock gene expression. J Biol Rhythms 23:103-116.
Riede SJ, van der Vinne V, and Hut RA (2017) The flexible clock: predictive and reactive homeostasis, energy balance and the circadian regulation of sleep-wake timing. J Exp Biol 220:738-749.
Roces F (1995) Variable Thermal Sensitivity as Output of a Circadian Clock Controlling the Bimodal Rhythm of Temperature Choice in the Ant Camponotus Mus. Journal of Comparative Physiology a-Sensory Neural and Behavioral Physiology 177:637-643.
Roces F, Farina WM, and Josens RB (1998) Nectar feeding by the ant Camponotus mus: intake rate and crop filling as a function of sucrose concentration. J Insect Physiol 44:579-585.
Roces F, and Nunez JA (1989a) Brood Translocation and Circadian Variation of Temperature Preference in the Ant Camponotus-Mus. Oecologia 81:33-37.
Roces F, and Nunez JA (1989b) Brood translocation and circadian variation of temperature preference in the ant Camponotus mus. Oecologia 81:33-37.
Rodriguez-Zas SL, Southey BR, Shemesh Y, Rubin EB, Cohen M, Robinson GE, and Bloch G (2012) Microarray Analysis of Natural Socially-Regulated Plasticity in Circadian Rhythms of Honey Bees. J Biol Rhythm 27:12-24.
Rubin EB, Shemesh Y, Cohen M, Elgavish S, Robertson HM, and Bloch G (2006) Molecular and phylogenetic analyses reveal mammalian-like clockwork in the honey bee (Apis mellifera) and shed new light on the molecular evolution of the circadian clock. Genome Res 16:1352-1365.
Rutila JE, Suri V, Le M, So WV, Rosbash M, and Hall JC (1998) CYCLE is a second bHLH-PAS clock protein essential for circadian rhythmicity and transcription of Drosophila period and timeless. Cell 93:805-814.
Sato T, and Kawamura H (1984) Circadian rhythms in multiple unit activity inside and outside the suprachiasmatic nucleus in the diurnal chipmunk (Eutamias sibiricus). Neurosci Res 1:45-52.
Schindelin J, Arganda-Carreras I, Frise E, Kaynig V, Longair M, Pietzsch T, Preibisch S, Rueden C, Saalfeld S, Schmid B, Tinevez J-Y, White DJ, Hartenstein V, Eliceiri K, Tomancak P, and Cardona A (2012) Fiji: an open-source platform for biological-image analysis. Nat Meth 9:676-682.
Schlichting M, and Helfrich-Förster C (2015a) Chapter Five - Photic Entrainment in Drosophila Assessed by Locomotor Activity Recordings. In Methods in Enzymology, A Sehgal, ed, pp 105-123, Academic Press.
Schlichting M, and Helfrich-Förster C (2015b) Photic Entrainment in Drosophila Assessed by Locomotor Activity Recordings. Methods in Enzymology 552:105-123.

Schmid B, Helfrich-Förster C, and Yoshii T (2011) A new ImageJ plug-in "ActogramJ" for chronobiological analyses. J Biol Rhythms 26:464-467.
Schulze J, Neupert S, Schmidt L, Predel R, Lamkemeyer T, Homberg U, and Stengl M (2012) Myoinhibitory peptides in the brain of the cockroach Leucophaea maderae and colocalization with pigment-dispersing factor in circadian pacemaker cells. J Comp Neurol 520:1078-1097.
Searle I, and Coupland G (2004) Induction of flowering by seasonal changes in photoperiod. The EMBO Journal 23:1217-1222.
Sehgal A, Price JL, Man B, and Young MW (1994) Loss of circadian behavioral rhythms and per RNA oscillations in the Drosophila mutant timeless. Science 263:1603-1606.
Sehgal A, Rothenfluh-Hilfiker A, Hunter-Ensor M, Chen Y, Myers MP, and Young MW (1995) Rhythmic expression of timeless: a basis for promoting circadian cycles in period gene autoregulation. Science 270:808-810.
Seluzicki A, Flourakis M, Kula-Eversole E, Zhang L, Kilman V, and Allada R (2014) Dual PDF signaling pathways reset clocks via TIMELESS and acutely excite target neurons to control circadian behavior. PLoS Biol 12:e1001810.
Shafer OT, Rosbash M, and Truman JW (2002) Sequential nuclear accumulation of the clock proteins period and timeless in the pacemaker neurons of Drosophila melanogaster. J Neurosci 22:5946-5954.
Sharma VK, Lone SR, Goel A, and Chandrashekaran MK (2004) Circadian consequences of social organization in the ant species Camponotus compressus. Naturwissenschaften 91:386-390.
Shemesh Y, Cohen M, and Bloch G (2007) Natural plasticity in circadian rhythms is mediated by reorganization in the molecular clockwork in honeybees. The FASEB Journal 21:2304-2311.
Shemesh Y, Eban-Rothschild A, Cohen M, and Bloch G (2010) Molecular Dynamics and Social Regulation of Context-Dependent Plasticity in the Circadian Clockwork of the Honey Bee. The Journal of Neuroscience 30:12517-12525.
Shiga S, Rao KR, and Nässel DR (1993) Pigment-dispersing hormone immunoreactive neurons in the blowfly nervous system. Acta Biol Hung 44:55-59.
Simola DF, Graham RJ, Brady CM, Enzmann BL, Desplan C, Ray A, Zwiebel LJ, Bonasio R, Reinberg D, Liebig J, and Berger SL (2016) Epigenetic (re)programming of caste-specific behavior in the ant Camponotus floridanus. Science 351:aac6633.
Siwicki KK, Eastman C, Petersen G, Rosbash M, and Hall JC (1988) Antibodies to the period gene product of Drosophila reveal diverse tissue distribution and rhythmic changes in the visual system. Neuron 1:141-150.
Smyllie NJ, Pilorz V, Boyd J, Meng QJ, Saer B, Chesham JE, Maywood ES, Krogager TP, Spiller DG, Boot-Handford R, White MR, Hastings MH, and Loudon AS (2016) Visualizing and Quantifying Intracellular Behavior and Abundance of the Core Circadian Clock Protein PERIOD2. Curr Biol 26:1880-1886.
Soares PAO, Delabie JHC, Zanuncio JC, and Serrao JE (2008) Neural plasticity in the brain of workers of the carpenter ant Camponotus rufipes (Hymenoptera : Formicidae). Sociobiology 51:705-717.
Soehler S, Neupert S, Predel R, and Stengl M (2008) Examination of the role of FMRFamide-related peptides in the circadian clock of the cockroach Leucophaea maderae. Cell Tissue Res 332:257-269.
Sohler S, Neupert S, Predel R, Nichols R, and Stengl M (2007) Localization of leucomyosuppressin in the brain and circadian clock of the cockroach Leucophaea maderae. Cell Tissue Res 328:443-452.
Stefanini M, De Martino C, and Zamboni L (1967) Stefanini M, De Martino C, Zamboni LFixation of ejaculated spermatozoa for electron microscopy. Nature 216: 173-174. pp 173-174.

Stengl M, and Homberg U (1994) Pigment-dispersing hormone-immunoreactive neurons in the cockroach Leucophaea maderae share properties with circadian pacemaker neurons. Journal of Comparative Physiology A 175:203-213.

Strausfeld NJ (1989) Beneath the compound eye: neuroanatomical analysis and physiological correlates in the study of insect vision. In Facets of vision, pp 317-359, Springer.

Sumiyoshi M, Sato S, Takeda Y, Sumida K, Koga K, Itoh T, Nakagawa H, Shimohigashi Y, and Shimohigashi M (2011) A circadian neuropeptide PDF in the honeybee, Apis mellifera: cDNA cloning and expression of mRNA. Zoological science 28:897-909.

Toma DP, Bloch G, Moore D, and Robinson GE (2000) Changes in period mRNA levels in the brain and division of labor in honey bee colonies. Proceedings of the National Academy of Sciences of the United States of America 97:6914-6919.

Tomioka K, and Yoshii T (2006) Entrainment of Drosophila circadian rhythms by temperature cycles*. Sleep and Biological Rhythms 4:240-247.

van der Veen DR, Riede SJ, Heideman PD, Hau M, van der Vinne V, and Hut RA (2017) Flexible clock systems: adjusting the temporal programme. Philosophical transactions of the Royal Society of London Series B, Biological sciences 372.

van der Vinne V, Riede SJ, Gorter JA, Eijer WG, Sellix MT, Menaker M, Daan S, Pilorz V, and Hut RA (2014a) Cold and hunger induce diurnality in a nocturnal mammal. Proc Natl Acad Sci U S A 111:15256-15260.

van der Vinne V, Simons MJ, Reimert I, and Gerkema MP (2014b) Temporal niche switching and reduced nest attendance in response to heat dissipation limits in lactating common voles (Microtus arvalis). Physiology & behavior 128:295-302.

Van Pelt AF (1966) Activity and Density of Old-Field Ants of the Savannah River Plant, South Carolina. Journal of the Elisha Mitchell Scientific Society 82:35-43.

Vasilef I (2011) QtiPlot: data analysis and scientific visualization. Version 09 8.

Walsh JP, and Tschinkel WR (1974) Brood recognition by contact pheromone in the red imported fire ant, Solenopsis invicta. Anim Behav 22:695-704.

Weber NA (1972) Gardening Ants, the Attines. American Philosophical Society.

Wei H, el Jundi B, Homberg U, and Stengl M (2010) Implementation of pigment-dispersing factor-immunoreactive neurons in a standardized atlas of the brain of the cockroach Leucophaea maderae. J Comp Neurol 518:4113-4133.

Weiss R, Dov A, Fahrbach SE, and Bloch G (2009) Body size-related variation in Pigment Dispersing Factor-immunoreactivity in the brain of the bumblebee Bombus terrestris (Hymenoptera, Apidae). J Insect Physiol 55:479-487.

Wilson EO (1980a) Caste and division of labor in leaf-cutter ants (Hymenoptera: Formicidae: Atta). Behav Ecol Sociobiol 7:143-156.

Wilson EO (1980b) Caste and Division of Labor in Leaf-Cutter Ants (Hymenoptera: Formicidae: Atta): I. The Overall Pattern in A. sexdens. Behav Ecol Sociobiol 7:143-156.

Yoshii T, Wülbeck C, Sehadova H, Veleri S, Bichler D, Stanewsky R, and Helfrich-Förster C (2009) The Neuropeptide Pigment-Dispersing Factor Adjusts Period and Phase of Drosophila's Clock. J Neurosci 29:2597-2610.

Yu Q, Jacquier AC, Citri Y, Hamblen M, Hall JC, and Rosbash M (1987) Molecular mapping of point mutations in the period gene that stop or speed up biological clocks in Drosophila melanogaster. Proc Natl Acad Sci U S A 84:784-788.

Yuan Q, Metterville D, Briscoe AD, and Reppert SM (2007) Insect cryptochromes: gene duplication and loss define diverse ways to construct insect circadian clocks. Mol Biol Evol 24:948-955.

Závodská R, Šauman I, and Sehnal F (2003) Distribution of PER protein, pigment-dispersing hormone, prothoracicotropic hormone, and eclosion hormone in the cephalic nervous system of insects. J Biol Rhythm 18:106-122.

Zerr DM, Hall JC, Rosbash M, and Siwicki KK (1990) Circadian fluctuations of period protein immunoreactivity in the CNS and the visual system of Drosophila. J Neurosci 10:2749-2762.
Zheng X, Koh K, Sowcik M, Smith CJ, Chen D, Wu MN, and Sehgal A (2009) An isoform-specific mutant reveals a role of PDP1 epsilon in the circadian oscillator. J Neurosci 29:10920-10927.
Zube C, Kleineidam CJ, Kirschner S, Neef J, and Rössler W (2008) Organization of the olfactory pathway and odor processing in the antennal lobe of the ant Camponotus floridanus. The Journal of Comparative Neurology 506:425-441.

CURRICULUM VITAE

Education

10/14-12/17:	**Doctoral Researcher**: Julius-Maximilians-University of Würzburg Focus: Neurobiology and Genetics, Sociobiology Thesis: Characterization of the circadian clock of different Camponotus species
04/12-09/14:	**Master of Science Biology**: Julius-Maximilians-University of Würzburg Focus: Neurobiology and Genetics, Sociobiology Thesis: Characterization of the circadian clock of the carpenter ant *Camponotus floridanus* on the molecular and behavioral level
10/09-03/13:	**Bachelor of Science Biology**: Julius-Maximilians-University of Würzburg Focus: Neurobiology and Genetics, Biochemistry, Sociobiology Thesis: Das neuronale Netzwerk der inneren Uhr der Honigbiene (*Apis mellifera*, LINNAEUS 1758)
09/99-06/08:	**University Entrance Diploma**: Armin Knab Gymnasium Kitzingen

Meetings attended

04/14:	Clock Club Meeting, Kassel
05/14:	ASU - UWue international symposium and workshop "Frontiers in insect behavior, social organization and evolution", Würzburg
10/14:	SFB 1047- Timing Meeting 2014
03/15:	Eleventh Göttingen Meeting of the German Neuroscience Society
05/15:	SFB 1047- Timing Meeting 2015

07/15: Sleep and Circadian Neuroscience Summer School, Oxford

09/15: 108. Jahrestagung der Deutschen Zoologischen Gesellschaft, Graz

08/16: International Union for the Study of Social Insects (IUSSI) 2016

03/17: Twelfth Göttingen Meeting of the German Neuroscience Society

Posters

2014 Kay J, Menegazzi P, Müller S, Roces F, Helfrich-Förster C;
"The circadian clock of the carpenter ant *C. floridanus*:
genes,neurons and behavior" presented at the Clock Club
Meeting in Kassel, 22.04.2014

2014 Kay J, Beer K, Menegazzi P, Helfrich-Förster C;
"Molecular characterization of the circadian clock in selected
Hymenopteran species" presented at the SFB 1047- Timing
Meeting 2014 session 1, 30.09.14

2015 Kay J, Menegazzi P, Müller S, Roces F, Helfrich-Förster C;
"Investigating the circadian clock of the carpenter ant *C. floridanus*
genes, neurons and behavior" presented at the Eleventh Göttingen
Meeting of the German Neuroscience Society, 19.03.15 and the SFB
1047- Timing Meeting 2015, 31.05.15

2015 Kay J, Menegazzi P, Winnebeck E, Mildner S, Roces F, Helfrich-Förster C;
"The endogenous clock of the carpenter ant *C. floridanus*:
Genes, Neurons and Behavior" presented at the Sleep and Circadian
Neuroscience Summer School in Oxford, 20.07.15

2015 Kay J, Menegazzi P, Winnebeck E, Mildner S, Roces F, Helfrich-Förster C;
"Investigating the circadian clock of the carpenter ant

	C. floridanus" presented at the 108. Jahrestagung der Deutschen Zoologischen Gesellschaft in Graz, 12.09.15
2016	Kay J, Menegazzi P, Winnebeck E, Helfrich-Förster C; "First characterization of the circadian clock of *C. floridanus*" presented at the Meeting of the International Union for the Study of Social Insects (IUSSI) in Helsinki, 10.08.2016
2017	Kay J, Menegazzi P, Winnebeck E, Helfrich-Förster C; "The circadian clock of *C. floridanus*: PER&PDF expression in the brain" presented at the Twelfth Göttingen Meeting of the German Neuroscience Society, 25.03.2017

Publications

In preparation	Kay J, Menegazzi P, Beer K, Mildner S, Roces F, Helfrich-Förster C; The circadian clock of the ant *Camponotus floridanus*: A first characterization

AFFIDAVIT

I hereby confirm that my thesis entitled „The circadian clock of the carpenter ant *Camponotus floridanus*“ is the result of my own work. I did not receive any help or support from commercial consultants. All sources and / or materials applied are listed and specified in the thesis.

Furthermore, I confirm that this thesis has not yet been submitted as part of another examination process neither in identical nor in similar form.

Place, Date Signature

EIDESSTATTLICHE ERKLÄRUNG

Hiermit erkläre ich an Eides statt, die Dissertation „Die circadiane Uhr der Rossameise *Camponotus floridanus*“ eigenständig, d.h. insbesondere selbständig und ohne Hilfe eines kommerziellen Promotionsberaters, angefertigt und keine anderen als die von mir angegebenen Quellen und Hilfsmittel verwendet zu haben.

Ich erkläre außerdem, dass die Dissertation weder in gleicher noch in ähnlicher Form bereits in einem anderen Prüfungsverfahren vorgelegen hat.

Ort, Datum Unterschrift

ACKNOWLEDGEMENTS:

I gratefully thank everyone who made this dissertation possible. First of all I would like to thank my entire committee for their advice and patience, and the DFG for funding. I am very grateful to Prof. Dr. Charlotte Förster for introducing me to the fascinating research field of chronobiology, and offering me the possibility to work on this project. Her advice and help have guided me from my Bachelor to my Master and finally to this dissertation and without her this would not have been possible. All members of the department for Neurobiology and Genetics of the University of Würzburg, I thank for their support, many interesting conversations and helpful advice on my project. Special thanks go to Dr. Pamela Menegazzi, Katharina Beer and Enrico Bertolini for accompanying me throughout my project, sharing and discussing new insights and teaching me new methods (and of course the Sprizz). Of the Department of Zoology II of the University of Würzburg, I would like to specially thank Prof. Dr. Flavio Roces for his guidance and advice in the work with social insects and the provision of ants for my project, and Dr. Stephanie Mildner for teaching me her methods in working with these ants, explaining and supplying working material and experimental setups and discussion on the topic. Of the same department, I thank Annekathrin Lindenberg and Cornelia Grübel for their help with new techniques and comments, and Dr. Claudia Groh for valuable advice on my project. Prof. Dr. Monika Stengl I thank for interesting discussions and suggestions on my project. I would also like to generally thank all members of the SFB 1047 for their interest and comments. My friends and my family I thank for their constant support and patience. Special thanks go to my brother Julian Kay for help with all things technical, Lucas Landgrebe, Wiebke Sickel and Mira Becker for generally keeping up my motivation and energy levels (and dealing with my crazy ant-loving self), Steffi Klisch and Heiko Hartlieb for stopping me from making a fool of myself and all members of Würzburg Swing ‘n’ Blues who danced me through stressful times. Without any of you, this would have been a lot harder. If I forgot anybody, I´m sorry I couldn´t brain anymore, I´m still very grateful to you.